Thermodynamics of Hot Hadronic Gases at Finite Baryon Densities

A THESIS
SUBMITTED TO THE FACULTY OF THE GRADUATE SCHOOL
OF THE UNIVERSITY OF MINNESOTA
BY

Michael Glenn Albright

IN PARTIAL FULFILLMENT OF THE REQUIREMENTS
FOR THE DEGREE OF
Doctor of Philosophy

Joseph Kapusta, Advisor

November, 2015

Acknowledgements

First, I would like to express my sincerest appreciation to my advisor, Joseph Kapusta, for all of his guidance and assistance throughout my time as a graduate student at the University of Minnesota. I would also like to thank Clint Young, my research collaborator, for his helpful suggestions. I would also like to thank my parents, Chris and Glenn, and my sister Jaime. Your love and support throughout the years made this possible. Finally, I thank the members of my thesis committee: Marco Peloso, Roberta Humphreys, and Roger Rusack.

This work was supported by the School of Physics and Astronomy at the University of Minnesota, by a University of Minnesota Graduate School Fellowship, and by the US Department of Energy (DOE) under Grant Number DE-FG02-87ER40328. I also acknowledge computational support from the University of Minnesota Supercomputing Institute. Programming their supercomputers was a fun and memorable experience.

Dedication

To my parents, Chris and Glenn, and my sister Jaime—thanks.

Abstract

In this thesis we investigate equilibrium and nonequilibrium thermodynamic properties of Quantum Chromodynamics (QCD) matter at finite baryon densities. We begin by constructing crossover models for the thermodynamic equation of state. These use switching functions to smoothly interpolate between a hadronic gas model at low energy densities to a perturbative QCD equation of state at high energy densities. We carefully design the switching function to avoid introducing first-, second-, or higher-order phase transitions which lattice QCD indicates are not present at small baryon chemical potentials. We employ three kinds of hadronic models in the crossover constructions, two of which include repulsive interactions via an excluded volume approximation while one model does not. We find that the three crossover models are in excellent agreement with accurate lattice QCD calculations of the equation of state over a wide range of temperatures and baryon chemical potentials. Hence, the crossover models should be very useful for parameterizing the equation of state at finite baryon densities, which is needed to build next-generation hydrodynamic simulations of heavy-ion collisions. We next calculate the speed of sound and baryon number fluctuations predicted by the crossover models. We find that crossover models with hadronic repulsion are most successful at reproducing the lattice results, while the model without repulsion is less successful, and hadron (only) models show poor agreement. We then compare the crossover models to net-proton fluctuation measurements from the STAR Collaboration at the Relativistic Heavy Ion Collider (RHIC). The comparisons suggest baryon number fluctuations freeze-out well below the chemical freeze-out temperature. We also search for signs of critical fluctuations in the STAR data, but we find no evidence for them at this time.

Finally, we derive kinetic theory formulas for the shear and bulk viscosity and thermal conductivity of hot hadronic matter. This generalizes previous works by incorporating baryon chemical potential and a vector mean field into the formalism. We show that the theory is thermodynamically self-consistent and it obeys the Landau-Lifshitz conditions of fit. The formulas should be very useful for predicting transport coefficients in future heavy-ion collision experiments at RHIC and other colliders.

This thesis is based upon work published in Refs. [1, 2, 3].

Contents

List of Tables

List of Figures

Chapter 1

Introduction

Quantum Chromodynamics (QCD) is the theory of quarks and gluons and the forces between them. (*Chromo* refers to the color charge of QCD, whose values are called red, green, and blue.) In the world around us, QCD confines quarks and gluons into color neutral bound states—protons and neutrons—which form the centers atoms, from which we are made. Interestingly, quarks and gluons can form different collective states of matter when compressed to higher densities or heated to larger temperatures. For instance, according to our current understanding of cosmology, in the first microseconds after the big bang (approximately 13.8 billion years ago), the universe was too hot and dense for protons or neutrons to stably exist—instead, the quarks and gluons in the universe formed a quark-gluon plasma [4]. As the universe expanded and cooled below a temperature[1] of 150 MeV (nearly 2 trillion kelvin), it changed phase from a quark-gluon plasma into a gas of bound states including protons, neutrons, pions, rho mesons, and so forth. Collectively, these bound states are referred to as hadrons, and a weakly-interacting collection of them is called a hadron gas. As the universe further expanded and cooled, the unstable hadrons decayed, yielding an early universe filled with protons, neutrons, leptons, and photons (along with dark matter).

Quark-gluon plasmas are also expected to form at cooler temperatures and greater baryon densities. Furthermore, theoretical calculations suggest this may become superconducting at very large baryon densities [5, 6]. This raises an obvious question of whether or not neutron stars, whose cores may be nearly ten times more dense than

[1] In this thesis, we use natural units such that $\hbar = c = k_B = 1$.

atomic nuclei [7], are sufficiently dense to host exotic phases of quarks and gluons. This is a topic of intense research [8].

Major research efforts are underway in the nuclear physics community aimed at discovering and understanding these various collective phases of quarks and gluons. This represents, in essence, a quest to understand the earliest moments of our ancient past. Part of the challenge is elucidating the properties of the various phases of matter, while another challenge is locating and characterizing the boundaries separating the different phases. The conjectured phase diagram of QCD is illustrated in Fig. 1.1. (See Ref. [9] for a review.) From the figure, we see the quark-gluon plasma exists at high temperatures and baryon chemical potentials[2] while the hadron gas occupies lower temperatures and chemical potentials. The boundary separating the two phases is believed to have interesting thermodynamic properties: theoretical modeling suggests the phase boundary is a line of first-order [10, 11, 12, 13] phase transitions at large baryon chemical potentials, while computational studies show the phase boundary is an analytic crossover at zero baryon chemical potential [14, 15]. This suggests the first-order line terminates at a critical point—a point of second-order phase transition—at some critical temperature and chemical potential [16, 17]. The exact location of the critical point is unknown, and its existence has not yet been experimentally confirmed.

Experimentally, the phases of QCD are probed using heavy-ion colliders—enormous particle accelerators which collide large atomic nuclei at relativistic speeds. The violent collisions convert the projectiles' kinetic energy into thermal energy, forming a hot and dense quark-gluon plasma not much bigger than an atomic nucleus, with maximum temperatures reaching into the trillions of degrees; in essence, it is like a droplet of the early universe. With no walls to contain the material, the fireball quickly expands and cools until the quarks and gluons become confined into hadrons. Then, the fireball expands and cools further until interactions between hadrons cease (an event called freeze-out) and particles stream outwards, ultimately passing through sensitive particle detectors. It is the goal of experimental physicists to reconstruct the properties of the hot QCD phases formed early in the collision from observations of the leftover debris. This is a challenging endeavor which requires careful comparison between experimental

[2] Baryon chemical potential is the thermodynamic variable conjugate to baryon density. Large baryon densities correspond to large baryon chemical potentials.

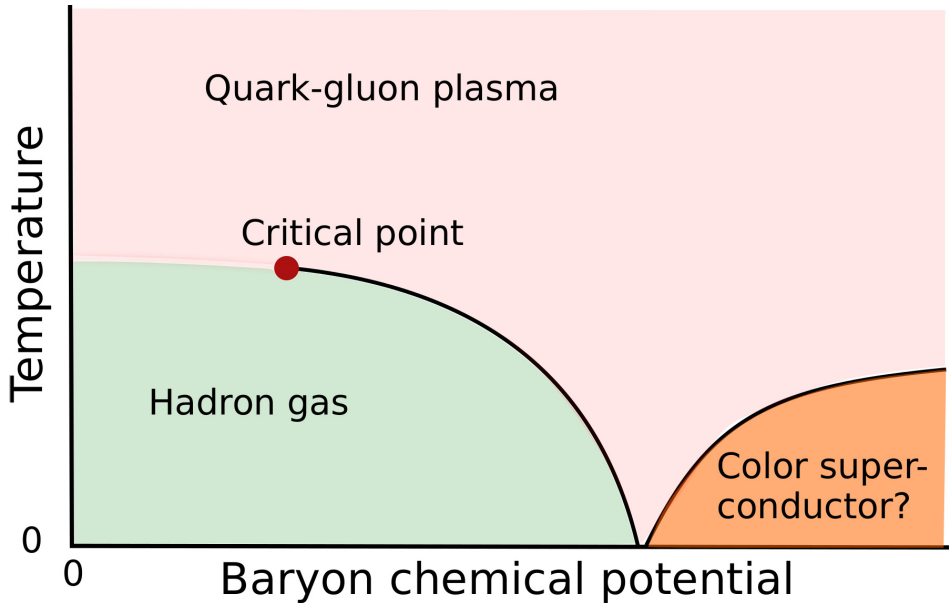

Figure 1.1: Conjectured phase diagram of QCD as a function of temperature and baryon chemical potential.

data and detailed simulations.

Heavy-ion collisions have a long history, going all the way back to the Bevalac at Lawrence Berkeley National Laboratory in the early 1970's and the Alternating Gradient Synchrotron (AGS) at Brookhaven National Laboratory in the 1980's [18]. A major goal was the creation of new forms of nuclear matter. Unfortunately, those early machines, which collided nuclei at energies of a few GeV per nucleon, did not have sufficient collision energy to create a quark-gluon plasma. Signatures of quark-gluon plasma were later observed at the more powerful Super Proton Synchrotron (SPS) at CERN [19], but some doubts remained. The Relativistic Heavy Ion Collider (RHIC) was constructed at Brookhaven to settle the issue. Completed in 2000, RHIC began colliding nuclei at ultra-relativistic energies of 200 GeV per nucleon pair, forming hotter and denser fluids with initial temperatures of 300-600 MeV [20]—well above the phase transition temperature. Within a few years, RHIC collisions had produced clear signs of a quark-gluon plasma [21, 22, 23, 24]. One major discovery was that the quark-gluon plasma behaved as a nearly ideal fluid [23, 25]. It has in fact been called a *perfect fluid* since its specific shear viscosity (that is, shear viscosity divided by entropy density) is among

the smallest of all known substances [26, 27, 28]. It is in fact very near a lower limit conjectured by string theory [29], which raises many tantalizing questions. In any case, hydrodynamic simulations with small but non-zero viscosities proved very successful at reproducing heavy-ion collision data from RHIC. Other interesting discoveries were jet quenching and collective flow [23, 25, 30, 31, 32]. These, along with the small specific shear viscosity, indicated that QCD is strongly interacting in the quark-gluon plasma formed at RHIC.

At the same time RHIC was making experimental breakthroughs, advances in computational modeling known as lattice QCD showed that the QCD phase transition is an analytic crossover at zero baryon chemical potential [14, 15], as opposed to the first-order phase transition which is expected at large baryon chemical potentials [10, 11, 12, 13]. This suggests the first-order transition line may terminate at a critical point at some unknown critical temperature and baryon chemical potential [16, 17]. With the quark-gluon plasma's existence confirmed, interest in recent years has turned towards locating the critical point. Experimentally, a beam energy scan program at RHIC has searched for signs of the critical point by colliding heavy ions at a variety of beam energies from $\sqrt{s_{NN}} = 7.7$ GeV to 200 GeV [33]. Varying the energy changes the chemical potential and initial temperature of the medium (higher collision energies yield larger initial temperatures and smaller baryon chemical potentials), enabling a scan across the phase diagram. Some have argued that the data shows hints of a critical point [34], but at present it is hard to claim any definitive signal. It seems that detecting the critical point will require greater effort from physicists.

Already, a second beam energy scan at RHIC is in the planning stage which will search for the critical point with greatly increased statistics and upgraded detectors [35]. Also, a new particle collider is under construction near Darmstadt, Germany. Called the Facility for Antiproton and Ion Research (FAIR), it will search for the critical point at even higher baryon chemical potentials than RHIC. To maximize the discovery potential, these experimental efforts must be accompanied by complementary improvements in theoretical modeling of QCD matter at moderate temperatures and large baryon chemical potentials, where the critical point is believed to lie. That is a major goal of this thesis.

Theoretical modeling of QCD and its various phases is a highly non-trivial endeavor.

Formally, it is straightforward to express thermodynamic properties of QCD matter (like the equation of state) in terms of path integrals, as the QCD Lagrangian is well known. However, no one knows how to solve the equations in general circumstances, and only in special cases has progress been made. Due to asymptotic freedom [36, 37], the QCD coupling constant weakens at temperatures far above the deconfinement transition temperature, so perturbation theory has been successfully applied there to compute various quantities, such as the equation of state. However, the coupling constant grows near the phase transition temperature, causing perturbative calculations to diverge and fail at lower temperatures.

In the special case where baryon chemical potential vanishes, the path integrals simplify enough to enable Monte-Carlo integration known as lattice QCD. With this technique, researchers use powerful supercomputers to solve the path integrals by discretizing space-time and numerically integrating over the fields. Thanks to the exponential growth of computing power over the decades, known as Moore's Law, lattice QCD has revolutionized our understanding of the QCD phase diagram at zero baryon chemical potential. For instance, it has identified the phase transition temperature as $T \approx 150$ MeV [38, 39, 40, 41] and shown us that the transition from a hadron gas to a quark-gluon plasma is a smooth crossover at zero chemical potential [14, 15]. However, lattice QCD suffers from the fermion sign problem [42] which renders calculations difficult to intractable at large baryon chemical potentials. There has been some progress at evading the sign problem using, for example, re-weighting and Taylor series expansion techniques, but in general they are only reliable for baryon chemical potentials smaller than the temperature [42].

Thus, at large baryon chemical potentials and at temperatures below the deconfinement transition, neither perturbation theory nor lattice QCD make reliable predictions about QCD matter. Unfortunately, those are exactly the conditions expected at RHIC's beam energy scan and at FAIR. Hence, in this thesis, we focus on hadron gas models. While these models are not derived directly from the QCD Lagrangian, they have been shown to match lattice QCD predictions below the deconfinement phase transition [43]. Hadron gas models have an advantage over lattice QCD in that calculations are tractable when baryon chemical potential is finite.

One goal of this thesis is to predict the thermodynamic equation of state of QCD

matter at large baryon chemical potentials over a range of temperatures. This is an interesting quantity for several reasons. First, state-of-the-art hydrodynamic simulation codes have proven themselves invaluable tools for modeling heavy-ion collisions and enabling discoveries, and all hydro codes require knowledge of the equation of state. This tells the program, for instance, how thermodynamic variables like pressure, energy density, temperature, etc., are related. In RHIC collisions at energies of 200 GeV, and in heavy-ion collisions at the Large Hadron Collider (LHC) at CERN, chemical potentials are tiny. (See for instance Ref. [44].) Hence, when modeling those collisions, hydrodynamic codes typically use an equation of state based on lattice QCD calculations, which assumes baryon chemical potential is zero. However, baryon chemical potentials are large in the RHIC beam energy scan, and they will be even larger at FAIR, and that alters the equation of state—for instance, pressure rises with baryon chemical potential. Hence, hydrodynamic codes need equation of state calculations which include large chemical potentials to support those new experiments. A second motivation is that the equation of state allows one to predict baryon number fluctuations. In Chapter 3, we compare our predicted fluctuations to experimental data from the STAR Collaboration at RHIC. By fitting our models to the STAR data, we infer the temperatures and chemical potentials at which fluctuations froze-out in collisions in the first beam energy scan at RHIC. This gives us information about the final moments of heavy-ion collisions as the fireballs disintegrate. Interestingly, we find that previous works may have overestimated the freeze-out temperatures. We also look for anomalously large fluctuations, which could pinpoint the location of the critical point, but we see no evidence of those in the current STAR data.

A second goal of this thesis is to develop a new framework for computing the shear and bulk viscosity and thermal conductivity of QCD matter at large baryon chemical potentials. These quantities are also needed for hydrodynamic simulations, but they could be even more valuable: in many substances, shear viscosity is a minimum and bulk viscosity a maximum at phase phase transitions [45]. Hence, it may be possible to detect phase transition boundaries from changes in the transport coefficients. In any regard, it is important to develop the mathematical tools to predict how the transport coefficients of QCD matter change with temperature and baryon chemical potential.

The outline of this thesis is as follows:

- In Chapter 2, we begin by reviewing the popular hadron resonance gas model, which is a simple but effective description for QCD matter below a temperature of 150 MeV. The hadron resonance gas model incorporates attractive interactions, but it neglects repulsion—something which is important as temperatures and baryon chemical potentials rise. We proceed to improve the model by incorporating repulsive forces through an excluded volume approximation, and we show this gives superior results at higher temperatures and baryon chemical potentials. For completeness, we also compare this to a similar excluded volume model found in the literature. We next develop phenomenological equations of state which use thermodynamic switching functions to smoothly interpolate from hadron gas models at low temperatures to perturbation theory at high temperatures. These crossover models are thermodynamically self-consistent, and we show that they are remarkably successful at reproducing lattice QCD calculations. Finally, we use the models to predict the equation of state at large baryon chemical potentials where lattice results are unavailable.

- In Chapter 3, we employ the crossover models from Chapter 2 to compute the speed of sound of QCD matter and the baryon number fluctuations. We then compare the fluctuation predictions to experimental data from the STAR Collaboration, and we fit the model predictions to the STAR data to infer the fluctuation freeze-out surface. An important discovery is that previous works may have overestimated the temperature at which baryon number fluctuations freeze-out. We also look for signatures of a critical point in the STAR data, but we find no clear signs of a critical point at this time.

- Finally, in Chapter 4, we derive a relativistic quasiparticle theory of transport coefficients of hadronic gases at moderate temperatures and large baryon chemical potentials. A novel contribution is showing how to incorporate attractive and repulsive interactions via scalar and vector mean fields all while maintaining thermodynamic self-consistency. We also show how to carefully obey the Landua-Lifshitz conditions of fit, and we show that this ensures that transport coefficients are non-negative, as thermodynamics requires.

Chapter 2

Equations of State

In this chapter, we develop models for calculating the thermodynamic equation of state of Quantum Chromodynamics (QCD). The models use thermodynamic switching functions to smoothly interpolate from a hadron gas phase at low temperatures and baryon chemical potentials to a quark-gluon plasma phase at high temperatures and chemical potentials. The resulting equations of state show remarkable agreement with lattice QCD calculations. We then use the models to predict the equation of state at large baryon chemical potentials where lattice QCD calculations become challenging due to the fermion sign problem.

2.1 Introduction

The equation of state of Quantum Chromodynamics at finite temperature is studied theoretically in a variety of ways. Starting from *low* temperatures one has a dilute gas of pions and nucleons. With increasing temperature hadron resonances are created and contribute to the equation of state. If the spectrum of resonances increases exponentially with mass then one reaches a Hagedorn limiting temperature which experiments and models suggest is about 160 MeV. This conclusion is based on the treatment of hadrons as point particles, which they are not. Starting from extremely *high* temperatures one can use perturbation theory to calculate the equation of state because QCD has the property of asymptotic freedom whereby the effective gauge coupling decreases logarithmically with temperature. As the temperature is lowered the coupling eventually

becomes large and perturbation theory is no longer useful. The only reliable approach for all temperatures is to do numerical calculations with lattice QCD.

The goal of this chapter is to find a means for switching from a hadron resonance gas at low temperature, preferably treating the hadrons not as point particles but as extended objects, to a plasma of weakly interacting quarks and gluons at high temperature. We will construct a switching function that does just that. The parameters will be adjusted to fit the lattice equation of state at zero chemical potentials. Then the model can make parameter-free predictions for both finite temperature and chemical potentials. Lattice calculations at finite chemical potentials face well-known problems [42], but comparison to one of them at a baryon chemical potential of 400 MeV is quite good. The equation of state constructed in this chapter can be used in hydrodynamical models of high energy heavy-ion collisions. It has the advantage that at the moment of freeze-out from fluid behavior to individual hadrons, one will know the chemical abundance of all the hadrons which then can either be compared to experimentally observed abundances or used as the initial condition for a cascade after-burner.

The outline of this chapter is as follows. In Sec. 2.2 we will review the hadron resonance model of point particles. In section 2.3 we will review and extend two versions of the excluded volume model which take into account the extended spatial size of hadrons. In Sec. 2.4, we describe the most recent calculations of perturbative QCD and compare it to the lattice equation of state to illustrate the problem we are addressing. In Sec. 2.5 we will construct a switching function, and adjust its parameters and the other parameters in the model by doing a chi-squared fit to both the pressure and the trace anomaly/interaction measure. The resulting parameters provide physical information, such as the size of hadrons and one optimum way to choose the scale of the running gauge coupling as a function of temperature and baryon chemical potential. In section 2.6 we will compare with lattice results at a baryon chemical potential of 400 MeV. Our conclusions are contained in section 2.7.

2.2 Hadron Resonance Gas

The equation of state of the hadronic phase is usually assumed to be a hadron resonance gas where all observed, and sometimes extrapolated, hadrons are included as free non-interacting point particles. According to the arguments by Dashen, Ma and Bernstein [46], this is a reasonable way to include attractive interactions. (Repulsive interactions will be addressed in the next section.) In thermodynamic equilibrium, each hadronic species labeled by a contributes to the pressure as

$$P_a^{\rm pt}(T,\mu_a) = g_a \int \frac{d^3p}{(2\pi)^3} \frac{|\mathbf{p}|^2}{3E_a} \frac{1}{{\rm e}^{\beta(E_a(p)-\mu_a)} \pm 1} \,. \tag{2.1}$$

(Note that we use natural units where $\hbar = c = k_B = 1$.) The sign is positive if the hadron a is a fermion and negative for bosons. The factor

$$\frac{1}{{\rm e}^{\beta(E_a(p)-\mu_a)} \pm 1} \tag{2.2}$$

appearing in Eq. (2.1) is the famous Fermi Dirac/Bose Einstein distribution function of quantum statistical mechanics. The inverse of temperature is denoted by β and μ_a is the particle chemical potential. The degeneracy of particle a of spin s_a is

$$g_a = (2s_a + 1) \,. \tag{2.3}$$

The energy E_a depends on momentum $\mathbf{p}$ and mass m_a as

$$E_a(p) = \sqrt{|\mathbf{p}|^2 + m_a^2} \,. \tag{2.4}$$

This is the standard energy equation of special relativity. Hence, Eq. (2.1) is valid at relativistic particle energies. We assume chemical equilibrium and we assume strange and electric chemical potentials vanish which is a good approximation for conditions probed in heavy-ion collision experiments [47]. Hence, the particle chemical potential is

$$\mu_a = b_a \mu \,, \tag{2.5}$$

where b_a is the baryon charge of particle a and μ is the baryon chemical potential. Note that b_a is $+1$ for baryons, -1 for antibaryons, and 0 for mesons. The total pressure is the sum of partial pressures:

$$P_{\rm pt}(T,\mu) = \sum_a P_a^{\rm pt}(T,\mu_a) \,. \tag{2.6}$$

The equilibrium number density of hadron species a is given by

$$n_a^{\rm pt}(T,\mu_a) = g_a \int \frac{d^3p}{(2\pi)^3} \frac{1}{{\rm e}^{\beta(E_a(p)-\mu_a)} \pm 1} \,. \tag{2.7}$$

Hence the equilibrium density of baryon charge is

$$n_{\rm pt}(T,\mu) = \sum_a b_a \, n_a^{\rm pt}(T,\mu_a) \,. \tag{2.8}$$

The equilibrium energy density of the hadron gas is

$$\epsilon_{\rm pt}(T,\mu) = \sum_a g_a \int \frac{d^3p}{(2\pi)^3} E_a \frac{1}{{\rm e}^{\beta(E_a(p)-\mu_a)} \pm 1} \,. \tag{2.9}$$

Finally, the entropy density is found through the thermodynamic relation

$$s_{\rm pt} = \frac{1}{T} \left(\epsilon_{\rm pt} + P_{\rm pt} - \mu n_{\rm pt} \right) \,. \tag{2.10}$$

Following a well-trodden path, we include all hadrons appearing in the most recent Particle Data Group compilation which consist of up, down, and strange quarks, with the exception of the σ meson—it is omitted as its contribution to averaged thermal observables is canceled by other repulsive channels [48]. For completeness, and for use by others, we provide a table of particles in Appendix A.

2.3 Excluded Volume Models

Hadrons are not point particles, and repulsive interactions can be implemented via an excluded volume approximation whereby the volume available for the hadrons to move in is reduced by the volume they occupy, as first suggested in Refs. [49, 50, 51]. There are at least two thermodynamically self-consistent versions of this model. Here we extend one of these models, referred to as model I [52], which was originally formulated at finite temperature, to include finite chemical potentials as well. Then we compare and contrast it to what we refer to as model II [53], which appeared a decade later. Model II has been compared to experimental data a number of times, such as in [54] and [55]. Our arguments are phrased in terms of classical statistics, or Boltzmann distributions, for clarity of presentation. However, this is not a limitation, and the extension to quantum statistics is deferred to later.

2.3.1 Model I

In the independent-particle approximation the partition function for a hadron of species a is Vz_a where V is the total volume of the system and

$$z_a = (2s_a + 1) \int \frac{d^3p}{(2\pi)^3} \mathrm{e}^{-\beta(E_a(p)-\mu_a)} \,. \tag{2.11}$$

In the canonical ensemble the total number of particles is fixed, whereas in the grand canonical ensemble only the average is. Let n denote the total number of species. The partition function in the grand canonical ensemble in the point particle approximation is

$$Z_{\mathrm{pt}} = \sum_{N=0}^{\infty} \sum_{N_1=0}^{\infty} \cdots \sum_{N_n=0}^{\infty} \delta_{N_1+\cdots N_n,N} \frac{(Vz_1)^{N_1}}{N_1!} \cdots \frac{(Vz_n)^{N_n}}{N_n!} \,, \tag{2.12}$$

where N is the total number of particles irrespective of species. The excluded volume approximation being applied here reduces the total volume V by the amount occupied by the N hadrons

$$V_{\mathrm{exI}} = \frac{1}{\epsilon_0} \left[\sum_{j=1}^{N_1} E_1(p_j) + \cdots \sum_{j=1}^{N_n} E_n(p_j) \right] \,. \tag{2.13}$$

The assumption is that the volume excluded by a hadron is proportional to its energy with the constant of proportionality ϵ_0 (dimension of energy per unit volume) being the same for all species. It is also assumed that hadrons are deformable so that there is no limitation by a packing factor as there would be for rigid spheres, for example. This is model I.

In the pressure ensemble [49, 50] the partition function is the Laplace transform of the grand canonical partition function in volume space.

$$\tilde{Z}(T, \mu, \xi) = \int dV \, Z(T, \mu, V) \mathrm{e}^{-\xi V} \tag{2.14}$$

In the present context the relevant integral is

$$\int_{V_{\mathrm{exI}}}^{\infty} dV (V - V_{\mathrm{exI}})^N \mathrm{e}^{-\xi V} = \frac{N!}{\xi^{N+1}} \mathrm{e}^{-\xi V_{\mathrm{exI}}} \,. \tag{2.15}$$

Then

$$\tilde{Z}_{\mathrm{exI}}(T, \mu, \xi) = \frac{1}{\xi} \sum_{N=0}^{\infty} \sum_{N_1=0}^{\infty} \cdots \sum_{N_n=0}^{\infty} \delta_{N_1+\cdots N_n,N} \frac{N!}{N_1! \cdots N_n!} \left(\frac{\tilde{z}_1}{\xi} \right)^{N_1} \cdots \left(\frac{\tilde{z}_n}{\xi} \right)^{N_n} \,, \tag{2.16}$$

where

$$\tilde{z}_a = (2s_a + 1) \int \frac{d^3p}{(2\pi)^3} \mathrm{e}^{-(\beta+\xi/\epsilon_0)E_a(p)} \mathrm{e}^{\beta\mu_a} \,. \tag{2.17}$$

The factor

$$\frac{N!}{N_1! \cdots N_n!}$$

is just the number of ways to choose N_1 particles of type 1, N_2 particles of type 2, etc. out of a total of $N = N_1 + \cdots + N_n$ particles. Hence

$$\tilde{Z}_{\mathrm{exI}}(T, \mu, \xi) = \frac{1}{\xi} \sum_{N=0}^{\infty} \left(\frac{\tilde{z}_1}{\xi} + \cdots \frac{\tilde{z}_n}{\xi} \right)^N = \left(\xi - \sum_{a=1}^{n} \tilde{z}_a \right)^{-1} \,. \tag{2.18}$$

In the pressure ensemble the pole ξ_{p} furthest to the right along the real axis determines the pressure as $\xi_{\mathrm{p}} = \beta P_{\mathrm{exI}}(\beta, \mu)$. Note that

$$\sum_{a=1}^{n} \tilde{z}_a = \beta_* P_{\mathrm{pt}}(\beta_*, \mu_*) \,, \tag{2.19}$$

where P_{pt} is the point particle pressure with effective inverse temperature $\beta_* = \beta + \xi_{\mathrm{p}}/\epsilon_0$ and baryon chemical potential $\mu_* = \beta\mu/\beta_*$. (The generalization to more than one conserved charge is obvious.) This implies that the pressure in the excluded volume approximation is expressed in terms of the point particle pressure as

$$P_{\mathrm{exI}}(T, \mu) = \frac{P_{\mathrm{pt}}(T_*, \mu_*)}{1 - P_{\mathrm{pt}}(T_*, \mu_*)/\epsilon_0} \tag{2.20}$$

with the real temperature and chemical potential expressed in terms of the effective ones by

$$T = \frac{T_*}{1 - P_{\mathrm{pt}}(T_*, \mu_*)/\epsilon_0} \tag{2.21}$$

$$\mu = \frac{\mu_*}{1 - P_{\mathrm{pt}}(T_*, \mu_*)/\epsilon_0} \,. \tag{2.22}$$

The baryon density, entropy density, and energy density are computed from the pressure using the standard thermodynamic formulas:

$$n_{\mathrm{exI}} = \left(\frac{P_{\mathrm{exI}}}{\partial\mu} \right)_T \tag{2.23}$$

$$s_{\mathrm{exI}} = \left(\frac{P_{\mathrm{exI}}}{\partial T} \right)_\mu \tag{2.24}$$

$$\epsilon_{\rm exI} = -P_{\rm exI} + Ts_{\rm exI} + \mu n_{\rm exI}\,. \tag{2.25}$$

Note that this ensures the model is thermodynamically self-consistent. After tedious algebra, we find

$$\begin{aligned} s_{\rm exI}(T,\mu) &= \frac{s_{\rm pt}(T_*,\mu_*)}{1+\epsilon_{\rm pt}(T_*,\mu_*)/\epsilon_0} && (2.26)\\ n_{\rm exI}(T,\mu) &= \frac{n_{\rm pt}(T_*,\mu_*)}{1+\epsilon_{\rm pt}(T_*,\mu_*)/\epsilon_0} && (2.27)\\ \epsilon_{\rm exI}(T,\mu) &= -P_{\rm exI}(T,\mu) + Ts_{\rm exI}(T,\mu) + \mu n_{\rm exI}(T,\mu) \\ &= \frac{\epsilon_{\rm pt}(T_*,\mu_*)}{1+\epsilon_{\rm pt}(T_*,\mu_*)/\epsilon_0}\,. && (2.28) \end{aligned}$$

Note that in this model there is a natural limiting energy density of ϵ_0. The model is solved using a numerical root finding algorithm to simultaneously solve Eqs. 2.21 and 2.22 for T_* and μ_* from the true T and μ, calculating the point particle properties with these values, and then computing thermodynamic properties in the excluded volume approximation.

It is rather tedious to present the derivation with quantum statistics. The result is simply to calculate the point particle quantities with the inclusion of Bose or Fermi statistics. The fundamental thermodynamic relations may easily be checked.

It is instructive to take the nonrelativistic limit with one species of particle with mass m and with classical statistics. Using $P_{\rm pt} = n_{\rm pt}T_*$, $\epsilon_{\rm pt} = (m + \frac{3}{2}T_*)n_{\rm pt}$, and assuming $T \ll m$ and $n_{\rm exI}T \ll \epsilon_0$, one finds the standard van der Waals equation of state $P_{\rm exI}(1 - v_0 n_{\rm exI}) = n_{\rm exI}T$ where $v_0 = m/\epsilon_0$.

2.3.2 Model II

Now let us consider a different version of the excluded volume approximation where a hadron of species a has a volume v_a. This is referred to as model II. Following the same procedure as for model I we find

$$\tilde{z}_a = (2s_a+1)\int \frac{d^3p}{(2\pi)^3} \mathrm{e}^{-\beta E_a(p)} \mathrm{e}^{\beta(\mu_a - v_a T\xi)}\,. \tag{2.29}$$

Thus the chemical potential for species a is shifted by the amount

$$\mu_a \to \bar{\mu}_a = \mu_a - v_a T\xi_{\rm p} = \mu_a - v_a P_{\rm exII}(T,\mu)\,. \tag{2.30}$$

Thus the pressure must be calculated self-consistently from the equation

$$P_{\rm exII}(T,\mu) = \sum_{a=1}^{n} P_a^{\rm pt}(T,\bar{\mu}_a) \tag{2.31}$$

using Eq. (2.30). Note that $P_a^{\rm pt}(T,\bar{\mu}_a)$ is the point particle pressure for species a with effective chemical potential $\bar{\mu}_a$. The application of standard thermodynamic identities to Eq. (2.31) yields the following expressions

$$\begin{aligned} n_{\rm exII}(T,\mu) &= \frac{\sum_a b_a\, n_a^{\rm pt}(T,\bar{\mu}_a)}{1+\sum_a v_a n_a^{\rm pt}(T,\bar{\mu}_a)} && (2.32)\\ s_{\rm exII}(T,\mu) &= \frac{\sum_a s_a^{\rm pt}(T,\bar{\mu}_a)}{1+\sum_a v_a n_a^{\rm pt}(T,\bar{\mu}_a)} && (2.33)\\ \epsilon_{\rm exII}(T,\mu) &= -P_{\rm exII}(T,\mu) + T s_{\rm exII}(T,\mu) + \mu n_{\rm exII}(T,\mu) \\ &= \frac{\sum_a \epsilon_a^{\rm pt}(T,\bar{\mu}_a)}{1+\sum_a v_a n_a^{\rm pt}(T,\bar{\mu}_a)}\,. && (2.34) \end{aligned}$$

One must pay attention to the notation used above: $n_a^{\rm pt}(T,\bar{\mu}_a)$ is the number density of particles of species a treated as noninteracting point particles, whereas the baryon density for point particles is $\sum_a b_a\, n_a^{\rm pt}(T,\mu_a)$, with b_a the baryon number of species a. In this version of the excluded volume model, one first uses numerical root finding to solve for the pressure $P_{\rm exII}(T,\mu)$ self-consistently using Eqs. (2.31) and (2.30). Note that the true T and μ are used. Then, one uses $P_{\rm exII}$ to compute the effective chemical potential $\bar{\mu}_a$ for each particle species a and then finds the remaining renormalized thermodynamic properties. Note that the chemical potential for each species is additively modified, not multiplicatively renormalized as in model I. Also, all of the shifts are negative. For example, the effective chemical potential for nucleons is $\mu - v_N P_{\rm exII}(T,\mu)$, for antinucleons it is $-\mu - v_N P_{\rm exII}(T,\mu)$, and for pions of any charge it is $-v_\pi P_{\rm exII}(T,\mu)$ (always negative). Here we choose v_a to be proportional to the mass, namely,

$$v_a = m_a/\epsilon_0 \tag{2.35}$$

where ϵ_0 is a constant with units of energy per volume. This should give results very similar to model I where the excluded volume is proportional to the single particle energy. This choice is also consistent with the MIT bag model. We also remark that with this choice there is only one free parameter (ϵ_0), unlike in other published works

where each v_a is an independent parameter. Hence, it will be easier to avoid over fitting when estimating the parameters of this model using the lattice QCD data.

A derivation which includes quantum statistics is straightforward. The obvious result is that one just calculates the point particle properties with the Bose-Einstein or Fermi-Dirac distributions instead of the Boltzmann distribution.

Next, we compare the three hadronic models, including quantum statistics, with lattice QCD calculations at zero baryon chemical potential. The lattice results to which we compare were reported in Ref. [56]. They included 2+1 flavors of quarks (strange quark heavier than up and down quarks). The temperature range sampled was from 100 to 1000 MeV, extending even beyond the highest temperatures expected at CERN's Large Hadron Collider (LHC). For both excluded volume models, we performed a chi-squared combined fit to the pressure and the trace anomaly for $T < 300$ MeV. The best-fit parameter for model I was $\epsilon_0 = (600.4\,\mathrm{MeV})^4$ with a chi-squared per degree of freedom of 9.93. The best-fit parameter for model II was $\epsilon_0 = (550.0\,\mathrm{MeV})^4$ with a chi-squared per degree of freedom of 8.94. The point model is parameter-free. The pressures are displayed in Fig. 2.1 while the trace anomaly $(\epsilon - 3P)/T^4$, also called the interaction measure, is visible in Fig. 2.2. We see that the excluded volume models have improved agreement with the lattice data at higher temperatures. However, all of the hadron models fail to agree with lattice QCD at high temperatures where the system transforms into a quark-gluon plasma.

2.4 Perturbative QCD

The equation of state of the quark-gluon plasma can be calculated using perturbation theory in the gauge coupling. Many papers have contributed to this endeavor since the first papers in the late 1970's. Here we use the latest results from Refs. [57] and [58] which computes the pressure including terms up to order $\alpha_s^3 \ln \alpha_s$. We assume 3 flavors of massless quarks. Note that both h_4 and h_6 depend on $\ln(\alpha_s/\pi)$:

$$P = \frac{8\pi^2}{45} T^4 \left[h_0 + h_2 \left(\frac{\alpha_s}{\pi}\right) + h_3 \left(\frac{\alpha_s}{\pi}\right)^{3/2} + h_4 \left(\frac{\alpha_s}{\pi}\right)^2 + h_5 \left(\frac{\alpha_s}{\pi}\right)^{5/2} + h_6 \left(\frac{\alpha_s}{\pi}\right)^3 \right] \quad (2.36)$$

where

$$h_0 = 1 + \frac{3N_f}{32} \left(7 + 120\hat{\mu}_q^2 + 240\hat{\mu}_q^4\right) \quad (2.37)$$

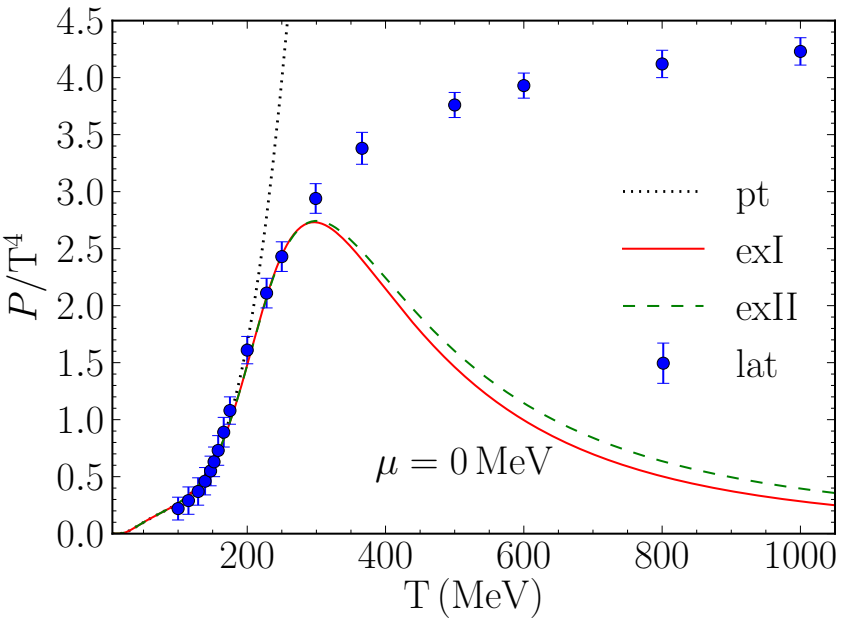

Figure 2.1: Pressure normalized by T^4 for the three hadronic models. The point model (pt) is parameter-free while the excluded volume models exI and exII were fit to lattice results from Ref. [56].

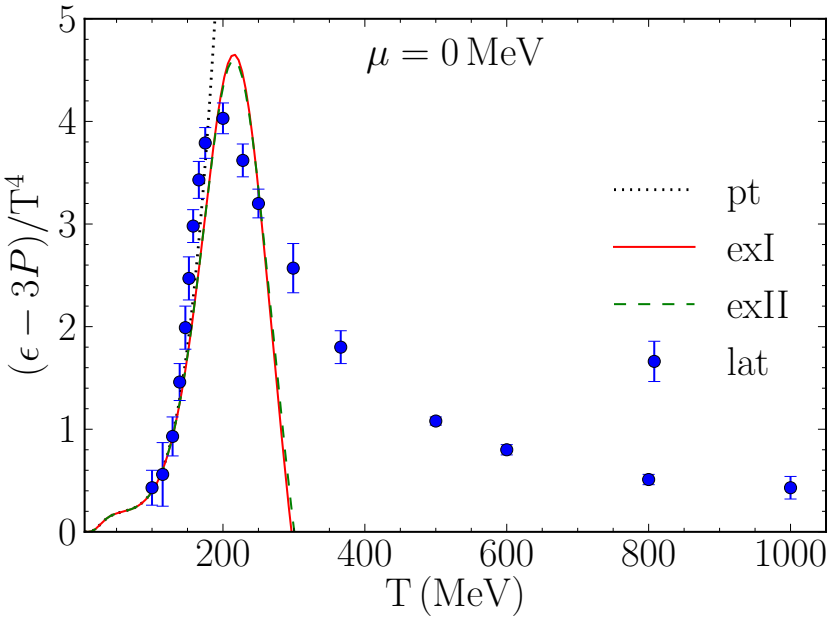

Figure 2.2: Trace anomaly normalized by T^4 for the three hadronic models. The point model (pt) is parameter-free while the excluded volume models exI and exII were fit to lattice results from Ref. [56].

$$h_2 = -\frac{15}{4}\left[1+\frac{N_f}{12}\left(5+72\hat{\mu}_q^2+144\hat{\mu}_q^4\right)\right] \tag{2.38}$$

$$h_3 = 30\left[1+\frac{N_f}{6}\left(1+12\hat{\mu}_q^2\right)\right]^{3/2} \tag{2.39}$$

$$\begin{aligned} h_4 &= 237.223+\left(15.963+124.773\ \hat{\mu}_q^2-319.849\hat{\mu}_q^4\right)N_f \\ &- \left(0.415+15.926\ \hat{\mu}_q^2+106.719\ \hat{\mu}_q^4\right)N_f^2 \\ &+ \frac{135}{2}\left[1+\frac{N_f}{6}\left(1+12\hat{\mu}_q^2\right)\right]\ln\left[\left(\frac{\alpha_s}{\pi}\right)\left(1+\frac{N_f}{6}\left(1+12\hat{\mu}_q^2\right)\right)\right] \\ &- \frac{165}{8}\left[1+\frac{N_f}{12}\left(5+72\hat{\mu}_q^2+144\hat{\mu}_q^4\right)\right]\left(1-\frac{2N_f}{33}\right)\ln\hat{M} \end{aligned} \tag{2.40}$$

$$\begin{aligned} h_5 &= -\sqrt{1+\frac{N_f}{6}\left(1+12\hat{\mu}_q^2\right)}\Bigg[799.149+\left(21.963-136.33\ \hat{\mu}_q^2+482.171\ \hat{\mu}_q^4\right)N_f \\ &+ \left(1.926+2.0749\ \hat{\mu}_q^2-172.07\ \hat{\mu}_q^4\right)N_f^2\Bigg] \\ &+ \frac{495}{12}\left(6+N_f(1+12\hat{\mu}_q^2)\right)\left(1-\frac{2N_f}{33}\right)\ln\hat{M} \end{aligned} \tag{2.41}$$

$$\begin{aligned} h_6 &= -\Bigg[659.175+\left(65.888-341.489\ \hat{\mu}_q^2+1446.514\ \hat{\mu}_q^4\right)N_f \\ &+ \left(7.653+16.225\ \hat{\mu}_q^2-516.210\ \hat{\mu}_q^4\right)N_f^2 \\ &- \frac{1485}{2}\left(1+\frac{1+12\hat{\mu}_q^2}{6}N_f\right)\left(1-\frac{2N_f}{33}\right)\ln\hat{M}\Bigg]\ln\left[\left(\frac{\alpha_s}{\pi}\right)\left(1+\frac{N_f}{6}(1+12\hat{\mu}_q^2)\right)4\pi^2\right] \\ &- 475.587\ln\left[\left(\frac{\alpha_s}{\pi}\right)4\pi^2 C_A\right]. \end{aligned} \tag{2.42}$$

For QCD we have $N_c = 3$, $C_A = 3$, and we take $N_f = 3$. The M is the renormalization scale which we will discuss shortly. If μ is the baryon chemical potential then $\mu_q = \mu/3$ is the quark chemical potential. The hat denotes division by $2\pi T$ so that $\hat{\mu}_q = \mu_q/(2\pi T)$ and $\hat{M} = M/(2\pi T)$. We use the 3-loop coupling constant from the Particle Data Group (PDG) [59] (we drop the b_3 term)

$$\begin{aligned} \alpha_s &= \frac{1}{b_0 t}\Bigg[1-\frac{b_1}{b_0^2}\frac{\ln t}{t}+\frac{b_1^2(\ln^2 t-\ln t-1)+b_0 b_2}{b_0^4 t^2} \\ &\quad -\frac{b_1^3(\ln^3 t-\frac{5}{2}\ln^2 t-2\ln t+\frac{1}{2})+3b_0 b_1 b_2\ln t}{b_0^6 t^3}\Bigg], \end{aligned} \tag{2.43}$$

where

$$b_0 = \frac{33 - 2N_f}{12\pi}$$
$$b_1 = \frac{153 - 19N_f}{24\pi^2}$$
$$b_2 = \frac{1}{128\pi^3}\left(2857 - \frac{5033}{9}N_f + \frac{325}{27}N_f^2\right) . \tag{2.44}$$

We will define the variable t shortly.

There are several issues with obtaining accurate numerical results. First, it was observed early on that the series (2.36) in α_s is oscillatory, so that at non-asymptotic temperatures the results depend to some degree on where the series is terminated. Second, one has some freedom in choosing the renormalization scale M for α_s. In Ref. [60] it was suggested to choose M^2 roughly equal to the average three-momentum of the quarks and gluons. For massless particles with quark chemical potential $\mu_q = \mu/3 = 0$, one finds $M \approx 3T$, the exact coefficient depending on whether they are bosons or fermions. For massless particles with $T = 0$, one finds $M \approx \mu_q$. Another commonly used argument for the choice of scale is that $M = \pi T$ since that is the smallest Matsubara frequency. We shall choose

$$M = C_M\sqrt{(\pi T)^2 + \mu_q^2} \tag{2.45}$$

and adjust the coefficient C_M to best represent the lattice results. What is important here is the relative proportion of T and μ_q, which is chosen on the basis of the above arguments.

The quantity labeled by t which enters into the solution of the 3-loop beta function for the running coupling (2.43) would usually be taken to be $t = \ln(M^2/\Lambda^2_{\overline{MS}})$. This results in a divergence of the running α_s at small but finite values of the temperature and chemical potential—the famous Landau pole—which causes unphysical behavior in the pressure at small temperatures and chemical potentials. In reality one would expect α_s to remain finite even at zero energy scale, although its value is most likely gauge-dependent. To address, this problem we choose

$$t = \ln\left(C_S^2 + M^2/\Lambda^2_{\overline{MS}}\right) , \tag{2.46}$$

where C_S is a constant used to eliminate the Landau pole; it will be adjusted to represent best the lattice results. The introduction of this constant does not change the

behavior of the perturbative expansion at asymptotically high temperatures because the applicability of perturbation theory is predicated on the assumption that $M \gg \Lambda_{\overline{MS}}$. The elimination of the Landau pole is crucial to obtaining a smooth crossover from one phase to the other, as we will see later. An alternative would be to take the running coupling from lattice QCD calculations, but we do not pursue that here. We recover the equation of state of Ref. [58] when $C_S = 0$, and take $\Lambda_{\overline{MS}} = 290$ MeV as in that paper.

It is straightforward to compute the other thermodynamic quantities like the energy, entropy, and baryon densities from derivatives of pressure (2.36) with respect to temperature and baryon chemical potential. Due to the complexity of Eq. (2.36), there are no convenient analytic formulas, so we simply evaluate these derivatives numerically with finite difference formulas.

We next compare the perturbative QCD result with lattice QCD and the point hadron model. Fig. 2.3 shows the pressure divided by T^4. The point hadron resonance gas represents the lattice result very well up to about $T = 200$ MeV and then greatly exceeds them. If we had included a full exponential spectrum of hadronic states, with level density proportional to $\exp(m/T_H)$ where $T_H = 160$ MeV is the Hagedorn temperature, the pressure would either end at a finite value or diverge at T_H, depending on the pre-exponential factor. This does not happen here because we include a very large but still finite number of hadronic states. The perturbative QCD result represents the lattice result very well down to a temperature of about 200 MeV. It appears from this figure that doing a little matching between the two limiting forms of the pressure in the vicinity of 200 MeV would achieve our goal.

Fig. 2.4 shows the trace anomaly $(\epsilon - 3P)/T^4$. The hadron resonance gas represents the lattice result very well up to a temperature of about 150 MeV and then greatly exceeds it. This is due to an increasing number of massive hadronic states with increasing temperature, massively diverging from a free massless gas which has $\epsilon = 3P$. The perturbative QCD result represents the lattice result very well down to a temperature of about 220 MeV. It also massively deviates at lower temperature because the renormalization group running coupling is becoming large, reflecting the intrinsic QCD scale $\Lambda_{\overline{MS}}$. Between these two limiting contributions there is a cusp around 190 MeV.

The perturbative QCD parameters were chosen by doing a chi-squared combined

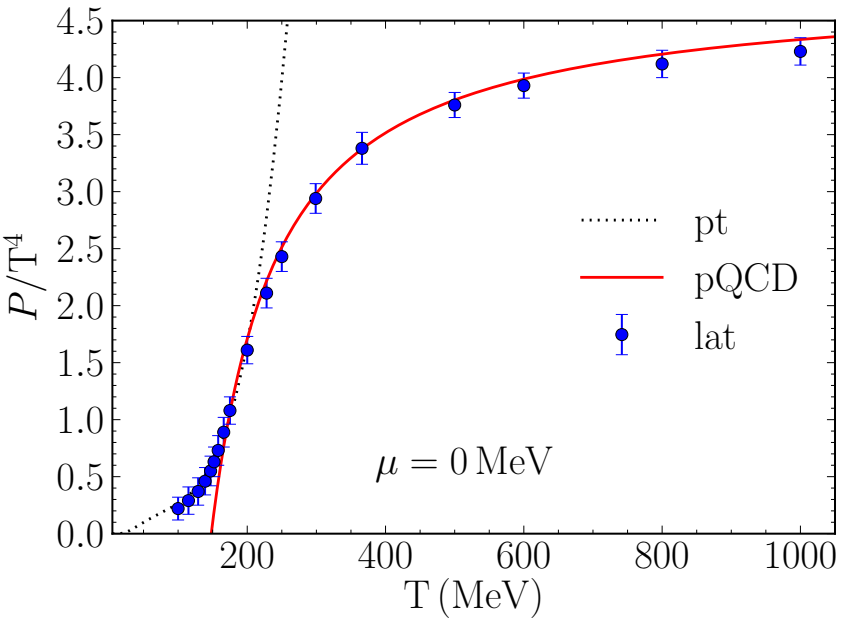

Figure 2.3: Pressure normalized by T^4. The dotted curve represents the parameter-free, point particle hadron resonance gas. The solid curve represents perturbative QCD with 2 parameters adjusted to fit the lattice result taken from Ref. [56].

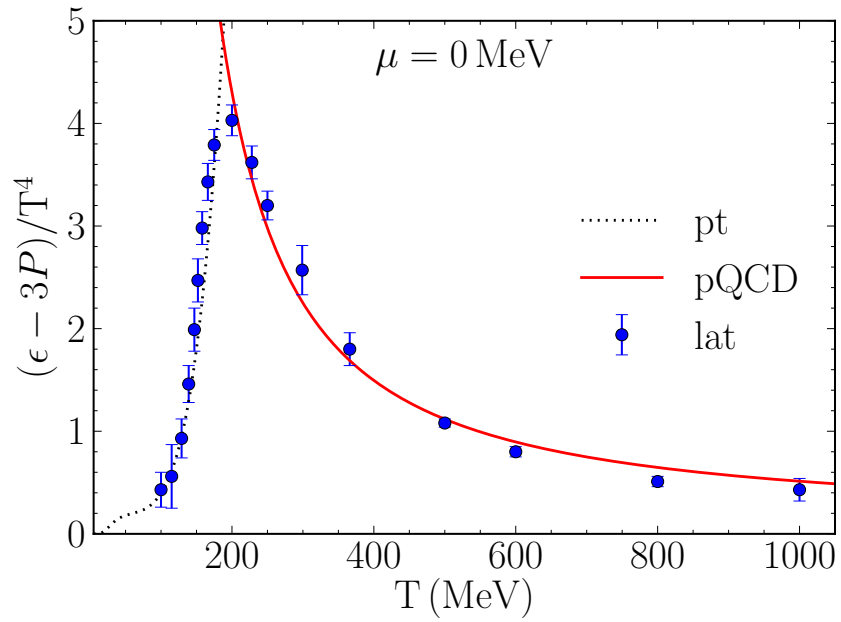

Figure 2.4: Trace anomaly normalized by T^4. The dotted curve represents the parameter-free, point particle hadron resonance gas. The solid curve represents perturbative QCD with 2 parameters adjusted to fit the lattice result taken from Ref. [56].

fit to the pressure and the trace anomaly for $T > 200$ MeV. For definiteness we fixed $\Lambda_{\overline{MS}} = 290$ MeV, but it should be noted that the choice is irrelevant since the value of C_M can be adjusted accordingly. The result of the fit is $C_M = 3.293$ and $C_S = 1.509$ with a chi-squared per degree of freedom of 1.397. This value of C_M is in the range usually considered, namely, $1 \leq C_M \leq 4$ [57, 58].

It would appear from these results that one could just terminate the hadron resonance gas contribution somewhat below 200 MeV and the perturbative QCD contribution somewhat above, and find an interpolating function to fill in the middle. The problem is that eventually one will find that some n'th order derivative of P with respect to T will become discontinuous at each of the matching points, leading to a phase transition of order n. This is unacceptable. We tried various matching functions, arguing that if n is large enough it would have no practical effects for use in modeling heavy-ion collisions, but we did not succeed. In addition, one would have to do this interpolation as a function of μ, and the equation of state for arbitrary T and μ is not known from lattice calculations.

2.5 Switching from Hadrons to Quarks and Gluons

In this section we study the problem of a smooth switching from a purely hadronic equation of state at low temperatures to a purely quark-gluon equation of state at high temperatures. We will introduce a thermodynamic switching function to accomplish this. We will also deduce best-fit values for ϵ_0 in the two excluded volume models, which is a physically interesting result in its own right.

The idea of a switching function has been used in atomic and molecular systems for a long time, usually with limited success. For example, it was found in [61], in the context of the properties of steam, that it is generally impossible to interpolate monotonically all thermodynamic functions over a range where a system has a transition from one phase to another. While it may be straightforward to make a switching function from a free energy $f_1(T)$ to $f_2(T)$, either its first or second derivative will deviate greatly from any kind of weighted average of the derivatives of f_1 and f_2 alone. Sometimes this is physical: in a first-order phase transition, the first derivative of the free energy $\partial f/\partial T$ is discontinuous at the transition temperature, corresponding to a discontinuous change

in heat capacity as well as a latent heat for the phase transition. However, lattice QCD calculations show no such discontinuities, at least for zero chemical potential, and the switching has to be done with great care.

We begin by constructing a pressure P which includes a hadronic piece P_h, a perturbative QCD piece P_{qg}, and a switching function S.

$$P(T,\mu) = S(T,\mu)P_{qg}(T,\mu) + [1 - S(T,\mu)]\, P_h(T,\mu) \tag{2.47}$$

Here P_h may be computed with any of the three hadronic models (pt, exI, exII). The switching function must approach zero at low temperatures and chemical potentials and approach one at high temperatures and chemical potentials. The switching function must also be very smooth to avoid introducing first, second, or higher-order phase transitions. We choose the following functional form

$$\begin{aligned} S(T,\mu) &= \exp\{-\theta(T,\,\mu)\} \\ \theta(T,\mu) &= \left[\left(\frac{T}{T_0}\right)^r + \left(\frac{\mu}{\mu_0}\right)^r\right]^{-1} \end{aligned} \tag{2.48}$$

with integer r. This function is infinitely differentiable, and goes to zero faster than any power of T as $T \to 0$ (when $\mu = 0$). It has three parameters. However, we will choose $\mu_0 = 3\pi T_0$. There are two reasons for this choice. First, it is consistent with Eq. (2.45). Second, the crossover region at $\mu = 0$ occurs around $T = 170$ MeV, whereas the crossover or phase transition is estimated to occur around $\mu = 1.25$ GeV when $T = 0$; see Ref. [62].

The other thermodynamic variables must be calculated from the pressure like before. We find

$$s = Ss_{qg} + (1 - S)\, s_h + \frac{r\theta^2}{T}\left(\frac{T}{T_0}\right)^r (P_{qg} - P_h)\, S \tag{2.49}$$

$$n = Sn_{qg} + (1 - S)\, n_h + \frac{r\theta^2}{\mu}\left(\frac{\mu}{\mu_0}\right)^r (P_{qg} - P_h)\, S \tag{2.50}$$

$$\epsilon = -P + Ts + \mu n\,. \tag{2.51}$$

Note that since we derived these quantities from the pressure using standard thermodynamics formulas, we ensure that the crossover models are thermodynamically self-consistent.

We now have two parameters in the switching function, two parameters in the perturbative QCD equation of state, and one parameter in the excluded volume equation of state (ϵ_0 not necessarily the same for both models). We now do a search on the parameters in each of the three models to obtain the best overall chi-squared fit to both the pressure and the trace anomaly. Quantum statistics are used for the hadronic piece of the equation of state. The results of the fit are shown in Figs. 2.5 and 2.6. The switching function is shown in Fig. 2.7, and the best-fit parameters are shown in Table 2.1.

	$\epsilon_0^{1/4}$ (MeV)	r	T_0 (MeV)	C_S	C_M	χ^2/dof
pt	NA	4	145.33	4.196	2.855	0.558
pt	NA	5	157.44	3.896	2.965	0.616
exI	306.50	5	177.12	4.281	3.352	0.342
exI	342.27	4	175.21	1.573	3.614	0.461
exII	279.71	5	177.65	4.325	3.351	0.343
exII	316.28	4	175.33	1.510	3.608	0.457

Table 2.1: First and second best-fit parameters for switching function equations of state built with pt, exI, and exII hadronic models. Fitting was done at $\mu = 0$ with lattice data from Ref. [56]. The last column gives each fit's χ^2 per degree of freedom.

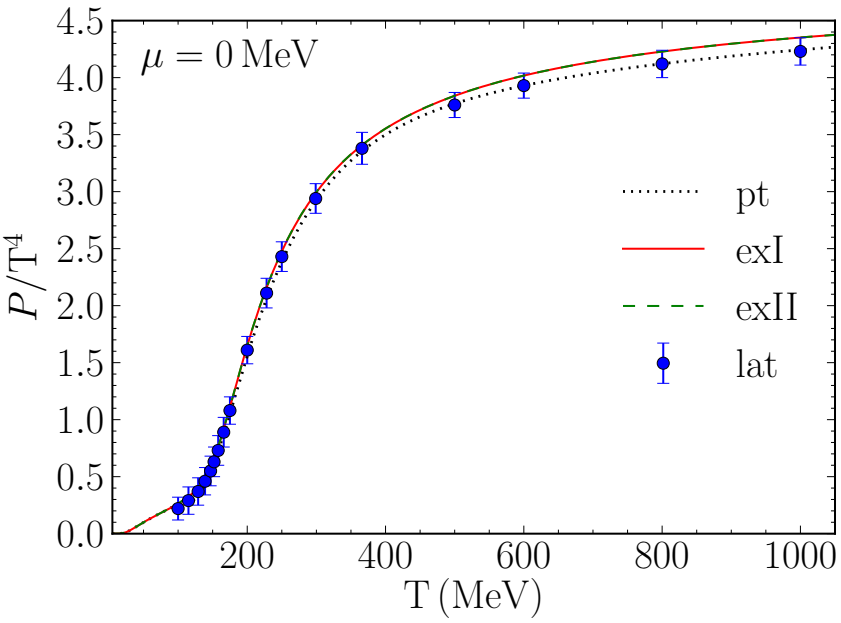

Figure 2.5: Pressure of crossover models using those parameters from Table 2.1 that minimize the χ^2 per degree of freedom. Lattice data is from Ref. [56].

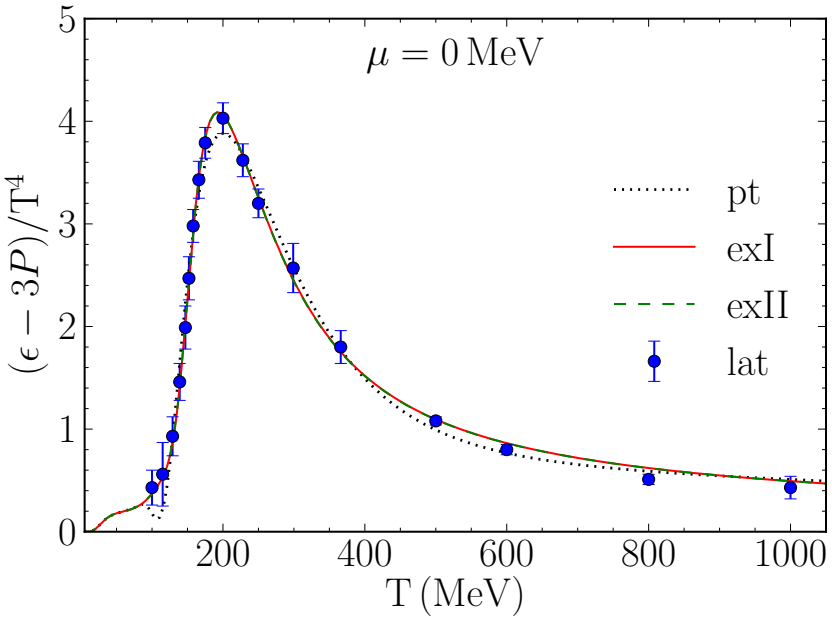

Figure 2.6: Trace anomaly of crossover models using those parameters from Table 2.1 that minimize the χ^2 per degree of freedom. Lattice data is from Ref. [56].

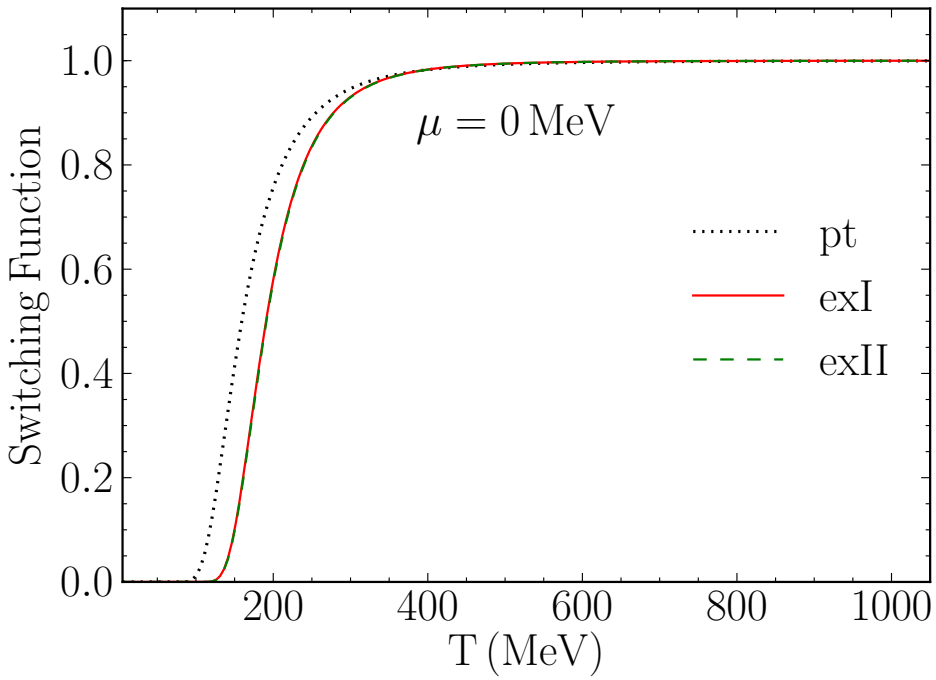

Figure 2.7: Switching function.

Some points to remark on follow.

(a) There is essentially no noticeable difference between the model I and model II curves. The only physical difference between these models is whether the volume excluded by a hadron is proportional to its total energy or to its mass. At low temperatures, the particle number density is so low that the excluded volumes do not matter, and both model I and II reduce to the point particle model.

(b) In excluded volume model I, ϵ_0 is the limiting energy density as T becomes large while the pressure increases linearly with T. In model II, both the energy density and the pressure grow slightly faster than T. Hence $P_h/T^4 \sim 1/T^3$ at high temperature. When multiplied by $1 - S$ the hadrons contribute much less than the quarks and gluons, which behave approximately as $P_{qg}/T^4 \sim$ constant.

(c) The best fit for model I is obtained with $\epsilon_0 = 1.149$ GeV/fm^3 and for model II it is $\epsilon_0 = 797$ MeV/fm^3. These can be used to infer the hard core radius of the proton or neutron to be 0.580 fm for model I and 0.655 fm for model II, very sensible numbers.

(d) For the point hadron gas model the best fit is obtained with $r = 4$ while the second best fit is obtained with $r = 5$. For the excluded volume models it is just the opposite. However, the difference in the chi-squared between those two values of r is very small.

(e) The value of T_0 for the point hadron gas is about 30 MeV smaller than for the excluded volume models. Thus the switching from hadrons to quarks and gluons occurs at a lower temperature. The reason is that P_h for the point hadron model grows much faster with T than for the excluded volume models; see Fig. 2.1 and point (b). That fast growth must be cut-off by the switching function. An unnatural consequence is that there is a minor dip in the trace anomaly near a temperature of 115 MeV.

2.6 Nonzero Chemical Potential

In Figs. 2.8 and 2.9, we compare the hadron (only) models with lattice results for $\mu = 400$ MeV. Similar to the case at $\mu = 0$, we see good agreement at $T < 150$ MeV for

all models, and excluded volume models perform better at higher temperatures.

Next, we compare the crossover models to lattice results for $\mu = 400$ MeV in Figs. 2.10 and 2.11. We see the crossover models perform much better than hadron (only) models. The two excluded volume crossover models agree very well with the lattice results. The crossover model with point hadrons does not agree as well. It should be emphasized that there are no free parameters in making these comparisons. All parameters were fixed already using lattice data at $\mu = 0$.

In Figs. 2.12 and 2.13 we show crossover model predictions for the larger value $\mu =$ 600 MeV. The difference between the two excluded volume crossover models continues to be insignificant, but now there are large—factor of 2—differences between them and the point hadron crossover model in the vicinity of $T = 150$ MeV.

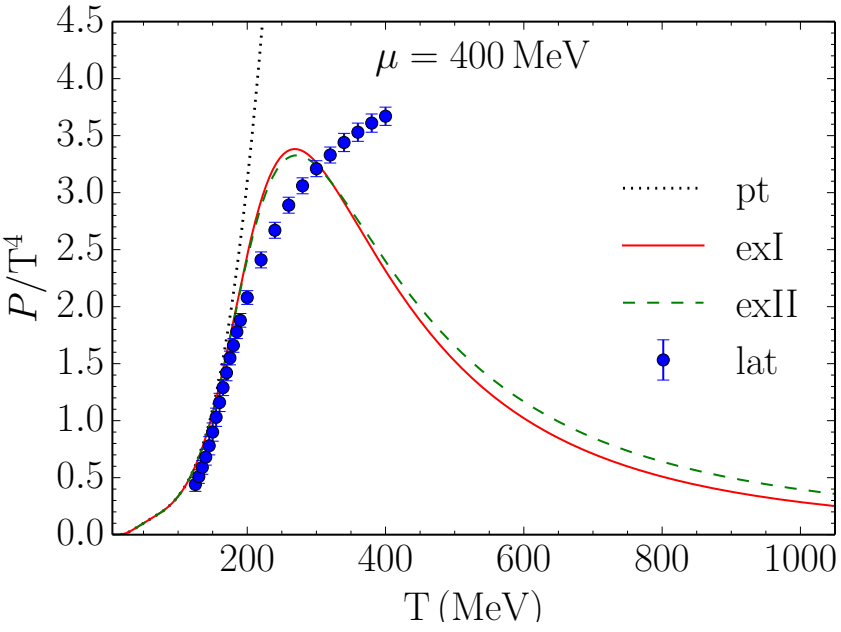

Figure 2.8: Pressure of hadron (only) models. Lattice data is from Ref. [63].

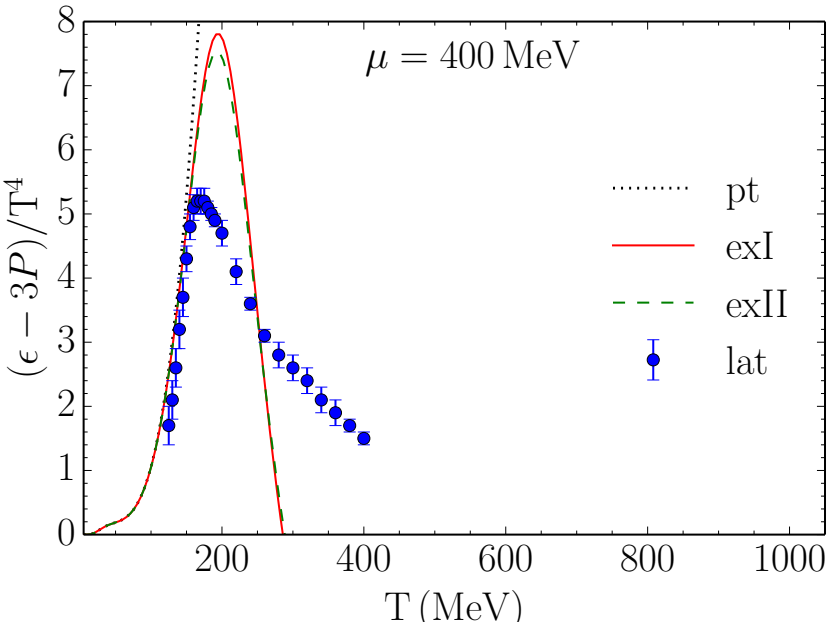

Figure 2.9: Trace anomaly of hadron (only) models. Lattice data is from Ref. [63].

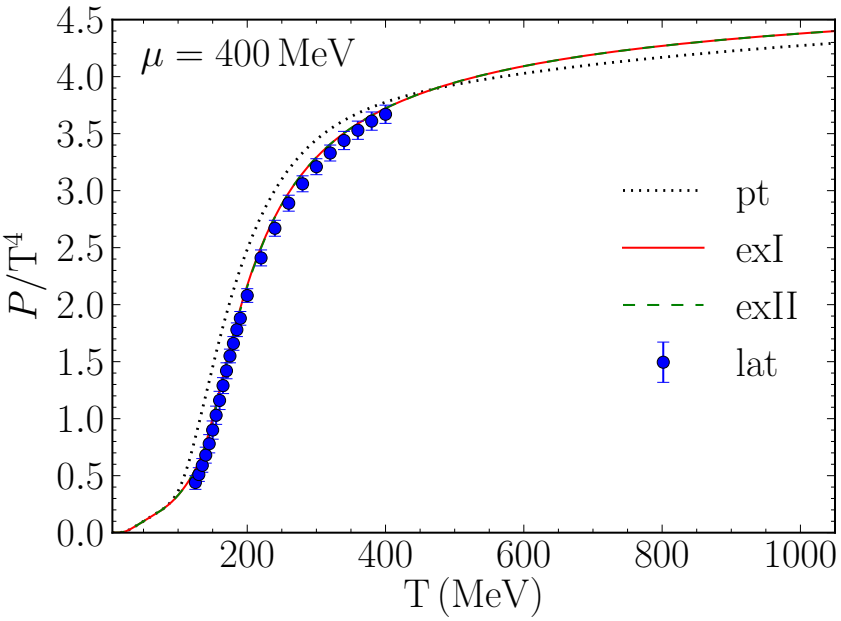

Figure 2.10: Pressure of crossover models. Lattice data is from Ref. [63].

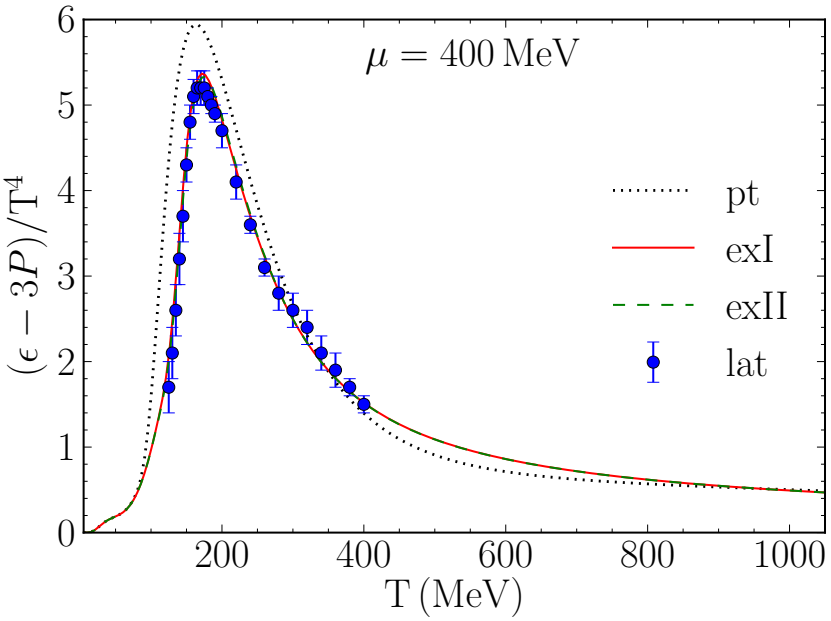

Figure 2.11: Trace anomaly of crossover models. Lattice data is from Ref. [63].

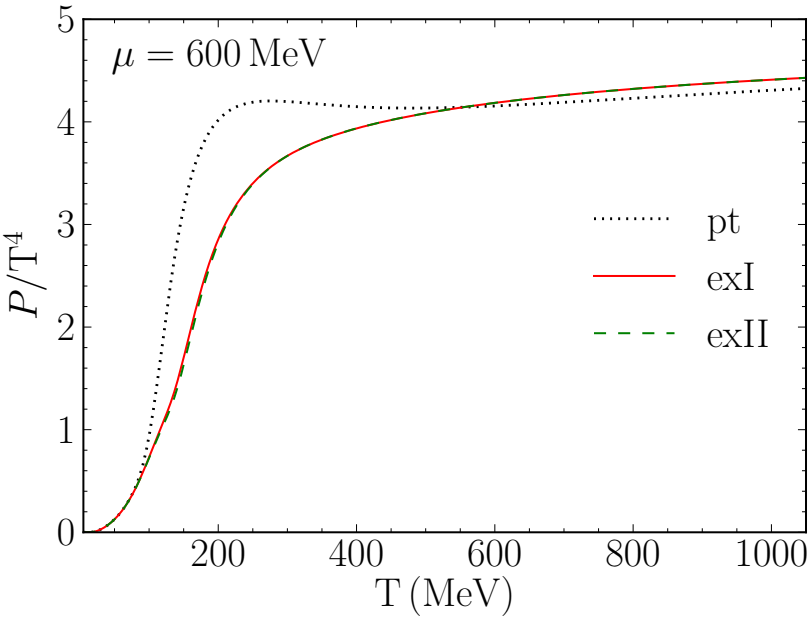

Figure 2.12: Pressure of crossover models.

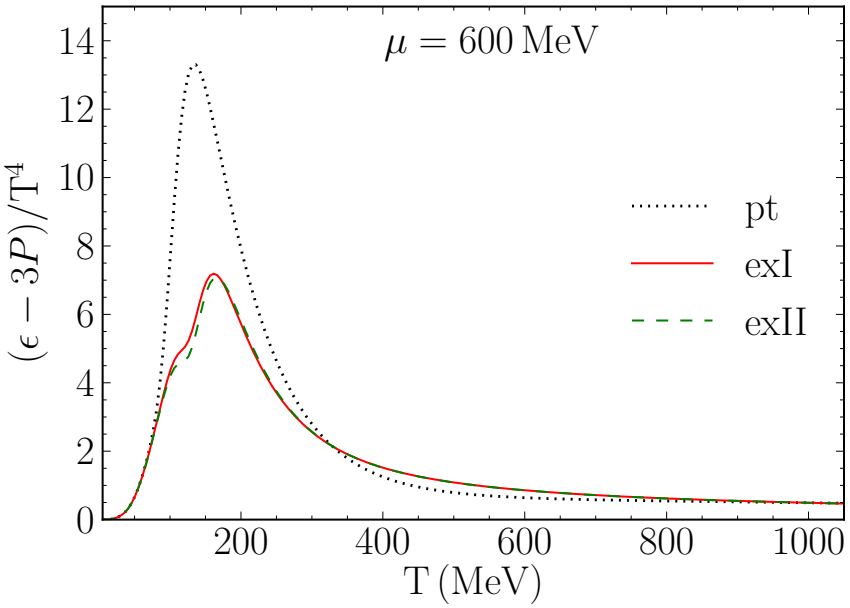

Figure 2.13: Trace anomaly of crossover models.

2.7 Conclusion

In this chapter, we matched three semi-realistic hadronic equations of state at low energy densities to a perturbatively computed equation of state of quarks and gluons at high energy densities. All three hadronic equations of state include all known hadronic resonances, which approximates attractive interactions among hadrons. The other two include, in addition, repulsive interactions in the form of excluded volumes occupied by hadrons of finite spatial extent. A switching function was employed to make the crossover transition from one phase to another without introducing a thermodynamic phase transition. A chi-squared fit to accurate lattice calculations at zero chemical potentials, with temperatures $100 < T < 1000$ MeV, fixes the various parameters in the models. These parameters quantify the behavior of the QCD running gauge coupling and the physical size of hadrons. Notably, the hard core radius of protons and neutrons turns out to be 0.62 ± 0.04 fm, a very sensible range that lends credence to the models.

The most physically reasonable models include the excluded volume effect. Not only do they include the effects of attractive and repulsive interactions among hadrons, but they also represent the lattice results the best. As pointed out by [61], it is very important to make the best possible approximation to the equation of state in two different phases when attempting to match them, especially when there is no true thermodynamic phase transition, but only a crossover.

The equations of state constructed in this chapter do not result in a phase transition, at least not for the temperatures and baryon chemical potentials investigated. It might be possible to introduce a thermodynamic phase transition with a different form of switching function, one that has some singularities built into it. It remains to be seen how well these equations of state will represent experimental data on high energy heavy-ion collisions when implemented in hydrodynamic simulations.

Chapter 3

Fluctuations and Freeze-Out

In this chapter, we use the equations of state developed in Chapter 2 to investigate the speed of sound and the baryon number fluctuations of QCD matter at finite temperatures and baryon chemical potentials. The speed of sound is important because its prediction is needed to build next-generation hydrodynamic simulations—for example, it dictates the velocity at which disturbances propagate through the fluid. Baryon number fluctuations are interesting because they could be used to locate the critical point, which should induce large critical fluctuations. We compare fluctuations predicted from our models (which do not contain a critical point) to data from the STAR Collaboration; there is good agreement between the models and data, so we find no clear signature of critical fluctuations.

3.1 Introduction

In Chapter 1, we discussed the motivation for the beam energy scan at the Relativistic Heavy Ion Collider (RHIC), which is to search for a critical end point in the QCD phase diagram. This is also a goal for the Facility for Antiproton and Ion Research (FAIR) which is currently under construction in Germany. Various models and theoretical arguments suggest that there is a curve in the plane of temperature T versus baryon chemical potential μ representing a line of first-order phase transitions. This curve is expected to terminate in a second-order phase transition at some critical T_c and μ_c. There is no agreement on the numerical values, but the expectation is that T_c is less

than 160 MeV and μ_c is greater than a few hundred MeV. (For reviews, see Refs. [16] and [17].) More generally, one would like to create matter in heavy-ion collisions with moderate temperatures and high baryon densities to study the type of matter that exists in proto-neutron and neutron stars. The challenge is entropy. One needs high enough collision energies to create matter at high energy density, but the collision energies cannot be too high because the entropy per baryon also increases with collision energy and that means high temperatures and low chemical potentials.

Recently, the STAR Collaboration at RHIC has reported measurements of the moments of net-proton (proton minus antiproton) multiplicity distributions in Au-Au collisions during the first beam energy scan [33]. These moments have been proposed as good observables for critical behavior [64, 65, 66]. The measurements were performed at beam energies $\sqrt{s_{NN}}$ = 7.7, 11.5, 19.6, 27, 39, 62.4, and 200 GeV per nucleon pair. This is remarkable as the two lowest energies are below the injection energy of 19.6 GeV. Here we focus on the most central collisions which are in the range 0-5%.

In Chapter 2, we constructed several equations of state which smoothly interpolate between a hadron resonance gas with excluded volumes to a perturbative QCD plasma of quarks and gluons as the temperature and/or chemical potential is raised. The handful of parameters were adjusted to reproduce the pressure and interaction measure (also called trace anomaly) calculated with lattice QCD for T between 100 and 1000 MeV with $\mu = 0$. With no further free parameters the crossover equation(s) of state represented the lattice results at $\mu = 400$ MeV just as well. In this chapter we compare the third and fourth moments of the baryon distribution from these crossover equations of state to the STAR data. Fukushima [67] made a similar comparison using a point particle hadron resonance gas and a relativistic mean field model with vector and scalar interactions. Borsányi *et al.* [68] compared their lattice QCD results to the second moments at $\sqrt{s_{NN}}$ = 27, 39, 62.4, and 200 GeV and to the third moment obtained by averaging over these energies.

The outline of this chapter is as follows. In Sec. 3.2 we briefly review the equations of state used here. We also compare them to each other and to lattice QCD calculations of the sound speed as a function of temperature, both for $\mu = 0$ and $\mu = 400$ MeV. We make similar comparisons for the susceptibility and for the fourth moment, or kurtosis, for $\mu = 0$ in Sec. 3.3. In Sec. 3.4 we make comparisons to the STAR data assuming

that the fluctuations are determined at the time of average chemical freeze-out. In order to represent the STAR data better, in Sec. 3.5 we consider the possibility that the fluctuations are determined significantly after the average chemical freeze-out. Our conclusions are contained in Sec. 3.6.

3.2 Speed of Sound

In Chapter 2, we constructed a pressure $P(T,\mu)$ which includes a hadronic piece P_h, a perturbative QCD piece P_{qg}, and a switching function S:

$$P(T,\mu) = S(T,\mu)P_{qg}(T,\mu) + [1 - S(T,\mu)]\, P_h(T,\mu) \tag{3.1}$$

The hadronic piece consists of a resonance gas comprising all the known hadrons as presented in the particle data tables [59]; an explicit list may be found in the Appendix A. In one case the hadrons were treated as point particles. We also used two excluded volume models for the resonance gas. For model I, the assumption is that the volume excluded by a hadron is proportional to its energy E with the constant of proportionality ϵ_0 (dimension of energy per unit volume) being the same for all species. For model II, the assumption is that the volume excluded by a hadron is proportional to its mass m. It is assumed in both models that hadrons are deformable so that there is no limitation by a packing factor as there would be for rigid spheres, for example. We refer to these three hadronic equations of state as pt, exI, and exII. Philosophically these excluded volume models are similar but the mathematics to compute their partition functions is rather different. Quantum statistics are used for the hadronic piece of the equation of state.

For the perturbative QCD piece we use the latest calculation which is valid up order $\alpha_s^3 \ln \alpha_s$ - see Eq. (2.36). This piece involves two parameters, both relating to the energy scale used in the renormalization group running coupling.

The $S(T,\mu)$ is a switching function which must approach zero at low temperatures and chemical potentials and approach one at high temperatures and chemical potentials. The switching function must also be infinitely differentiable to avoid introducing first-, second-, or higher-order phase transitions, which lattice QCD has shown are not present

at small values of μ. The following functional form was chosen:

$$\begin{aligned} S(T,\mu) &= \exp\{-\theta(T,\,\mu)\} \\ \theta(T,\mu) &= \left[\left(\frac{T}{T_0}\right)^r + \left(\frac{\mu}{3\pi T_0}\right)^r\right]^{-1} \end{aligned} \tag{3.2}$$

with integer r. This function goes to zero faster than any power of T as $T \to 0$ (when $\mu = 0$). It has two parameters, T_0 and r.

We now have two parameters in the switching function, two parameters in the perturbative QCD equation of state, and one parameter in the excluded volume equation of state (ϵ_0 not necessarily the same for both models). We did a search on the parameters in each of the three models to obtain the best overall chi-squared fit to both the pressure P/T^4 and the trace anomaly $(\epsilon - 3P)/T^4$ to the data in Ref. [56]. The best-fit parameters are listed in Table 2.1. From the table, we see that the value of T_0 for the point hadron gas is significantly smaller than for the excluded volume models, and so the switching from hadrons to quarks and gluons occurs at a lower temperature. The reason is that P_h for the point hadron model grows much faster with T than for the excluded volume models, and that fast growth must be cut off by the switching function. An unnatural consequence is that there is a minor dip in the trace anomaly near a temperature of 115 MeV in the point particle model. As we will describe shortly, this unphysical artifact causes the point crossover model to make unrealistic predictions for the speed of sound and baryon fluctuations which disagree with lattice QCD results.

Although we show some results with the point hadron resonance gas in what follows, it has a second fatal flaw when used as the hadronic piece in a crossover equation of state. If the point particle hadron resonance gas has a mass spectrum which grows exponentially like a Hagedorn gas, rather than with a large but finite number of hadronic resonances, then the hadronic piece has a pressure which either diverges or reaches a maximum at the Hagedorn temperature $T_H \approx 160$ MeV. Then the crossover or switching method of Eq. (3.1) fails to produce a smooth crossover. With the inclusion of excluded volumes for the hadrons this is not the case.

A more sensitive test of the agreement between the crossover models and lattice QCD is the speed of sound c_s given by $c_s^2 = \partial P/\partial\epsilon$, where the derivative is taken at

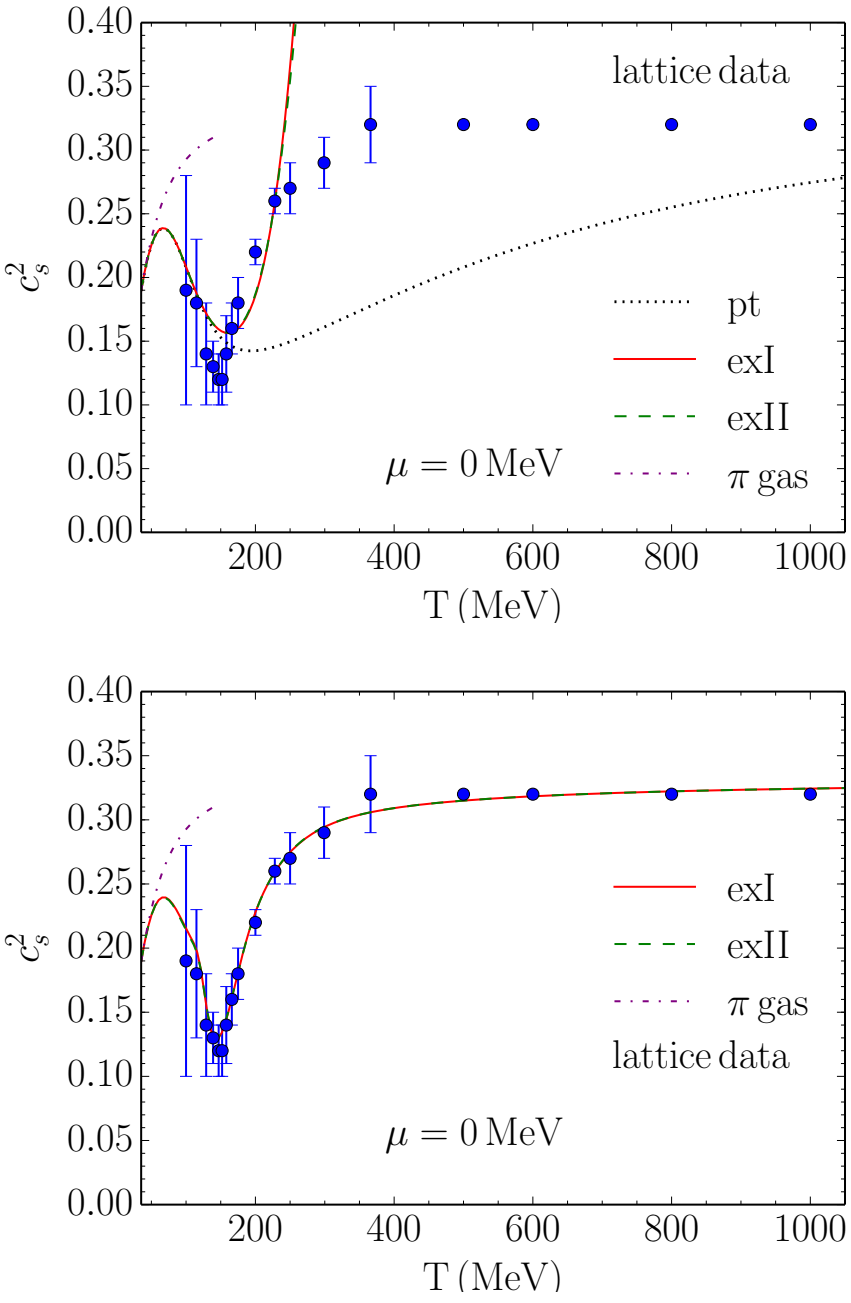

Figure 3.1: The square of the sound speed as a function of temperature for zero baryon chemical potential. The points are from lattice QCD [56]. The dashed line is for a noninteracting massive pion gas. The top panel shows the sound speed for hadronic resonance gases, including those for point hadrons and for the two excluded volume models. The bottom panel shows the full crossover equations of state.

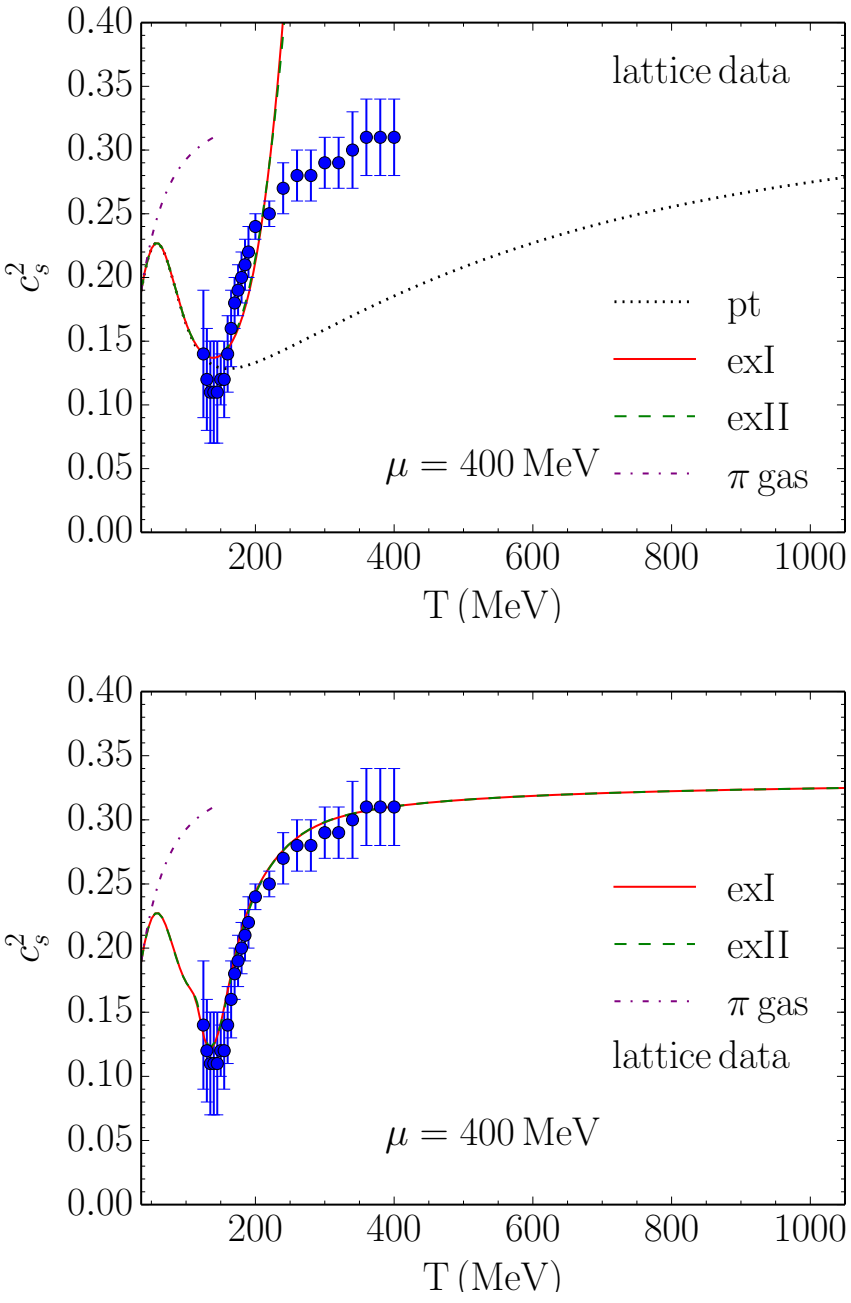

Figure 3.2: The square of the sound speed as a function of temperature for a baryon chemical potential of 400 MeV. The points are from lattice QCD [63]. The dashed line is for a noninteracting massive pion gas. The top panel shows the sound speed for hadronic resonance gases, including those for point hadrons and for the two excluded volume models. The bottom panel shows the full crossover equations of state.

constant entropy per baryon. In terms of the susceptibilities

$$\chi_{xy} = \frac{\partial^2 P(T,\mu)}{\partial x \partial y} \tag{3.3}$$

where x and y may be T or μ, it is

$$c_s^2 = \frac{n^2\chi_{TT} - 2sn\chi_{\mu T} + s^2\chi_{\mu\mu}}{w(\chi_{TT}\chi_{\mu\mu} - \chi_{\mu T}^2)} \,. \tag{3.4}$$

Note that n, s, and w are the baryon, entropy, and enthalpy densities, respectively. (See Appendix B for further details on the theory of sound.) Whereas the trace anomaly depends on first-order derivatives of the pressure, the sound speed depends also on second-order derivatives. A comparison to lattice QCD is shown in Fig. 3.1 for $\mu = 0$ [56] and in Fig. 3.2 for $\mu = 400$ MeV [63]. In both figures the top panel shows the hadronic piece only; in other words, set $S(T,\mu) = 0$. (It might be mentioned that the excluded volume parameter ϵ_0 was adjusted to try to give a better fit to the pressure and trace anomaly of lattice QCD.) The bottom panel shows the full crossover equation of state. The crossover equation of state using point hadrons has an unnatural temperature dependence around 115 MeV (see comment above) which causes unphysical behavior in the speed of sound, so we do not show it in these figures. In both panels the dashed curve shows the sound speed for a massive noninteracting pion gas, which is the natural limit as the temperature goes to zero. The hadronic piece only gives a qualitative representation of the lattice data, where the full crossover equation of state reproduces it very well.

It is possible to switch smoothly between the excluded volume and the perturbative QCD equations of state thanks to the existence of a region of overlap where both equations of state match the lattice data. Ultimately, the switching is possible not because of the choice of $S(T,\mu)$, but by the improved description of the physics of hadronic gas, making it accurate to higher temperatures.

3.3 Susceptibility, Skewness and Kurtosis

Let Q represent some conserved charge (in this work we focus on the net baryon number.) In an ensemble of events, Q will have a mean value M and a variance σ^2. In equilibrium,

these quantities may be computed from the grand canonical partition function Z, which can be written very generally as a sum over quantum states s as

$$Z = \sum_s e^{-\beta(E_s - Q_s\mu)} \,. \tag{3.5}$$

For example, the first two moments of charge are

$$M = \langle Q \rangle = (Z)^{-1} \sum_s Q_s e^{-\beta(E_s - Q_s\mu)} = T \frac{\partial}{\partial \mu} \ln Z \,, \tag{3.6}$$

$$\left\langle Q^2 \right\rangle = (Z)^{-1} \sum_s Q_s^2 e^{-\beta(E_s - Q_s\mu)} = T^2 (Z)^{-1} \frac{\partial^2}{\partial \mu^2} Z \,. \tag{3.7}$$

Writing the fluctuation as $\delta Q = Q - M$, we can compute the variance as

$$\sigma^2 = \left\langle \delta Q^2 \right\rangle = \left\langle Q^2 \right\rangle - M^2 = T^2 \frac{\partial^2}{\partial \mu^2} \ln Z \,. \tag{3.8}$$

In equilibrium, the partition function and pressure are related by the identity

$$P = \frac{T}{V} \ln Z \,, \tag{3.9}$$

where V is the volume of the system. Hence, in equilibrium M and σ^2 can be computed directly from derivatives of the pressure, which is convenient since both the hadronic models and crossover models predict the pressure. Recalling our definition of susceptibility from Eq. (3.3), we find

$$M = V \chi_\mu \tag{3.10}$$

and

$$\sigma^2 = VT \chi_{\mu\mu} \,. \tag{3.11}$$

It is convenient to take ratios such that the volume cancels:

$$\frac{\sigma^2}{M} = T \frac{\chi_{\mu\mu}}{\chi_\mu} \,. \tag{3.12}$$

The next higher moments are the skewness

$$S = \frac{\langle \delta Q^3 \rangle}{\sigma^3} \tag{3.13}$$

and kurtosis

$$\kappa = \frac{\langle \delta Q^4 \rangle}{\sigma^4} - 3 \,. \tag{3.14}$$

For a finite-size system, such as the matter formed in heavy-ion collisions, it is convenient and useful to consider the scaled skewness and kurtosis, which are intensive quantities. For a system in equilibrium they are

$$S\sigma = T\frac{\chi_{\mu\mu\mu}}{\chi_{\mu\mu}} \tag{3.15}$$

and

$$\kappa\sigma^2 = T^2\frac{\chi_{\mu\mu\mu\mu}}{\chi_{\mu\mu}}\,. \tag{3.16}$$

Again, these are easily evaluated for either the hadronic or crossover models since both sets of models predict the pressure. One general statement that can be made is $S\sigma = 0$ if the baryon chemical potential μ vanishes. The reason is that the pressure is an even function of the baryon chemical potential, hence all odd derivatives vanish when $\mu = 0$.

Consider a point particle hadron resonance gas. When Boltzmann statistics are adequate for the baryons, the pressure takes the form

$$P(T,\mu) = P_b(T)\cosh(\mu/T) + P_m(T)\,, \tag{3.17}$$

where $P_m(T)$ is the pressure contributed by the mesons, and $P_b(T)$ is the baryonic pressure when $\mu = 0$. Then $S\sigma = \tanh(\mu/T)$ and $\kappa\sigma^2 = 1$. This is a very strong prediction. For comparison, consider a noninteracting gas of massless quarks and gluons. The pressure takes the form

$$P(T,\mu) = a_0T^4 + a_2T^2\mu^2 + a_4\mu^4\,, \tag{3.18}$$

where a_0, a_2, and a_4 are constants. Then $S\sigma = 12a_4\mu T/(a_2T^2 + 6a_4\mu^2)$ and $\kappa\sigma^2 = 12a_4T^2/(a_2T^2 + 6a_4\mu^2)$. The dependence on the ratio μ/T is very different for these two equations of state.

The kurtosis has been computed by lattice QCD [69] and the results are shown in Fig. 3.3 (the skewness is obviously zero.) The top panel shows a comparison to the point hadron resonance gas and the two excluded volume hadron resonance gases. The kurtosis for the point particle hadron resonance gas is essentially 1, but deviates very slightly with increasing temperature due to quantum statistics. The kurtosis for the excluded hadron resonance gas does decrease significantly with temperature, but it does not quantitatively reflect the lattice QCD kurtosis. Also shown in the top panel is the

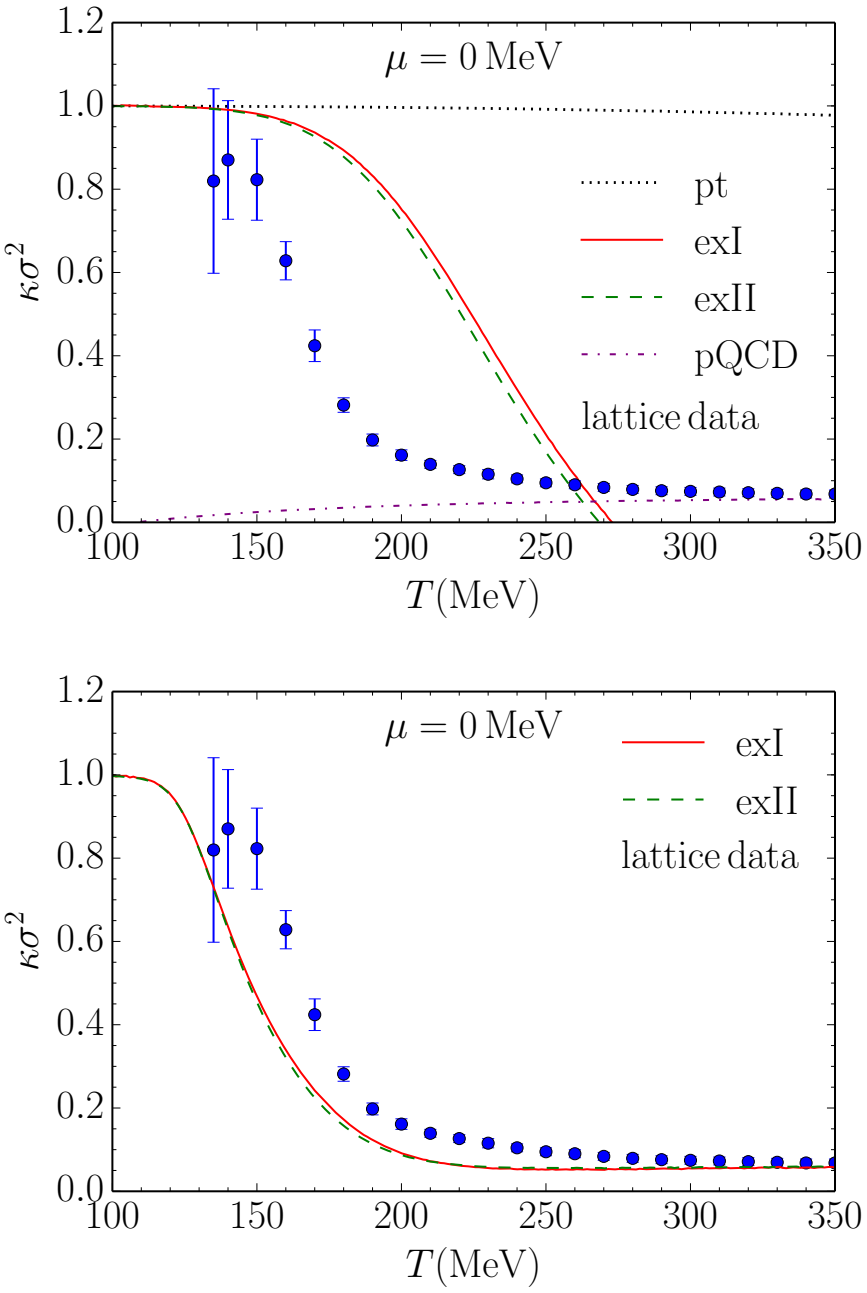

Figure 3.3: The kurtosis as a function of temperature for zero baryon chemical potential. The points are from lattice QCD [69]. The top panel shows the kurtosis for hadronic resonance gases, including those for point hadrons and for the two excluded volume models. It also shows the purely perturbative QCD result for quarks and gluons. The bottom panel shows the full crossover equations of state.

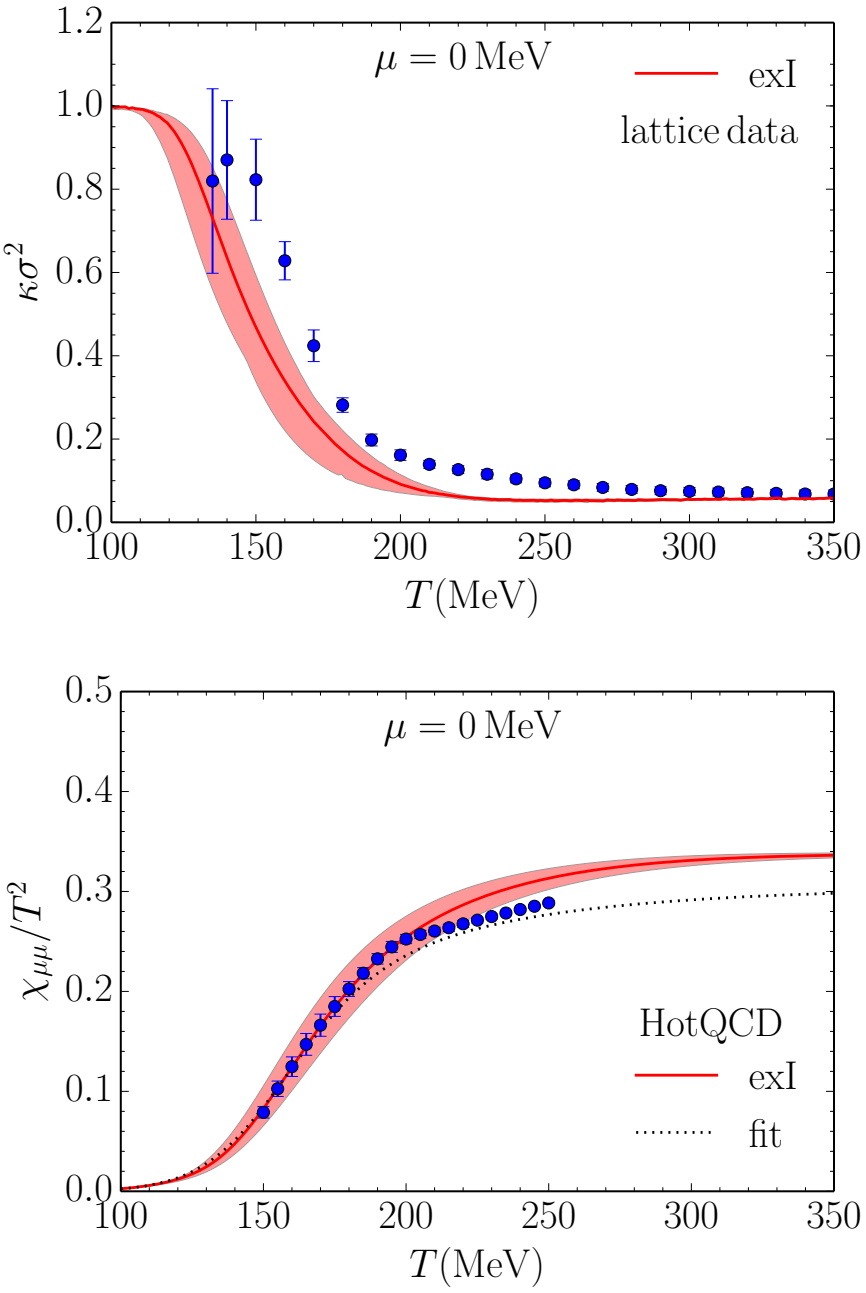

Figure 3.4: The top panel shows the kurtosis as a function of temperature for zero baryon chemical potential. The points are from lattice QCD [69]. The curve is the same as the crossover from the previous figure. The shaded region shows the uncertainty when fitting the crossover equation of state parameters to lattice QCD at zero chemical potential. The bottom panel shows the susceptibility as a function of temperature for zero baryon chemical potential. The dotted curve is the parameterization from the lattice calculations in Ref. [63] while the points are from the HotQCD Collaboration [70].

kurtosis from perturbative QCD. Deviation from a noninteracting gas of massless quarks and gluons is evident and is due to the running of the renormalization group coupling α_s with T and μ. Lattice QCD clearly shows the transition from a hadron resonance gas at low temperature to a plasma of quarks and gluons at high temperature. The bottom panel shows the comparison with the full crossover equations of state exI and exII. Qualitatively the agreement is very good, the crossover equations of state having the correct limits when T becomes small and when it becomes large. However, in the intermediate region between 150 and 300 MeV, the kurtosis from the crossover equations of state is too small compared to lattice QCD. This is due to the perturbative equation of state lying below the lattice data. While this deserves further exploration, it is most likely inconsequential for the following sections, where lower temperatures are relevant.

To see whether the discrepancy in the kurtosis can be resolved by the fitting procedure to the pressure and trace anomaly, we show the band of uncertainty in the crossover parameters in the top panel of Fig. 3.4. Clearly it cannot. Since the kurtosis involves the fourth derivative of the pressure with respect to chemical potential, it is a very sensitive measure of the equation of state. The discrepancy might be due to a slightly inaccurate parameterization of the crossover between hadrons and quarks and gluons, although the agreement with the pressure, trace anomaly, and sound speed at $\mu = 0$ and $\mu = 400$ MeV makes this problematic. In the bottom panel of Fig. 3.4 we show the susceptibility in comparison to two lattice calculations. The dotted curve is from Ref. [63], whereas here the data points come from the HotQCD Collaboration [70]. There is good agreement between the two lattice calculations. The crossover equation of state is also in good agreement at and below 200 MeV, which is what matters for comparison with the STAR heavy-ion data. At temperatures of 250–350 MeV the crossover equation of state gives a result too large, by about 10%, in comparison to lattice QCD. It should be pointed out that a free gas of massless quarks and gluons gives $\chi_{\mu\mu}/T^2 = 1/3$. It is easily shown that including a strange mass of order 100 MeV changes that value only about 0.1%.

3.4 Comparison to STAR Data: Chemical Freeze-Out

In this section, we compare to the data taken during the first beam energy scan at RHIC by the STAR Collaboration [33]. In order to make the comparison we need to have an estimate of the temperature and chemical potential at the time the fluctuations are frozen out. Following Fukushima [67] we use the conditions at the time of average chemical freeze-out as presented in Ref. [44]. The chemical potential is parameterized as a function of $\sqrt{s_{NN}}$ by

$$\mu(\sqrt{s_{NN}}) = \frac{d}{1 + e\sqrt{s_{NN}}} \tag{3.19}$$

and then the temperature by

$$T(\mu) = a - b\mu^2 - c\mu^4 \,. \tag{3.20}$$

The five constants in these parameterizations are $a = 0.166$ GeV, $b = 0.139$ GeV^{-1}, $c = 0.053$ GeV^{-3}, $d = 1.308$ GeV, and $e = 0.273$ GeV^{-1}.

In Fig. 3.5 we show the skewness as a function of beam energy. First, consider the top panel which displays the hadronic and perturbative QCD pieces only. The perturbative QCD piece is always small and goes to zero with increasing energy. The reason is that the chemical potential goes to zero with increasing energy, and the skewness vanishes for zero chemical potential as discussed in the previous section. The point particle hadron gas closely follows the formula $S\sigma = \tanh(\mu/T)$ with only a minor correction for quantum statistics. Qualitatively it follows the trend of the data. The two excluded volume models are similar but lie somewhat closer to the data. The bottom panel shows the skewness from the full crossover equations of state with the excluded volume approximations in the hadronic piece. (We do not show the crossover with point hadrons for the same reason as with the sound speed.) These lie significantly below the data and do far worse than the pure hadronic pieces only. Mathematically the reason for this is that the switching function is reducing the hadronic contribution and increasing the perturbative QCD contribution.

In Fig. 3.6 we show the kurtosis as a function of beam energy. The top and bottom panels display the same equations of state as in Fig. 3.5. The kurtosis for the point hadron resonance gas would be exactly 1 if classical statistics were used; it drops slightly below 1 at low energy due to the slight effect of quantum statistics. It cannot be said

to represent the data very well; certainly it does not have the dip that the data has at the 19.6 GeV beam energy. The pure hadronic excluded volume equations of state lie closer to the data but do not reproduce such a strong dip at the aforementioned energy.

As in the previous section, we show the band of uncertainty in the crossover parameters for exI in Fig. 3.7 for the skewness (top panel) and kurtosis (bottom panel). These uncertainties are not large enough to explain the STAR data. As a final check, we also plot the crossover model baryon number variance over the mean in Fig. 3.8. We again find poor agreement between the crossover model and the STAR data.

This leaves us with a puzzle. The crossover equations of state exI and exII do an excellent job of reproducing the pressure, the trace anomaly, and the sound speed as calculated with lattice QCD as a function of temperature between 100 and 1000 MeV and for a baryon chemical potential of 0 and 400 MeV. They also reproduce the lattice results relatively well for the kurtosis for zero chemical potential. Yet they do not adequately describe the STAR data as well as the purely hadronic equation of state, which does a much worse job of reproducing the lattice results. Why is that?

3.5 Comparison to STAR Data: Post-Chemical Freeze-Out

The lack of agreement between the crossover equations of state and the STAR data is significant. We have already compared the crossover equations of state with lattice QCD in detail previously, with very positive results. One possibility, which we explore here, is that the baryon fluctuations are not frozen out at the same time as average chemical freeze-out. Indeed, it is well known that kinetic freeze-out occurs after average chemical freeze-out when the temperature is lower [71, 72]. A hint in this direction is that both the skewness and kurtosis decrease with increasing temperature when the chemical potential is fixed. To get closer agreement with the STAR data, we ought to consider the possibility that the baryon fluctuations freeze-out occurs at lower temperatures than assumed earlier.

As an example, consider changing the parameter a in Eq. (3.20) from 166 to 140 MeV. Such a lower temperature is roughly consistent with kinetic freeze-out [71, 72]. The results are shown in Figs. 3.9 and 3.10 for the crossover equation of state exI (the results

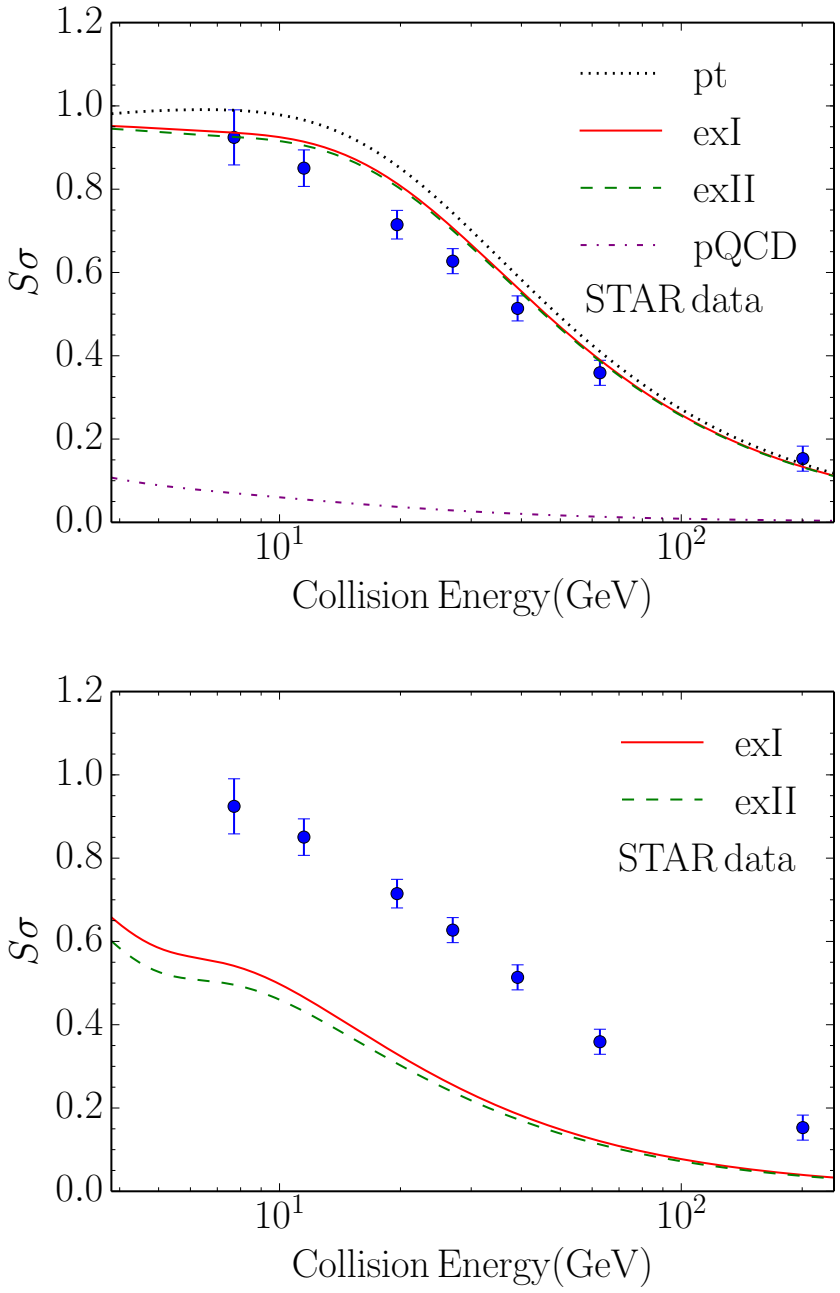

Figure 3.5: The skewness as a function of collision energy per nucleon pair. The points are from STAR measurements. The top panel shows the skewness for excluded volume hadronic resonance gases. It also shows the purely perturbative QCD result for quarks and gluons. The bottom panel shows the full crossover equations of state. The energy dependence of the temperature and chemical potential are determined by the conditions at average chemical freeze-out as in Eq. (3.20).

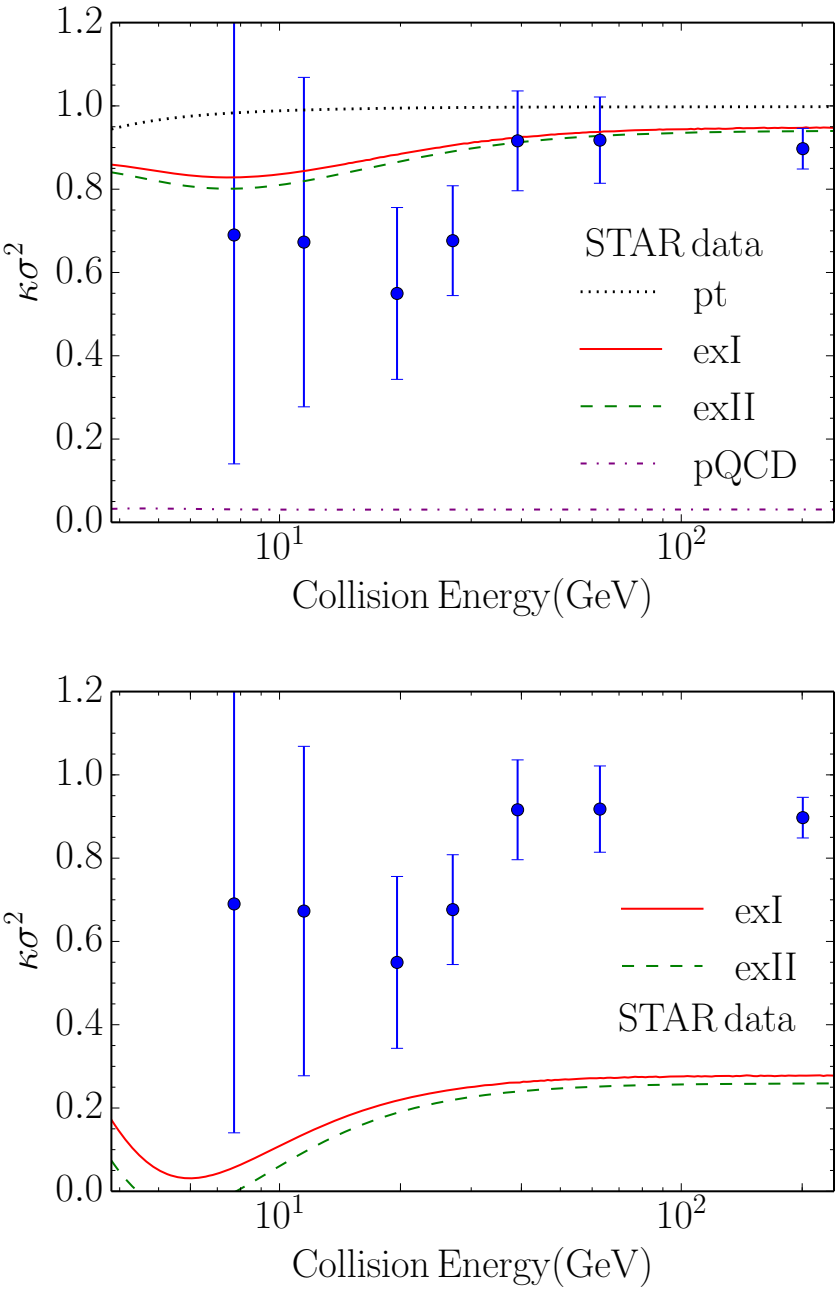

Figure 3.6: The kurtosis as a function of collision energy per nucleon pair. The points are from STAR measurements. The top panel shows the kurtosis for excluded volume hadronic resonance gases. It also shows the purely perturbative QCD result for quarks and gluons. The bottom panel shows the full crossover equations of state. The energy dependence of the temperature and chemical potential are determined by the conditions at average chemical freeze-out as in Eq. (3.20).

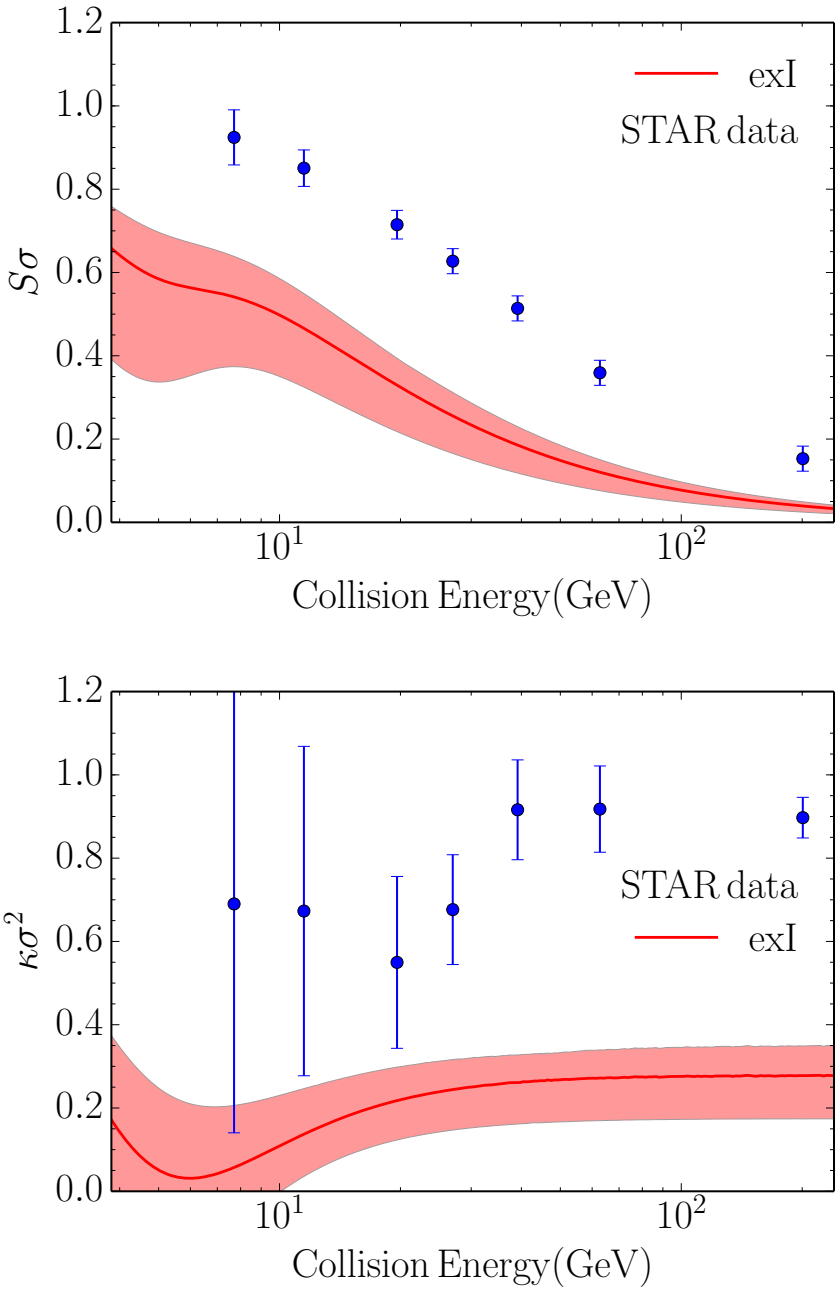

Figure 3.7: The skewness (top panel) and kurtosis (bottom panel) for the crossover model exI. The shaded region shows the uncertainty when fitting the crossover equation of state parameters to lattice QCD at zero chemical potential. The energy dependence of the temperature and chemical potential are determined by the conditions at average chemical freeze-out as in Eq. (3.20).

for exII are nearly identical). Now the agreement is quite acceptable. The exceptional points are the kurtoses at the three highest beam energies for which the theory is below the data. This may very well be associated with the fact that the kurtosis for the excluded volume crossover equations of state, at zero chemical potential, lie below the lattice results, as shown in Figs. 3.3 and 3.4.

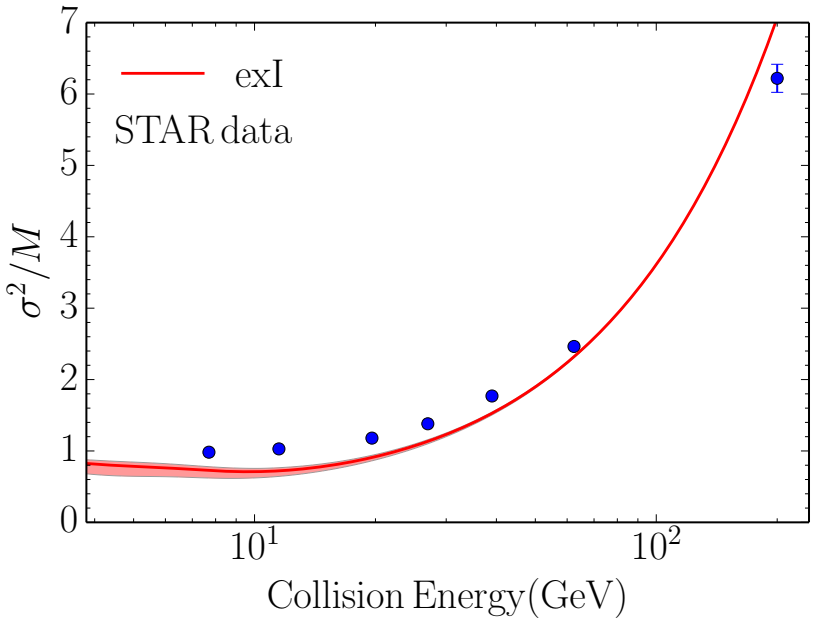

Figure 3.8: Ratio of variance to mean for the crossover equation of state compared to the measurements by the STAR Collaboration. The energy dependence of the temperature and chemical potential are determined by the conditions at average chemical freeze-out as in Eq. (3.20).

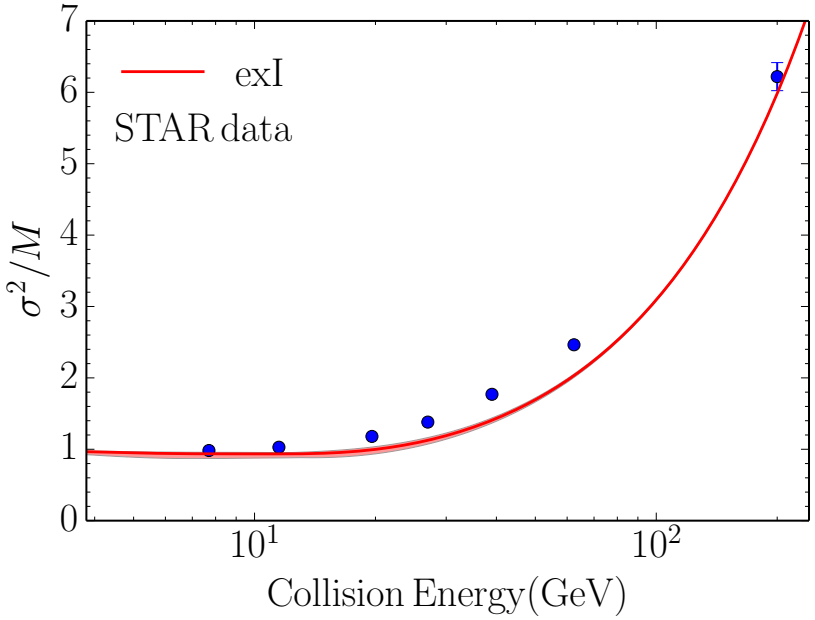

Figure 3.9: Ratio of variance to mean for the crossover equation of state compared to the measurements by the STAR Collaboration. The energy dependence of the temperature and chemical potential are determined as in Eq. (3.20) but with a temperature which is 26 MeV lower than in Figs. 3.5 to 3.8 ($a = 140$ MeV).

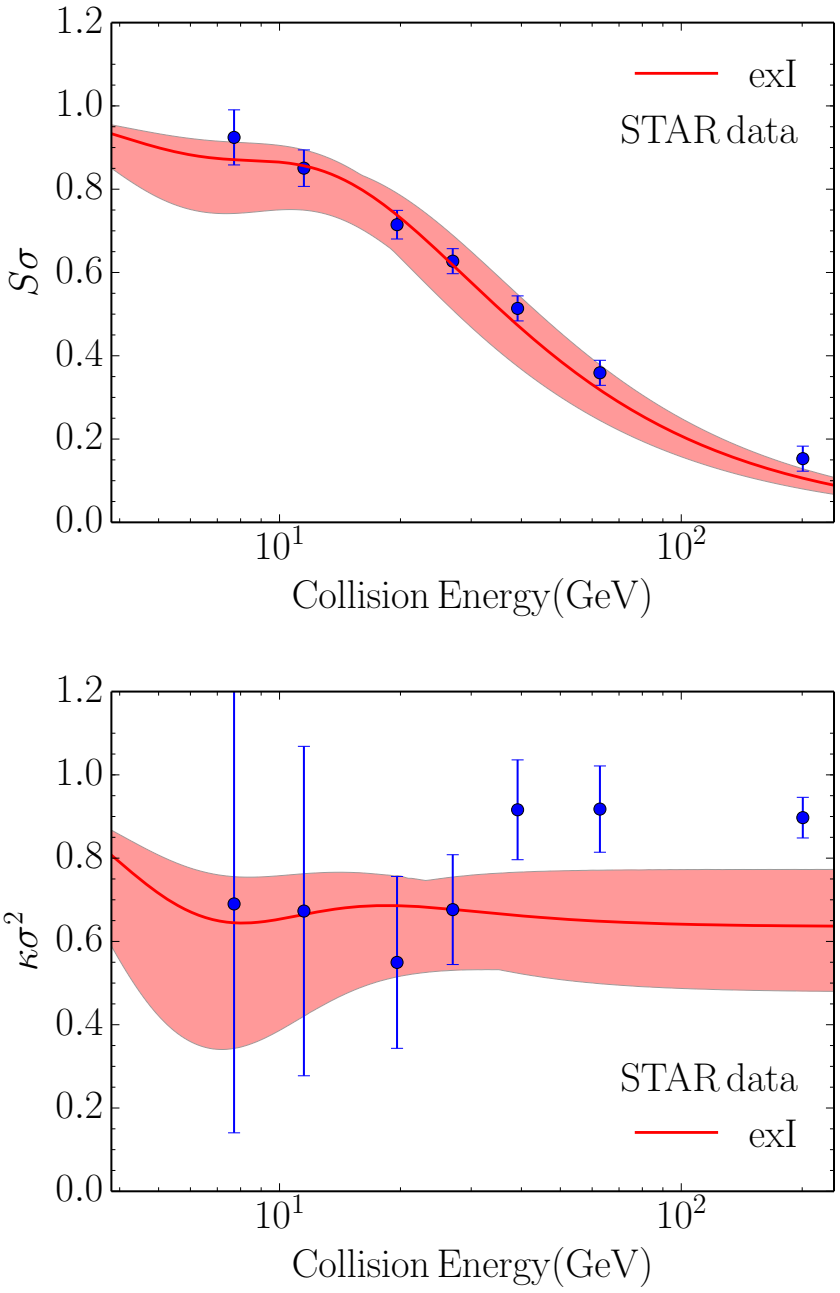

Figure 3.10: The skewness (top panel) and kurtosis (bottom panel) for the crossover model exI. The shaded region shows the uncertainty when fitting the crossover equation of state parameters to lattice QCD at zero chemical potential. The energy dependence of the temperature and chemical potential are determined as in Eq. (3.20) but with a temperature which is 26 MeV lower than in Figs. 3.5 to 3.8 ($a = 140$ MeV).

It is interesting to plot the ratio κ/S^2 since this is independent of the variance. The result, using $a = 140$ MeV as in Figs. 3.9 and 3.10, is shown in Fig. 3.11. The agreement at the four lowest beam energies is excellent. Again, the biggest discrepancies are at the highest beam energies. As there is no discrepancy for $\sqrt{s_{NN}} = 7.7$, 11.5, 19.6, and 27 GeV, and the crossover models lack a critical point, it would be difficult to argue for a critical point in this energy range—at least under the assumptions made here.

Suppose that at each beam energy we wanted to fit the experimental measurements of $\kappa\sigma^2$ and $S\sigma$. Assuming an equation of state, one can always find a T and μ at each energy to fit this data. Using the crossover equation of state exI, we show the results in Fig. 3.12. Three features in Fig. 3.12 are notable. The first is that T initially increases with μ. This feature is easily explained from the STAR data. From Fig. 3.6, we see that as $\sqrt{s_{NN}}$ decreases below 200 GeV (hence, as μ increases), the experimentally measured $\kappa\sigma^2$ decreases. From the lattice results shown in Fig. 3.3, we know that $\kappa\sigma^2$ is inversely related to T (at least for small μ). Hence, the inferred T should grow with μ (for small values of μ). It is interesting to note that a similar behavior was found in Ref. [73], where the point hadron resonance gas model was fit to the variance at all but the lowest energy of $\sqrt{s_{NN}} = 7.7$ GeV. The second feature is that T is definitely smaller than inferred from the average chemical freeze-out. The third is that at large μ, corresponding to small $\sqrt{s_{NN}}$, there is a very large uncertainty in μ. This uncertainty is a direct consequence of the experimental uncertainties. As a final point, we note that one can perform a similar fit to temperature and baryon chemical potential using $\kappa\sigma^2$, $S\sigma$, and σ^2/M. Now there are only two free variables for every three data points, so a fit is not guaranteed. The results are shown in Fig. 3.13, albeit without fitting uncertainties. As on can see, the additional data had no significant impact on the fitted freeze-out surface.

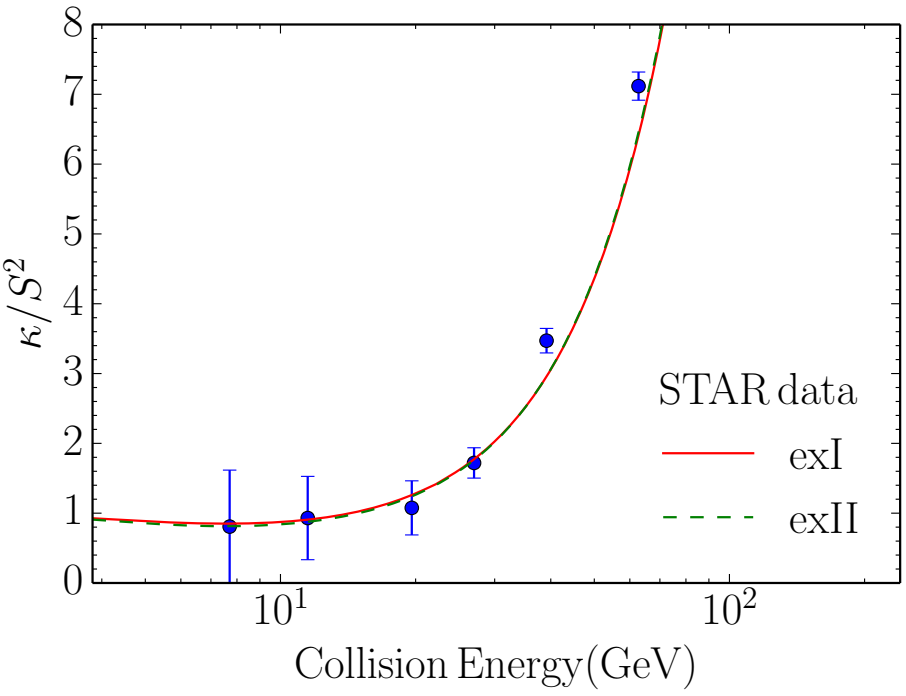

Figure 3.11: Ratio of kurtosis to the square of skewness for the two crossover equations of state compared to the measurements by the STAR Collaboration.

3.6 Conclusion

In this chapter, we compared crossover equations of state with lattice QCD results and with the measurements of the first beam energy scan at RHIC. The previously constructed crossover equations of state interpolated between perturbative QCD at high energy density to a hadronic resonance gas at low energy density. The hadronic resonance gas, with excluded volume effects included, gave excellent agreement with the sound speed as calculated on the lattice. Unsatisfactory results were found when hadrons were treated as point particles.

Skewness and kurtosis of the baryon number fluctuations are very sensitive measures of the equation of state because they involve third and fourth derivatives of the pressure with respect to the chemical potential. The crossover equation of state agreed best with lattice QCD calculations when excluded volume effects in the hadronic sector were taken into account. Henceforth we rejected the crossover equation of state with point hadrons.

The crossover equations of state are in qualitative agreement but in quantitative disagreement with experimental measurements of the skewness and kurtosis when it is assumed that the fluctuations were frozen out at the same time as average chemical freeze-out. When baryon fluctuations are allowed to freeze out at lower temperatures, much better agreement is obtained, except for the higher beam energies. This conclusion is supported by other studies.

There are obvious questions that deserve further investigation. How accurate are the lattice QCD results, especially at nonzero chemical potential? How accurately does the crossover equation of state need be known to replicate the lattice QCD equation of state, given that the skewness and kurtosis involve third and fourth derivatives of the pressure? Our study does not include the requirement that the system have zero net strangeness, which is probably not a major factor but still needs investigation. A serious issue is the phenomenology connecting the experimental measurements to the equation of state. For example, the experimental measurements have a lower momentum-space cutoff for protons of 400 MeV. Such cutoff effects have been investigated in Refs. [74] and [75]. However, in general these cutoff effects are not so straightforward when the equation of state includes interactions.

Our study does not suggest evidence for a critical point, but clearly there is much

work to be done, both theoretically and experimentally.

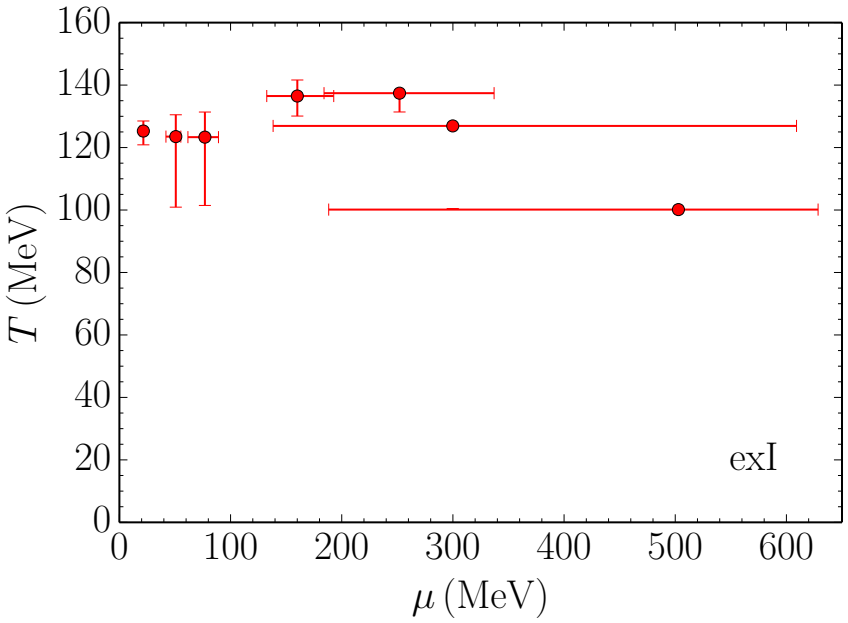

Figure 3.12: A fit to the STAR measurements of the temperature and chemical potential at each beam energy using the crossover equation of state exI.

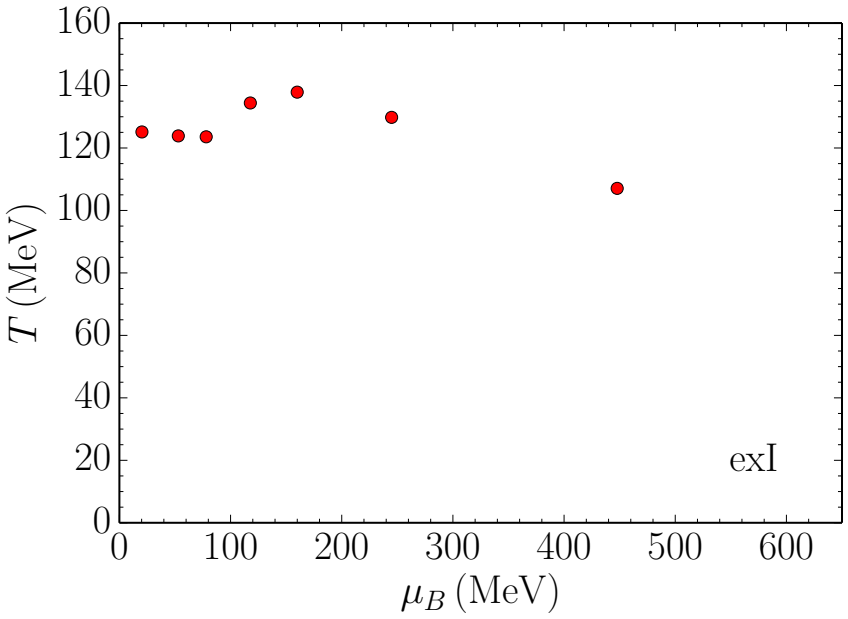

Figure 3.13: A fit (including σ^2/M) to the STAR measurements of the temperature and chemical potential at each beam energy using the crossover equation of state exI. Fitting uncertainties are omitted.

Chapter 4

Quasiparticle Theory of Transport Coefficients in Hadronic Matter at Finite Temperature and Baryon Density

In Chapters 2 and 3, we investigated the equation of state of QCD at finite baryon chemical potentials μ. In this chapter, we derive new formulas to compute the shear and bulk viscosities and thermal conductivity of hot hadronic matter with $\mu > 0$. To do so, we develop a flexible, thermodynamically consistent framework of hadronic quasiparticles with medium-dependent quasiparticle masses and with a scalar and vector mean field. This may be considered a natural generalization of Ref. [76] to incorporate nonzero baryon chemical potential, along with the concomitant vector mean field which is generated by large baryon densities.

4.1 Introduction

Transport coefficients of hot QCD matter, like the shear and bulk viscosities and thermal conductivity, are especially interesting quantities to study for several reasons. First, they are essential theoretical inputs for hydrodynamic simulations, which are critical

tools for interpreting heavy-ion collision data. In hydrodynamic simulations, the shear and bulk viscosities influence the predictions of various observables, such as the elliptic flow coefficients v_n and the hadron transverse momentum (p_T) spectrum [77, 78, 79, 80]. Furthermore, the temperature and chemical potential dependence of transport coefficients may reveal the location of phase transitions: in many physical systems, the shear viscosity is a minimum and the bulk viscosity a maximum at the phase transition [45]. A third motivation is investigating the KSS lower bound [29] on the shear viscosity to entropy density $\eta/s \geq 1/4\pi$ for strongly-coupled conformal theories and its implications for QCD.

In principle, the transport coefficients can be computed directly from QCD using the Kubo formulas [81]. However, QCD is strongly coupled at energies accessible to heavy-ion collision experiments, complicating first-principles calculations. There were some early attempts to employ lattice QCD [82, 83], but even today it is challenging to achieve a large enough grid with a small enough grid spacing to accurately compute transport coefficients. Furthermore, lattice QCD simulations are currently very difficult at finite baryon chemical potential due to the well-known fermion sign problem. Hence, many of the early works [84, 85, 86, 87] computed transport coefficients of quark-gluon plasmas, or hadronic gases with a few species of particles, using the Boltzmann equation in the relaxation time approximation. These early works did not include mean fields or medium-dependent masses.

Later on, Jeon [88] and Jeon and Yaffe [89] computed the shear and bulk viscosities of a hot, weakly-coupled scalar field theory using perturbation theory. Amazingly, they showed that their complicated perturbative calculation of transport coefficients was reproduced by a simpler kinetic theory of quasiparticles with temperature-dependent masses and a scalar mean field. The same conclusion was found for hot, weakly-coupled QCD and QED [90, 91, 92, 93, 94, 95, 96, 97]. This was also consistent with an earlier analysis of transport in a nucleon plus σ meson system, which similarly found that renormalized quasiparticle masses were required [98]. Though astounding, this makes intuitive sense: kinetic theory is widely used to model nonequilibrium systems, and renormalized particle masses are ubiquitous in finite-temperature field theories. (They are also present in Fermi liquid theory [99].) Also, temperature- and chemical

potential-dependent masses allow quasiparticle models to generate more realistic, non-ideal gas, equations of state [100]. Furthermore, as Gorenstein and Yang pointed out [101], the scalar mean field is essential for maintaining thermodynamic self-consistency when masses depend on temperature and/or chemical potential. Hence, it seems kinetic theories of quasiparticles with medium-dependent masses and mean fields are powerful theoretical tools, though thermodynamic consistency must be carefully maintained.

More recently, the conjecture of a lower bound on η/s by Kovtun, Son, and Starinets from AdS/CFT [29] ignited a flurry of additional work. There were several more lattice calculations [102, 103, 104, 105]. There were also many studies with Boltzmann equations—most of them without medium-dependent masses or mean fields. Shear viscosity was computed for pion-nucleon gases at low temperatures and varying chemical potentials in [106, 107]. Bulk viscosity of cool pion gases was computed using chiral perturbation theory in [107, 108]. Shear viscosity in mixtures of hadrons with excluded volumes were calculated in [109, 110, 111].

There were a few attempts to employ the more powerful quasiparticle models with medium-dependent masses to compute transport coefficients. In an early work, Sasaki and Redlich applied kinetic theory and the relaxation time approximation to a quasiparticle model to compute the bulk viscosity near a chiral phase transition [112]. Later, Chakraborty and Kapusta developed a comprehensive theory of shear and bulk viscosities in hadronic gases [76]. That work included multiple hadron species with temperature-dependent masses and a scalar mean field in a thermodynamically self-consistent way. They derived formulas for shear and bulk viscosity and provided both relaxation time approximation formulas and more general integral equations. However, they did not include chemical potentials, hence, thermal conductivity was not considered in that work. Bluhm, Kämpfer, and Redlich used a similar quasiparticle formalism to study the shear and bulk viscosity of gluon matter in [113] (also without chemical potentials). Thus, a natural question is, how does the formalism of [76] generalize to finite baryon chemical potential? Also, what is the formula for thermal conductivity?

Several papers have tried different ansatzes for generalized viscosity formulas (in the relaxation time approximation) when the baryon chemical potential is non-zero. Chen, Liu, Song, and Wang calculated the shear and bulk viscosities of weakly-coupled quark-gluon plasma at finite temperature and chemical potential in [114] using a quasiparticle

model with medium-dependent masses and a scalar mean field. Khvorostukhin, Toneev, and Voskresensky compared three ansatzes for the generalized bulk viscosity formula [115] of a hadron gas with medium-dependent masses and a scalar mean field; see also [116, 117]. Interestingly, Khvorostukhin's quasiparticle model also included a vector (ω) mean field [116, 115]; as is well known, they are important to account for repulsive forces in hadronic matter with large baryon densities. This type of model is quite relevant for studying the moderate temperature hadronic matter formed in the beam energy scan at RHIC. It is also relevant for experiments at the Super Proton Synchrotron Heavy Ion and Neutrino Experiment (SHINE) at CERN and at the future Facility for Antiproton and Ion Research (FAIR). Given the usefulness of this kind of model, it is desirable to put the results on a firmer theoretical foundation and (ideally) determine which of the ansatzes presented in [114] and [115] are correct.

In this work, we present detailed derivations of the formulas for the shear and bulk viscosities and thermal conductivity of a gas of hadronic quasiparticles. We include a scalar and a vector mean field, where the mean fields and the quasiparticle masses depend on temperature and baryon chemical potential. Generalization to multiple scalar and vector fields is straightforward but not included here for clarity of presentation. Starting from the quasiparticle dispersion relation, we obtain the Boltzmann equation, and then use the Chapman-Enskog expansion to derive formulas for the transport coefficients. At each step we ensure that thermodynamic self-consistency is maintained, and we carefully enforce the Landau-Lifshitz conditions of fit; we later show this is vital to obtaining the correct results. We derive both relaxation time approximation formulas and more general integral equations. Finally, we show that the formulas for shear and bulk viscosities are straightforward generalizations of previous results [76, 89] if one recalls that entropy per baryon is conserved in ideal hydrodynamics (neglecting viscous effects). Classical statistics are used in the main text for ease of presentation, but results which include quantum statistics are presented in Sec. 4.10, albeit without detailed derivations.

4.2 Quasiparticles

In this section we discuss quasiparticle dispersion relations for baryons and mesons. In the simplest mean field approach all hadrons acquire effective masses in the medium. In addition, baryons acquire effective chemical potentials. We will focus attention on baryons since the inclusion of the baryon chemical potential is the new feature of this work compared to Ref. [76].

The piece of the Lagrangian involving baryons is

$$\mathcal{L}_{\rm baryon} = \sum_a \bar{\psi}_a (i \not{\partial} - m_a + g_{\sigma a}\sigma - g_{\omega a} \not{\omega}) \psi_a \,. \tag{4.1}$$

Here a refers to the species of baryon. For simplicity of presentation we include only a generic scalar meson σ and a generic vector meson ω. When evaluating the partition function there enters an additional term of the form $\mu \bar{\psi}_a \gamma^0 \psi_a$, where μ is the baryon chemical potential. Since we are using Dirac spinors both particles and antiparticles are included. Baryons have chemical potential μ while antibaryons have chemical potential $-\mu$. Let b_a denote the baryon charge, which is $+1$ for baryons, -1 for antibaryons and 0 for mesons. Then the chemical potential of hadron a is

$$\mu_a = b_a \mu \,. \tag{4.2}$$

Note that hadrons contain electric and strange charges in addition to baryon charge, so in principle this expression should contain additional terms. However, the electric and strange chemical potentials are typically small in heavy-ion collisions [47], so those extra terms are tiny; hence, we ignore them here.

For a uniform medium in thermal equilibrium the meson fields acquire space-time independent nonzero mean values denoted by $\bar{\sigma}$ and $\bar{\omega}^\mu$; in the rest frame of the medium the spatial part of the vector field vanishes on account of rotational symmetry, $\bar{\boldsymbol{\omega}} = 0$, but in a general frame of reference it does not. The dispersion relation for baryon a is

$$E_a(\mathbf{p}) = \sqrt{(\mathbf{p} - g_{\omega a}\bar{\boldsymbol{\omega}})^2 + m_a^{*2}} + g_{\omega a}\bar{\omega}^0 \tag{4.3}$$

and for antibaryon $\bar{a}$

$$E_{\bar{a}}(\mathbf{p}) = \sqrt{(\mathbf{p} + g_{\omega a}\bar{\boldsymbol{\omega}})^2 + m_a^{*2}} - g_{\omega a}\bar{\omega}^0 \,. \tag{4.4}$$

The kinetic momentum $\mathbf{p}^*$ is related to the canonical momentum $\mathbf{p}$ by

$$\mathbf{p}_a^* = \mathbf{p} - g_{\omega a}\bar{\boldsymbol{\omega}} \tag{4.5}$$

for baryons and by

$$\mathbf{p}_{\bar{a}}^* = \mathbf{p} + g_{\omega a}\bar{\boldsymbol{\omega}} \tag{4.6}$$

for antibaryons. Mesons do not couple to the vector field, so every meson a has $g_{\omega a} = 0$. Particles and antiparticles have a common mass m_a^*. In this mean field approach it is given by

$$m_a^* = m_{\bar{a}}^* = m_a - g_{\sigma a}\bar{\sigma}\,, \tag{4.7}$$

so we require $g_{\sigma a} = g_{\sigma\bar{a}}$.

We can succinctly combine the dispersion relations for baryons, mesons, and their antiparticles into a uniform set of expressions. For antibaryons $\bar{a}$, we define $g_{\omega\bar{a}} = -g_{\omega a}$. For mesons a we have $g_{\omega a} = 0$. Then, for any particle or antiparticle a, we have

$$E_a(\mathbf{p}) = \sqrt{(\mathbf{p} - g_{\omega a}\bar{\boldsymbol{\omega}})^2 + m_a^{*2}} + g_{\omega a}\bar{\omega}^0 \tag{4.8}$$

and

$$\mathbf{p}_a^* = \mathbf{p} - g_{\omega a}\bar{\boldsymbol{\omega}}\,. \tag{4.9}$$

A more convenient way to think about the dispersion relations is to recognize a shift in both the mass and chemical potential of quasiparticles and anti-quasiparticles. They both have energy

$$E_a^*(\mathbf{p}^*) = \sqrt{\mathbf{p}^{*2} + m_a^{*2}} \tag{4.10}$$

while the chemical potentials shift like

$$\mu_a^* = b_a\mu - g_{\omega a}\bar{\omega}^0\,, \tag{4.11}$$

where b_a is the baryon charge of particle a. Mesons do not have a baryon charge or couple to the vector field, hence meson formulas in the mean field approximation simplify to

$$E(\mathbf{p}) = E^*(\mathbf{p}) = \sqrt{\mathbf{p}^2 + m^{*2}} \tag{4.12}$$

and

$$\mu_a^* = 0\,. \tag{4.13}$$

Note that the kinetic and canonical momenta are the same for mesons. The effective masses and effective chemical potentials can be found self-consistently once one fixes the Lagrangian.

In equilibrium, the phase space density for a particle (or antiparticle) of type a is given by

$$f_a(\mathbf{x}, \mathbf{p}^*, t) = \frac{1}{\mathrm{e}^{(p^\mu u_\mu - \mu_a)/T} - (-1)^{2s_a}} \,. \tag{4.14}$$

Here s_a denotes the spin and u^μ is the fluid four-velocity. These are relativistic versions of Fermi-Dirac or Bose-Einstein distributions, depending on whether particle a is a fermion or boson. In the fluid rest frame, $p^\mu u_\mu = E_a$, so in that frame $p^\mu u_\mu - \mu_a = E_a^* - \mu_a^*$. Thus in the rest frame

$$f_a(\mathbf{x}, \mathbf{p}^*, t) = \frac{1}{\mathrm{e}^{(E_a^* - \mu_a^*)/T} - (-1)^{2s_a}} \,. \tag{4.15}$$

Later on we will simplify our results by using classical statistics, although that approximation is not necessary. Results including quantum statistics are given in Sec. 4.10. Momentum space integration will be abbreviated as

$$d\Gamma_a^* = (2s_a + 1)\frac{d^3p_a^*}{(2\pi)^3} \tag{4.16}$$

indicating that the kinetic momentum is chosen as the independent variable, and the spin degeneracy is included.

Once again, in this chapter we use natural units where $\hbar = c = k_B = 1$.

4.3 Boltzmann Equation

The general form of the Boltzmann equation for the distribution function $f_a(\mathbf{x}, \mathbf{p}^*, t)$ is

$$\frac{df_a}{dt}(\mathbf{x}, \mathbf{p}^*, t) = \frac{\partial f_a}{\partial t} + \frac{\partial f_a}{\partial x^i}\frac{dx^i}{dt} + \frac{\partial f_a}{\partial p^{*i}}\frac{dp^{*i}}{dt} = \mathcal{C}_a \,. \tag{4.17}$$

Note that we use Einstein notation where repeated tensor indices (like i above) are summed over. In this thesis, sums over Roman tensor indices like i, j, k run over spacial coordinates 1-3 while sums over Greek tensor indices like μ, ν, α run over space-time coordinates 0-3.

The right-hand-side of Eq. (4.17) is the collision term which will be discussed later. Here we focus on the left-hand-side. It involves the trajectory $\mathbf{x}(t)$ and $\mathbf{p}^*(t)$ between collisions. This trajectory is in general not a straight line because the particle is moving in a mean field which can be space and time dependent.

The velocity is

$$\frac{dx^i}{dt} = \frac{\partial E_a}{\partial p_a^i} = \frac{p^{*i}}{E_a^*} \,. \tag{4.18}$$

The relativistic version of Newton's Second Law is

$$\frac{dp_a^i}{dt} = -\left(\frac{\partial E_a}{\partial x^i}\right)_p \,. \tag{4.19}$$

Note that it is p that is held fixed, not p^*. The right-hand-side is

$$\left(\frac{\partial E_a}{\partial x^i}\right)_p = \frac{m_a^*}{E_a^*}\frac{\partial m_a^*}{\partial x^i} - g_{\omega a}\frac{\partial \bar{\omega}^j}{\partial x^i}\frac{p^{*j}}{E_a^*} + g_{\omega a}\frac{\partial \bar{\omega}^0}{\partial x^i} \,. \tag{4.20}$$

The left-hand-side of Newton's Second Law can be written in terms of the kinetic momentum as

$$\frac{dp_a^i}{dt} = \frac{dp^{*i}}{dt} + g_{\omega a}\frac{d\bar{\omega}^i}{dt} = \frac{dp^{*i}}{dt} + g_{\omega a}\left(\frac{\partial \bar{\omega}^i}{\partial t} + \frac{p^{*j}}{E_a^*}\frac{\partial \bar{\omega}^i}{\partial x^j}\right) \,. \tag{4.21}$$

The time derivatives of $\mathbf{x}$ and $\mathbf{p}^*$ can now be replaced in Eq. (4.17) to put the Boltzmann equation in the form

$$\frac{df_a}{dt}(\mathbf{x},\mathbf{p}^*,t) = \frac{\partial f_a}{\partial t} + \frac{p^{*i}}{E_a^*}\frac{\partial f_a}{\partial x^i}$$

$$-\frac{\partial f_a}{\partial p^{*i}}\left\{\frac{m_a^*}{E_a^*}\frac{\partial m_a^*}{\partial x^i} + g_{\omega a}\left[\frac{\partial \bar{\omega}^0}{\partial x^i} + \frac{\partial \bar{\omega}^i}{\partial t} + \frac{p^{*j}}{E_a^*}\left(\frac{\partial \bar{\omega}^i}{\partial x^j} - \frac{\partial \bar{\omega}^j}{\partial x^i}\right)\right]\right\} = \mathcal{C}_a \,. \tag{4.22}$$

This can be simplified by making use of the kinetic four-momentum

$$p_a^{*\mu} = (E_a^*, \mathbf{p}^*) \tag{4.23}$$

and the field strength tensor

$$\bar{\omega}^{\alpha\beta} \equiv \partial^\alpha \bar{\omega}^\beta - \partial^\beta \bar{\omega}^\alpha \,. \tag{4.24}$$

The final form is

$$\frac{df_a}{dt}(\mathbf{x},\mathbf{p}^*,t) = \frac{p^{*\mu}}{E_a^*}\partial_\mu f_a - \left[\frac{m_a^*}{E_a^*}\frac{\partial m_a^*}{\partial x^i} + g_{\omega a}\frac{p_\mu^*}{E_a^*}\,\bar{\omega}^{\mu i}\right]\frac{\partial f_a}{\partial p^{*i}} = \mathcal{C}_a \,. \tag{4.25}$$

4.4 Energy-Momentum Tensor and Baryon Current

In this section we present the structure of the energy-momentum tensor $T^{\mu\nu}$ and of the baryon current J^{μ}. In terms of temperature, chemical potential, and flow four-velocity u^{μ} they are

$$T^{\mu\nu} = -Pg^{\mu\nu} + wu^{\mu}u^{\nu} + \Delta T^{\mu\nu} \tag{4.26}$$

and

$$J^{\mu} = nu^{\mu} + \Delta J^{\mu}\,, \tag{4.27}$$

where $P(T,\mu)$ is the pressure, $s = \partial P/\partial T$ is the entropy density, $n = \partial P/\partial \mu$ is the baryon density, $\epsilon = -P + Ts + \mu n$ is the energy density, and $w = \epsilon + P$ is the enthalpy density. In the Landau-Lifshitz approach, which we use, u^{μ} is the four-velocity of energy transport. Recall from special relativity, if $\mathbf{v}$ is the local three-velocity of the fluid, then the four-velocity is defined as

$$u^{\mu} = (\frac{1}{\sqrt{1-\mathbf{v}^2}}, \frac{\mathbf{v}}{\sqrt{1-\mathbf{v}^2}})\,, \tag{4.28}$$

where natural units have $c = 1$. Our metric (written as a matrix) is

$$g = \begin{pmatrix} 1 & 0 & 0 & 0 \\ 0 & -1 & 0 & 0 \\ 0 & 0 & -1 & 0 \\ 0 & 0 & 0 & -1 \end{pmatrix}. \tag{4.29}$$

Note that $g_{\mu\nu}$ denotes the (μ,ν) component of the matrix. Together, these imply that

$$u_{\mu}u^{\mu} = g_{\mu\nu}u^{\mu}u^{\nu} = 1\,. \tag{4.30}$$

The $\Delta T^{\mu\nu}$ and ΔJ^{μ} are the nonequilibrium (i.e., dissipative) parts. In the next section, we will show they are given by

$$\Delta T^{\mu\nu} = \eta\left(D^{\mu}u^{\nu} + D^{\nu}u^{\mu} + \tfrac{2}{3}\Delta^{\mu\nu}\partial_{\rho}u^{\rho}\right) - \zeta\Delta^{\mu\nu}\partial_{\rho}u^{\rho} \tag{4.31}$$

and

$$\Delta J^{\mu} = \lambda\left(\frac{nT}{w}\right)^2 D^{\mu}\left(\frac{\mu}{T}\right). \tag{4.32}$$

Here η, ζ and λ are the shear viscosity, bulk viscosity, and thermal conductivity, respectively. The other symbols are

$$D = u^\rho \partial_\rho \,, \tag{4.33}$$

$$D^\mu = \partial^\mu - u^\mu D \,, \tag{4.34}$$

$$\Delta^{\mu\nu} = u^\mu u^\nu - g^{\mu\nu} \,. \tag{4.35}$$

Physically, D represents a time derivative in the local rest frame of the fluid, D^μ becomes a spacial gradient in the local rest frame of the fluid, and $\Delta^{\mu\nu}$ is a projector that kills components of a vector parallel to the fluid four-velocity. In the rest frame, we have $D = \partial_0$, $D_i = \partial_i$, $D_0 = 0$, $\Delta_{0\mu} = 0$, and $\Delta_{ij} = \delta_{ij}$.

Now that we have the forms of $T^{\mu\nu}$ and J^μ in terms of macroscopic thermodynamic variables, we must find the corresponding expressions in terms of the microscopic quasiparticles and mean fields. One expression for the former is

$$T^{\mu\nu} = \sum_a \int d\Gamma_a^* \frac{p_a^{*\mu} p_a^{*\nu}}{E_a^*} f_a + g^{\mu\nu} U(\bar{\sigma}, \bar{\omega}^\rho \bar{\omega}_\rho) + m_\omega^2 \bar{\omega}^\mu \bar{\omega}^\nu \,. \tag{4.36}$$

(Note that the sum over a runs over mesons, baryons, and their antiparticles.) The first term is familiar as the kinetic contribution. The second term is the usual meson field potential energy; it includes the mass terms $\frac{1}{2} m_\sigma^2 \bar{\sigma}^2$ and $-\frac{1}{2} m_\omega^2 \bar{\omega}^\rho \bar{\omega}_\rho$, plus any interaction terms which are more than two powers of the fields. Note that kinetic terms for the mean meson fields are not included because they are second order in space-time gradients and are not included in first-order viscous fluid dynamics. The last term is not obviously of the form of Eq. (4.26). However, when one remembers that T^{0i} is the energy flux in the direction i, and that E_a is the complete quasiparticle energy and not E_a^*, then one would write

$$T^{\mu\nu} = \sum_a \int d\Gamma_a^* \frac{p_a^{\mu} p_a^{*\nu}}{E_a^*} f_a + g^{\mu\nu} U(\bar{\sigma}, \bar{\omega}^\rho \bar{\omega}_\rho) \,. \tag{4.37}$$

Using $p_a^\mu = p_a^{*\mu} + g_{\omega a} \bar{\omega}^\mu$ we get

$$T^{\mu\nu} = \sum_a \int d\Gamma_a^* \frac{p_a^{*\mu} p_a^{*\nu}}{E_a^*} f_a + g^{\mu\nu} U(\bar{\sigma}, \bar{\omega}^\rho \bar{\omega}_\rho) + \bar{\omega}^\mu \sum_a g_{\omega a} \int d\Gamma_a^* \frac{p_a^{*\nu}}{E_a^*} f_a \,. \tag{4.38}$$

The vector mean field is determined by its equation of motion. Assuming an interaction only with the baryons (this assumption is easily relaxed) it is

$$\left(\partial^2 + m_\omega^2\right)\bar{\omega}^\nu = \sum_j g_{\omega j}\langle\bar{\psi}_j\gamma^\nu\psi_j\rangle \tag{4.39}$$

where the averaging refers to the quasiparticle distribution. Recognizing that the summation index j refers to both baryons and antibaryons, and dropping the d'Alembertian because of first-order viscous fluid dynamics, we can write

$$m_\omega^2\bar{\omega}^\nu = \sum_a g_{\omega a}\int d\Gamma_a^*\frac{p_a^{*\nu}}{E_a^*}f_a\,. \tag{4.40}$$

(We remind the reader that the coupling $g_{\omega a}$ is opposite in sign for baryons and antibaryons. It is zero for mesons.) Hence Eqs. (4.36) and (4.37) are the same.

In a similar way the scalar mean field is determined by its equation of motion. This turns out to be

$$\frac{\partial U(\bar{\sigma},\bar{\omega}^\rho\bar{\omega}_\rho)}{\partial\bar{\sigma}} = \sum_a g_{\sigma a}\int d\Gamma_a^*\frac{m_a^*}{E_a^*}f_a\,. \tag{4.41}$$

(Note that the coupling to scalar mesons of particles and antiparticles has the same sign, unlike the coupling to vector mesons.) In Appendix C, we show that conservation of energy and momentum also requires, in addition to Eqs. (4.40) and (4.41), that the potential U obeys the constraint

$$\frac{\partial U(\bar{\sigma},\bar{\omega}^\rho\bar{\omega}_\rho)}{\partial\left(\bar{\omega}^\rho\bar{\omega}_\rho\right)} = -\tfrac{1}{2}m_\omega^2\,. \tag{4.42}$$

The structure of the baryon current is readily deduced to be

$$J^\mu = \sum_a b_a\int d\Gamma_a^*\frac{p_a^{*\mu}}{E_a^*}f_a\,, \tag{4.43}$$

where b_a denotes the baryon number of particle a.

The macroscopic conservation laws for energy and momentum and baryon charge are written covariantly as

$$\partial_\mu T^{\mu\nu} = 0\,, \tag{4.44}$$

and

$$\partial_\mu J^\mu = 0\,. \tag{4.45}$$

These originate microscopically in the conservation of energy, momentum, and baryon charge in individual collisions between particles. One may describe this mathematically using the general expression [118]

$$\sum_a \int d\Gamma_a^* \chi_a \mathcal{C}_a = 0\,. \tag{4.46}$$

The χ_a represents the contribution from quasiparticle a to any conserved quantity, such as energy, momentum, or baryon number, while $\mathcal{C}_a$ is the collision integral. The derivation of the conservation laws (4.44) and (4.45) from Eq. (4.46) is straightforward but very lengthy and tedious, hence it is relegated to Appendix C. A key result is that Eqs. (4.40)-(4.42) guarantee that energy and momentum are conserved in the model. Not surprisingly, this is also crucial to maintaining the thermodynamic self-consistency of the model, as we discuss further in Appendix C.

It is straightforward and much less tedious to show that the mean field equation of state follows from the above expressions for $T^{\mu\nu}$ and J^μ when the system is uniform, time independent, and in thermal and chemical equilibrium.

4.4.1 Derivation of the Nonequilibrium Terms

The nonequilibrium terms of the baryon current and energy-momentum tensor are uniquely determined in first-order hydrodynamics by the thermodynamic requirement that entropy increase with time. Mathematically, this means that the divergence of the entropy 4-current must be positive: $\partial_\mu s^\mu > 0$. For further details, see Weinberg [119] and Landau and Lifshitz [120].

To start, we decompose the entropy current into the equilibrium part plus a deviation:

$$\partial_\mu s^\mu = \partial_\mu (s u^\mu) + \partial_\mu (\Delta s^\mu)\,. \tag{4.47}$$

Here s is the entropy density. Next, we seek an expression for $\partial_\mu(su^\mu)$. We start with the energy-momentum tensor:

$$\begin{aligned} T^{\mu\nu} &= -P g^{\mu\nu} + (\epsilon + P) u^\mu u^\nu + \Delta T^{\mu\nu} \\ &= -P g^{\mu\nu} + (Ts + \mu n) u^\mu u^\nu + \Delta T^{\mu\nu}\,. \end{aligned} \tag{4.48}$$

Energy and momentum conservation requires that the divergence of this tensor vanish:

$$\begin{aligned} 0 = \partial_\mu T^{\mu\nu} &= -\partial^\nu P + s u^\mu \partial_\mu (T u^\nu) + n u^\mu \partial_\mu (\mu u^\nu) \\ &\quad + T u^\nu \partial_\mu (s u^\mu) + \mu u^\nu \partial_\mu (n u^\mu) + \partial_\mu \Delta T^{\mu\nu} \,. \end{aligned} \tag{4.49}$$

We contract with u_ν and simplify using the following identities:

$$u_\nu u^\nu = 1 \,, \quad u_\nu \partial_\mu u^\nu = 0 \,, \quad u_\nu \partial^\nu = D \,.$$

We find

$$\begin{aligned} 0 &= -DP + sDT + nD\mu \\ &\quad + T\partial_\mu (s u^\mu) + \mu \partial_\mu (n u^\mu) + u_\nu \partial_\mu \Delta T^{\mu\nu} \,. \end{aligned} \tag{4.50}$$

The first line vanishes from the Gibbs-Duhem equation of thermodynamics. From conservation of baryon charge, we have

$$0 = \partial_\mu J^\mu = \partial_\mu (n u^\mu) + \partial_\mu (\Delta J^\mu) \,. \tag{4.51}$$

From the Landau-Lifshitz condition

$$u_\nu \Delta T^{\mu\nu} = 0 \,, \tag{4.52}$$

we find

$$u_\nu \partial_\mu \Delta T^{\mu\nu} = -\Delta T^{\mu\nu} \partial_\mu u_\nu \,. \tag{4.53}$$

Thus, Eq. (4.50) becomes

$$\partial_\mu (s u^\mu) = \frac{\mu}{T} \partial_\mu (\Delta J^\mu) + \frac{\Delta T^{\mu\nu}}{T} \partial_\mu u_\nu \,. \tag{4.54}$$

Using Eq. (4.54) with Eq. (4.47), we find

$$\partial_\mu s^\mu = \partial_\mu \left(\Delta s^\mu + \frac{\mu}{T} \Delta J^\mu \right) - \Delta J^\mu \, \partial_\mu \left(\frac{\mu}{T} \right) + \frac{\Delta T^{\mu\nu}}{T} \partial_\mu U_\nu \,. \tag{4.55}$$

We want Eq. (4.55) to consist of a sum of squares to ensure $\partial_\mu s^\mu > 0$, so we need

$$\Delta s^\mu = -\frac{\mu}{T} \Delta J^\mu \,. \tag{4.56}$$

At this point, we assume spacetime gradients are small, so in first-order hydrodynamics ΔJ^μ must be linear in gradients like $\partial^\mu (\mu/T)$. Since the baryon current must obey

the Landau-Lifshitz condition $u_\mu \Delta J^\mu = 0$, we see the baryon term must in fact be proportional to $D^\mu(\mu/T)$:

$$\Delta J^\mu = \lambda \left(\frac{Tn}{w}\right)^2 D^\mu \left(\frac{\mu}{T}\right) . \tag{4.57}$$

Here λ is the thermal conductivity and $w = (\epsilon + P)$ is the enthalpy density. $\Delta T^{\mu\nu}$ must be symmetric and linear in terms like $\partial_\mu u_\nu$, and it must obey the Landau-Lifshitz condition of fit $u_\mu \Delta T^{\mu\nu} = 0$. There are two possible combinations of gradients, so the general solution is

$$\Delta T^{\mu\nu} = \eta \left(D^\mu u^\nu + D^\nu u^\mu + \tfrac{2}{3}\Delta^{\mu\nu}\partial_\rho u^\rho\right) - \zeta \Delta^{\mu\nu}\partial_\rho u^\rho \, . \tag{4.58}$$

Here η and ζ are the shear and bulk viscosities.

To verify that these results are correct, we now evaluate Eq. (4.55). To simplify the expressions, we work in the local fluid rest frame where

$$D_0 = 0 \, , \quad D_i = \partial_i \, , \tag{4.59}$$

and

$$\Delta^{0\nu} = 0 \, , \quad \Delta^{ij} = \delta^{ij} \, , \tag{4.60}$$

where δ^{ij} is the Kronecker delta function. Thus in the rest frame, Eq. (4.55) simplifies to

$$\begin{aligned} \partial_\mu s^\mu &= \frac{\eta}{2T}\left(\partial_i u^j + \partial_j u^i - \tfrac{2}{3}\delta^{ij}\partial_\rho u^\rho\right)^2 + \frac{\zeta}{T}\left(\partial_\rho u^\rho\right)^2 \\ &\quad + \lambda \left(\frac{Tn}{w}\right)^2 \left(\partial_i \left(\frac{\mu}{T}\right)\right)^2 > 0 \, . \end{aligned} \tag{4.61}$$

This is a sum of squares as claimed, so entropy production is clearly positive.

4.5 Thermodynamic Consistency of the Quasiparticle Theory

In this section we demonstrate that the quasiparticle model is thermodynamically self-consistent. Thermodynamic self-consistency requires that the following identities hold:

$$\left(\frac{\partial P}{\partial \mu}\right)_T = n \tag{4.62}$$

$$T\left(\frac{\partial P}{\partial T}\right)_{\mu} = \epsilon + P - \mu n\,. \tag{4.63}$$

To start, we need an expression for the equilibrium pressure of the system in the fluid rest frame. We must be careful to include contributions from both quasiparticles and mean fields. Fortunately, the pressure is readily obtained from the spacial trace of energy-momentum tensor:

$$P = \tfrac{1}{3}\sum_{i=1}^{3} T^{ii}\,. \tag{4.64}$$

Using Eq. (4.36) for the energy-momentum tensor, and recalling that $\bar{\omega}^i = 0$ in the rest frame in equilibrium, we find

$$P = \sum_a \int d\Gamma_a^* \frac{|\mathbf{p}_a^*|^2}{3E_a^*} f_a^{\rm eq} - U\,. \tag{4.65}$$

We will also need the energy density, which is given by T^{00}. From Eq. (4.37), this is

$$\epsilon = \sum_a \int d\Gamma_a^* E_a f_a^{\rm eq} + U\,. \tag{4.66}$$

4.5.1 Expression for the Baryon Density

We begin with the baryon density expression (4.62). From Eq. (4.65), we see

$$\left(\frac{\partial P}{\partial \mu}\right)_T = \sum_a \int d\Gamma_a^* \frac{|\mathbf{p}_a^*|^2}{3E_a^*}\left[\left(\frac{\partial f_a^{\rm eq}}{\partial \mu}\right)_T - \frac{f_a^{\rm eq}}{E_a^*}\left(\frac{\partial E_a^*}{\partial \mu}\right)_T\right] - \left(\frac{\partial U}{\partial \mu}\right)_T\,. \tag{4.67}$$

Next, we rewrite the derivative of the distribution function as

$$\begin{aligned}
\left(\frac{\partial f_a^{\rm eq}}{\partial \mu}\right)_T &= f_a^{\rm eq}\frac{\partial}{\partial \mu}\left[-\beta(E_a^* - \mu_a^*)\right] \\
&= -\beta f_a^{\rm eq}\left[\left(\frac{\partial E_a^*}{\partial \mu}\right)_T - \left(\frac{\partial \mu_a^*}{\partial \mu}\right)_T\right] \\
&= \frac{\partial f_a^{\rm eq}}{\partial E_a^*}\left[\frac{1}{2E_a^*}\left(\frac{\partial m_a^{*2}}{\partial \mu}\right)_T - \left(\frac{\partial \mu_a^*}{\partial \mu}\right)_T\right]\,.
\end{aligned} \tag{4.68}$$

We insert Eq. (4.68) into Eq. (4.67). Then, for the integral term containing

$$\frac{\partial f_a^{\rm eq}}{\partial E_a^*}\,,$$

we change the integration variable from p_a^* to E_a^*, integrate by parts, and change the integration variable back to p_a^*. After canceling terms, we obtain

$$\left(\frac{\partial P}{\partial \mu}\right)_T = \sum_a \int d\Gamma_a^* f_a^{\rm eq} \frac{\partial}{\partial \mu} \left(\mu_a^* - E_a^*\right)_T - \left(\frac{\partial U}{\partial \mu}\right)_T . \tag{4.69}$$

We recall that $(\mu_a^* - E_a^*) = (\mu_a - E_a) = (b_a\mu - E_a)$. In Appendix C, we show that energy-momentum conservation implies (Eq. (C.30)):

$$\left(\frac{\partial U}{\partial \mu}\right)_T = -\sum_a \int d\Gamma_a^* \left(\frac{\partial E_a}{\partial \mu}\right)_T f_a^{\rm eq} . \tag{4.70}$$

Thus Eq. (4.69) becomes

$$\left(\frac{\partial P}{\partial \mu}\right)_T = \sum_a b_a \int d\Gamma_a^* f_a^{\rm eq} = n . \tag{4.71}$$

The integral is clearly the baryon density n, so we confirm Eq. (4.62).

4.5.2 Expression for the Entropy Density

Next, we prove the entropy density identity (4.63). Starting with Eq. (4.65) we find

$$\left(\frac{\partial P}{\partial T}\right)_\mu = \sum_a \int d\Gamma_a^* \frac{|\mathbf{p}_a^*|^2}{3E_a^*} \left[\left(\frac{\partial f_a^{\rm eq}}{\partial T}\right)_\mu - \frac{f_a^{\rm eq}}{E_a^*}\left(\frac{\partial E_a^*}{\partial T}\right)_\mu\right] - \left(\frac{\partial U}{\partial T}\right)_\mu . \tag{4.72}$$

Proceeding like before, we transform the derivative term

$$\begin{aligned}
\left(\frac{\partial f_a^{\rm eq}}{\partial T}\right)_\mu &= f_a^{\rm eq} \frac{\partial}{\partial T}\left[-\beta(E_a - \mu_a)\right] \\
&= -\beta f_a^{\rm eq}\left[\left(\frac{\partial E_a}{\partial T}\right)_\mu - \beta\left(E_a - \mu_a\right)\right] \\
&= \frac{\partial f_a^{\rm eq}}{\partial E_a^*}\left[\frac{1}{2E_a^*}\left(\frac{\partial m_a^{*2}}{\partial T}\right)_\mu + g_{\omega a}\left(\frac{\partial \bar{\omega}^0}{\partial T}\right)_\mu - \beta\left(E_a - \mu_a\right)\right] .
\end{aligned} \tag{4.73}$$

We insert Eq. (4.73) into Eq. (4.72). Once again, we focus on the term containing

$$\frac{\partial f_a^{\rm eq}}{\partial E_a^*} .$$

With that term, we again convert the integration variable from p_a^* to E_a^*, integrate by parts, and convert the integration variable back to p_a^*. After canceling terms we find

$$\left(\frac{\partial P}{\partial T}\right)_\mu = \frac{1}{T}\sum_a \int d\Gamma_a^* f_a^{\rm eq}\left[E_a + \frac{|\mathbf{p}_a^*|^2}{3E_a^*} - \mu_a - T\left(\frac{\partial E_a}{\partial T}\right)_\mu\right] - \left(\frac{\partial U}{\partial T}\right)_\mu . \tag{4.74}$$

We see the two right-most terms cancel if we use the identity (C.29) from Appendix C:

$$\left(\frac{\partial U}{\partial T}\right)_\mu = -\sum_a \int d\Gamma_a^* \left(\frac{\partial E_a}{\partial T}\right)_\mu f_a^{\rm eq}\,. \tag{4.75}$$

Recalling that $\mu_a = b_a\mu$, we see the μ_a term leads to the integral for baryon density (4.71), so we find

$$T\left(\frac{\partial P}{\partial T}\right)_\mu = \sum_a \int d\Gamma_a^* f_a^{\rm eq}\left[E_a + \frac{|\mathbf{p}_a^*|^2}{3E_a^*}\right] - \mu n\,. \tag{4.76}$$

Finally, we can see that the integral above is equal to $(\epsilon + P)$ if we add Eqs. (4.65) and (4.66). Thus we find

$$T\left(\frac{\partial P}{\partial T}\right)_\mu = Ts = \epsilon + P - \mu n\,. \tag{4.77}$$

Thus we verified Eq. (4.63), so the theory is indeed thermodynamically self-consistent.

4.6 Departures from Equilibrium of the Quasiparticle Distribution Function

To first order in departures from equilibrium, we can express the quasiparticle distribution function as

$$f_a = f_a^{\rm eq}\,(1 + \phi_a) \tag{4.78}$$

where $f_a^{\rm eq}$ is the distribution function in thermal and chemical equilibrium. The nonequilibrium part ϕ_a leads to the nonequilibrium contributions $\Delta T^{\mu\nu}$ and ΔJ^μ, so ϕ_a must contain the same space-time gradients as found in them. Therefore, ϕ_a must have the form

$$\phi_a = -A_a\partial_\rho u^\rho - B_a p_a^\nu D_\nu\left(\frac{\mu}{T}\right) + C_a p_a^\mu p_a^\nu\left(D_\mu u_\nu + D_\nu u_\mu + \tfrac{2}{3}\Delta_{\mu\nu}\partial_\rho u^\rho\right)\,. \tag{4.79}$$

The functions A_a, B_a and C_a only depend on momentum p while u^μ only depends on space-time coordinate x.

The departure from equilibrium of the quasiparticle distributions can be used to compute the departure from equilibrium of the energy-momentum tensor. It is convenient to work in the local rest frame. The variation of the space-space part of expression

(4.36) is

$$\delta T^{ij} = \sum_a \int d\Gamma_a^* \frac{p_a^{*i} p_a^{*j}}{E_a^*} \left(\delta f_a - f_a^{\rm eq} \frac{\delta E_a^*}{E_a^*} \right) + g^{ij} \delta U \,. \tag{4.80}$$

To obtain the variation in the mean field potential we start with the expression for the pressure $P(T,\mu) = P_0 - U$. Here P_0 is the kinetic contribution to the pressure from the quasiparticles. The entropy density is obtained from $s = \partial P(T,\mu)/\partial T$. This has three contributions: the first is from s_0 which is the same functional form as for particles with T- and μ-independent energies, the second is from the variation of the quasiparticle energies due to variations in T and μ, and finally there is the contribution $-\partial U/\partial T$ at fixed μ. The mean field carries no entropy, therefore the second and third terms must cancel. Using classical statistics for simplicity we have

$$P_0 = T \sum_a \int d\Gamma_a^* f_a^{\rm eq} \tag{4.81}$$

and thus

$$\left(\frac{\partial U}{\partial T} \right)_\mu = - \sum_a \int d\Gamma_a^* \left(\frac{\partial E_a}{\partial T} \right)_\mu f_a^{\rm eq} \,. \tag{4.82}$$

The same argument applies to differentiation with respect to μ, which gives the baryon density. The mean field carries no baryon number, so similarly

$$\left(\frac{\partial U}{\partial \mu} \right)_T = - \sum_a \int d\Gamma_a^* \left(\frac{\partial E_a}{\partial \mu} \right)_T f_a^{\rm eq} \,. \tag{4.83}$$

We remark that Eqs. (4.82) and (4.83) are simply Eqs. (C.29) and (C.30), which we derived in Appendix C by a different argument; namely, from conservation of energy and momentum.

Hence we conclude

$$\delta U = - \sum_a \int d\Gamma_a^* \delta E_a f_a^{\rm eq} \,, \tag{4.84}$$

where $E_a = E_a^* + g_{\omega a} \bar{\omega}^0$ and

$$\delta E_a = \frac{m_a^*}{E_a^*} \delta m_a^* + g_{\omega a} \delta \bar{\omega}^0 \,. \tag{4.85}$$

Now we come to the deviation in the quasiparticle distribution function. The f_a in general will have departures from the equilibrium form, but it can also change because the quasiparticle energy departs from its equilibrium value. Let us denote E_a^0 the

equilibrium value and E_a the total nonequilibrium energy; it is the latter which is conserved in the particle collisions. Similarly, we denote T^0 and μ^0 the equilibrium values. Then we write

$$\begin{aligned} f_a(E_a, T, \mu) &= f_a^{\rm eq}(E_a^0, T^0, \mu^0) + \delta f_a \,, \\ f_a(E_a, T, \mu) &= f_a^{\rm eq}(E_a, T^0, \mu^0) + \delta \tilde{f}_a \,. \end{aligned} \tag{4.86}$$

The deviations are related to each other by

$$\delta f_a = \delta \tilde{f}_a + \left(\frac{\partial f_a^{\rm eq}}{\partial E_a} \right)_{T^0,\,\mu^0} \delta E_a = \delta \tilde{f}_a - \frac{\delta E_a}{T} f_a^{\rm eq} \tag{4.87}$$

where the second equality follows when using classical statistics.

It is always the $\delta \tilde{f}_a$ which determine the transport coefficients. The reason is that since E_a is conserved in particle collisions, the collision integral must be expanded about E and not E_a^0. Therefore we express δT^{ij} in terms of $\delta \tilde{f}_a$ instead of δf_a.

$$\begin{aligned} \delta T^{ij} &= \sum_a \int d\Gamma_a^* \frac{p_a^{*i} p_a^{*j}}{E_a^*} \delta \tilde{f}_a - \sum_a \int d\Gamma_a^* \frac{p_a^{*i} p_a^{*j}}{E_a^*} \left(\frac{\delta E_a}{T} + \frac{\delta E_a^*}{E_a^*} \right) f_a^{\rm eq} \\ &+ \delta^{ij} \sum_a \int d\Gamma_a^* \delta E_a f_a^{\rm eq} \end{aligned} \tag{4.88}$$

The integrand of the second term depends only on the magnitude of $\mathbf{p}_a^*$, apart from the factor $p_a^{*i} p_a^{*j}$. Therefore, one may effectively make the replacement $p_a^{*i} p_a^{*j} \to \frac{1}{3} |\mathbf{p}_a^*|^2 \delta^{ij}$. Then the terms not involving $\delta \tilde{f}_a$ all have a factor of δ^{ij}. They can be written as a sum of

$$\delta \bar{\omega}^0 \sum_a g_{\omega a} \int d\Gamma_a^* \left(1 - \frac{|\mathbf{p}_a^*|^2}{3 T E_a^*} \right) f_a^{\rm eq} \tag{4.89}$$

and

$$\sum_a \delta m_a^* \int d\Gamma_a^* \frac{m_a^*}{E_a^*} \left(1 - \frac{|\mathbf{p}_a^*|^2}{3 T E_a^*} - \frac{|\mathbf{p}_a^*|^2}{3 E_a^{*2}} \right) f_a^{\rm eq} \,. \tag{4.90}$$

It can be shown that both of these integrate to zero using classical statistics. (For both integrals, the trick is to change the integration variable from p_a^* to E_a^*, then rewrite

$$-\frac{f_a^{\rm eq}}{T} = \frac{\partial f_a^{\rm eq}}{\partial E_a^*} \tag{4.91}$$

and integrate that term by parts, then convert the integration variable back to p_a^*.) Hence we find

$$\delta T^{ij} = \sum_a \int d\Gamma_a^* \frac{p_a^{*i} p_a^{*j}}{E_a^*} \delta \tilde{f}_a \tag{4.92}$$

as our final result.

The variation in the time-time component of the energy-momentum tensor, starting with either Eq. (4.36) or (4.37), is

$$\delta T^{00} = \sum_a \int d\Gamma_a^* E_a \delta f_a \,. \tag{4.93}$$

We use Eq. (4.87) for δf_a. The variation of the local energy E_a

$$\delta E_a = \frac{\delta m_a^{*2}}{2E_a^*} + g_{\omega a}\delta\bar{\omega}^0 \tag{4.94}$$

can be expressed in terms of the variations in temperature and chemical potential

$$\delta m_a^{*2} = \left(\frac{\partial m_a^{*2}}{\partial T}\right)_\mu \delta T + \left(\frac{\partial m_a^{*2}}{\partial \mu}\right)_T \delta\mu \,, \tag{4.95}$$

$$\delta\bar{\omega}^0 = \left(\frac{\partial \bar{\omega}^0}{\partial T}\right)_\mu \delta T + \left(\frac{\partial \bar{\omega}^0}{\partial \mu}\right)_T \delta\mu \,. \tag{4.96}$$

The variations δT and $\delta\mu$ are not independent. They are related by the hydrodynamic flow of the matter which to this order occurs at constant entropy per baryon $\sigma = s/n$. (See Appendix B for further discussion.) Dissipation should not be included since it would lead to second-order effects which are consistently neglected in first-order viscous fluid dynamics. The relation can be expressed in various ways, including these:

$$\left(\frac{\partial\mu}{\partial T}\right)_\sigma = \frac{\mu}{T}\frac{v_s^2}{v_n^2} = \frac{1}{T}\left[\mu + \frac{1}{v_n^2}\left(\frac{\partial P}{\partial n}\right)_\epsilon\right] = \frac{\chi_{TT} - \sigma\chi_{T\mu}}{\sigma\chi_{\mu\mu} - \chi_{\mu T}} \,. \tag{4.97}$$

Here $v_x^2 = (\partial P/\partial\epsilon)_x$ is the speed of sound at constant x. It is easily shown that

$$\begin{aligned} v_n^2 &= \frac{s\chi_{\mu\mu} - n\chi_{\mu T}}{T(\chi_{TT}\chi_{\mu\mu} - \chi_{\mu T}^2)} \,, \\ v_s^2 &= \frac{n\chi_{TT} - s\chi_{\mu T}}{\mu(\chi_{TT}\chi_{\mu\mu} - \chi_{\mu T}^2)} \,, \\ v_\sigma^2 &= \frac{v_n^2 Ts + v_s^2\mu n}{w} \,, \end{aligned} \tag{4.98}$$

relationships that are independent of the specific equation of state. Of course waves do not physically propagate at constant n or s, only at constant σ, but these definitions are useful for various intermediate steps in various applications. The other symbol represents the susceptibilities

$$\chi_{xy} = \frac{\partial^2 P(T,\mu)}{\partial x \partial y} \,. \tag{4.99}$$

Rather than thinking of m_a^* and $\bar{\omega}^0$ as functions of T and μ we can think of them as functions of T and σ. Then

$$\delta m_a^{*2} = \left(\frac{\partial m_a^{*2}}{\partial T}\right)_\sigma \delta T\,, \tag{4.100}$$

$$\delta \bar{\omega}^0 = \left(\frac{\partial \bar{\omega}^0}{\partial T}\right)_\sigma \delta T\,. \tag{4.101}$$

Next, we need to relate the variations in T and μ to the variation $\delta\tilde{f}_a$. The latter variation is done at fixed E_a and is

$$\delta\tilde{f}_a = f_a^{\rm eq}\left[E_a - \mu_a + T\left(\frac{\partial \mu_a}{\partial T}\right)_\sigma\right]\frac{\delta T}{T^2}\,. \tag{4.102}$$

(Recall that $\mu_a = b_a\mu$.) The term from Eq. (4.87) which needs to be rewritten is

$$\begin{aligned}\frac{\delta E_a}{T} f_a^{\rm eq} &= \frac{1}{E_a^*}\left[\frac{T^2\left(\partial m_a^{*2}/\partial T^2\right)_\sigma + g_{\omega a} T\left(\partial\bar{\omega}^0/\partial T\right)_\sigma E_a^*}{E_a - \mu_a + T\left(\partial\mu_a/\partial T\right)_\sigma}\right]\delta\tilde{f}_a \\ &= \left[\frac{T(\partial E_a/\partial T)_\sigma}{E_a - \mu_a + T\left(\partial\mu_a/\partial T\right)_\sigma}\right]\delta\tilde{f}_a\,. \end{aligned}\tag{4.103}$$

We reiterate that the temperature derivative of a function F depending on T and μ, taken at fixed entropy per baryon, is

$$\left(\frac{\partial F}{\partial T}\right)_\sigma = \left(\frac{\partial F}{\partial T}\right)_\mu + \left(\frac{\partial F}{\partial \mu}\right)_T\left(\frac{\partial \mu}{\partial T}\right)_\sigma = \left(\frac{\partial F}{\partial T}\right)_\mu + \frac{\mu}{T}\frac{v_s^2}{v_n^2}\left(\frac{\partial F}{\partial \mu}\right)_T\,. \tag{4.104}$$

The final expression is therefore

$$\delta T^{00} = \sum_a \int d\Gamma_a^* E_a\left\{1 - \frac{T(\partial E_a/\partial T)_\sigma}{E_a - \mu_a + T\left(\partial\mu_a/\partial T\right)_\sigma}\right\}\delta\tilde{f}_a\,. \tag{4.105}$$

When the baryon density goes to zero this reduces to the formula known in the literature.

The time-space component has the very natural form

$$\delta T^{0j} = \sum_a \int d\Gamma_a^* \frac{p_a^{*j}}{E_a^*} E_a \delta f_a\,. \tag{4.106}$$

To express this in terms of $\delta\tilde{f}_a$, we note that the last term on the right-hand-side of Eq. (4.87) is spherically symmetric in momentum space and therefore that term integrates

to zero. This is not true of the other term because the deviation ϕ_a does have terms that depend on the direction of the momentum. Therefore

$$\delta T^{0j} = \sum_a \int d\Gamma_a^* \frac{p_a^{*j}}{E_a^*} E_a \delta \tilde{f}_a \,. \tag{4.107}$$

Lastly we need the variations in the baryon current. The steps are by now very familiar. The results are

$$\delta J^0 = \sum_a b_a \int d\Gamma_a^* \left\{ 1 - \frac{T(\partial E_a/\partial T)_\sigma}{E_a - \mu_a + T\left(\partial \mu_a/\partial T\right)_\sigma} \right\} \delta \tilde{f}_a \tag{4.108}$$

and

$$\delta J^i = \sum_a b_a \int d\Gamma_a^* \frac{p_a^{*i}}{E_a^*} \delta \tilde{f}_a \,. \tag{4.109}$$

4.7 General Formulas for the Transport Coefficients

Suppose that we know the scalars A_a, B_a, and C_a in Eq. (4.79) as functions of the magnitude of the momentum $\mathbf{p}_a^*$. Then in the local rest frame we should equate the hydrodynamic expression ΔT^{ij} from Eq. (4.31) with the quasiparticle expression δT^{ij} from Eq. (4.92), the latter being

$$\begin{aligned} \delta T^{ij} &= \sum_a \int d\Gamma_a^* \frac{p_a^{*i} p_a^{*j}}{E_a^*} \Big[- A_a \partial_\rho u^\rho - B_a p_a^\nu D_\nu \left(\frac{\mu}{T}\right) \\ &+ C_a p_a^\mu p_a^\nu \left(D_\mu u_\nu + D_\nu u_\mu + \tfrac{2}{3} \Delta_{\mu\nu} \partial_\rho u^\rho \right) \Big] f_a^{\rm eq} \,. \end{aligned} \tag{4.110}$$

The B_a integrates to zero by symmetry. In the local rest frame the derivative $\partial_k u_0 = 0$, so the the summation over μ and ν is a sum over spatial indices kl only. In the A_a term we can use

$$p_a^{*i} p_a^{*j} \to \tfrac{1}{3} |\mathbf{p}_a^*|^2 \delta_{ij}$$

and in the C_a term we can use

$$p_a^{*i} p_a^{*j} p_a^{*k} p_a^{*l} \to \tfrac{1}{15} |\mathbf{p}_a^*|^4 (\delta_{ij}\delta_{kl} + \delta_{ik}\delta_{jl} + \delta_{il}\delta_{jk})$$

because in the local rest frame $\mathbf{p} = \mathbf{p}^*$. Equating the tensorial structures then gives us the shear viscosity

$$\eta = \frac{2}{15} \sum_a \int d\Gamma_a^* \frac{|\mathbf{p}_a^*|^4}{E_a^*} f_a^{\rm eq} C_a \tag{4.111}$$

and the bulk viscosity

$$\zeta = \frac{1}{3}\sum_a \int d\Gamma_a^* \frac{|\mathbf{p}_a^*|^2}{E_a^*} f_a^{\rm eq} A_a \,. \tag{4.112}$$

For the baryon current we compare the ΔJ^i from Eq. (4.32) with the dissipative part of Eq. (4.43) in the local rest frame. The latter is

$$\delta J^i = \sum_a b_a \int d\Gamma_a^* \frac{p_a^{*i}}{E_a^*} \left[-B_a p_a^\nu D_\nu \left(\frac{\mu}{T}\right)\right] f_a^{\rm eq} \,. \tag{4.113}$$

Obviously the A_a and C_a terms integrate to zero on account of symmetry. After some manipulation this results in an expression for the thermal conductivity

$$\lambda = \frac{1}{3}\left(\frac{w}{nT}\right)^2 \sum_a b_a \int d\Gamma_a^* \frac{|\mathbf{p}_a^*|^2}{E_a^*} f_a^{\rm eq} B_a \,. \tag{4.114}$$

To solve for the functions A_a, B_a, and C_a we turn to the Chapman-Enskog method. This entails expanding both sides of the Boltzmann equation (4.25) to first order in the ϕ_a. It leads to integral equations which in general must be solved numerically.

Here we follow the notation of Ref. [76]. Including 2-to-2, 2-to-1 and 1-to-2 processes, and using classical statistics (these restrictions are easily relaxed) the collision integral is

$$\begin{aligned} \mathcal{C}_a \;=\; & \sum_{bcd} \frac{1}{1+\delta_{ab}} \int d\Gamma_b^*\, d\Gamma_c^*\, d\Gamma_d^*\, W(a,b|c,d)\{f_c f_d - f_a f_b\} \\ & + \sum_{cd} \int d\Gamma_c^*\, d\Gamma_d^*\, W(a|c,d)\{f_c f_d - f_a\} \\ & + \sum_{bc} \int d\Gamma_b^*\, d\Gamma_c^*\, W(c|a,b)\{f_c - f_a f_b\} \,. \end{aligned} \tag{4.115}$$

The W are given as

$$W(a,b|c,d) = \frac{(2\pi)^4 \delta^4(p_a + p_b - p_c - p_d)}{2E_a^* 2E_b^* 2E_c^* 2E_d^*} |\overline{\mathcal{M}(a,b|c,d)}|^2 \tag{4.116}$$

and

$$W(a|c,d) = \frac{(2\pi)^4 \delta^4(p_a - p_c - p_d)}{2E_a^* 2E_c^* 2E_d^*} |\overline{\mathcal{M}(a|c,d)}|^2 \,. \tag{4.117}$$

The use of E_a^* instead of E_a in the denominators ensures that the phase space integration is Lorentz covariant. Also note that, following Larionov [121], we use dimensionless

matrix elements $\mathcal{M}$ averaged over spin in both initial and final states. This is necessary to balance the degeneracy factors in the $d\Gamma_a^*$. We use chemical equilibrium (for example, $a+b \leftrightarrow c+d$ gives $f_a^{\rm eq} f_b^{\rm eq} = f_c^{\rm eq} f_d^{\rm eq}$.) Then the collision integral becomes

$$\begin{aligned}
\mathcal{C}_a &= f_a^{\rm eq} \sum_{bcd} \frac{1}{1+\delta_{ab}} \int d\Gamma_b^*\, d\Gamma_c^*\, d\Gamma_d^*\, f_b^{\rm eq} W(a,b|c,d)\, [\phi_c + \phi_d - \phi_a - \phi_b] \\
&+ f_a^{\rm eq} \sum_{cd} \int d\Gamma_c^*\, d\Gamma_d^*\, W(a|c,d)\, [\phi_c + \phi_d - \phi_a] \\
&+ f_a^{\rm eq} \sum_{bc} \int d\Gamma_b^*\, d\Gamma_c^*\, f_b^{\rm eq} W(c|a,b)\, [\phi_c - \phi_a - \phi_b] \; . \qquad (4.118)
\end{aligned}$$

This constitutes the right-hand-side of the Boltzmann equation.

The left-hand-side of the Boltzmann equation (4.25) is computed using the local equilibrium form of the distribution function

$$f_a^{\rm eq}(x,\mathbf{p}^*) = \exp\left[-\frac{u_\alpha(x) p_a^\alpha}{T(x)}\right] \exp\left[\frac{\mu_a(x)}{T(x)}\right] = \exp\left[-\frac{u_\alpha(x) p_a^{*\alpha}}{T(x)}\right] \exp\left[\frac{\mu_a^*(x)}{T(x)}\right] \; . \qquad (4.119)$$

Here the flow velocity, temperature and chemical potential all depend on x. Although not explicitly indicated, p_a^α depends on x via the dependence of m_a^* and $\bar{\omega}^\alpha$ on x, while E_a^* depends on x via m_a^* only. The left-hand-side must be expressed in terms of the same space-time gradients as ϕ_a, namely $\partial_\rho u^\rho$, $D_\nu\,(\mu/T)$, and $\left(D_\mu u_\nu + D_\nu u_\mu + \frac{2}{3}\Delta_{\mu\nu}\partial_\rho u^\rho\right)$. The derivation is long and tedious; hence, it is left to Appendix D. Space-time derivatives of T and μ are expressed in terms of the relevant tensor structures by using the ideal fluid dynamics equations for conservation of energy, momentum and baryon number. Some useful intermediate results are

$$\begin{aligned}
DT &= -v_n^2 T\, \partial_\rho u^\rho \, , \\
D\mu &= -v_s^2 \mu\, \partial_\rho u^\rho \, . \qquad (4.120)
\end{aligned}$$

To facilitate comparison to other works (e.g., Ref. [112]), we note that the prior equations are often written in an equivalent form

$$\begin{aligned}
DT &= -T \left(\frac{\partial P}{\partial \epsilon}\right)_n \partial_\rho u^\rho \, , \\
D\mu &= -\left[\mu \left(\frac{\partial P}{\partial \epsilon}\right)_n + \left(\frac{\partial P}{\partial n}\right)_\epsilon\right] \partial_\rho u^\rho \, . \qquad (4.121)
\end{aligned}$$

Thus we can also write

$$v_s^2 = \left(\frac{\partial P}{\partial \epsilon}\right)_n + \frac{1}{\mu}\left(\frac{\partial P}{\partial n}\right)_\epsilon . \tag{4.122}$$

However, throughout this chapter we shall use Eq. (4.120) and forgo the forms found in (4.121).

In Appendix D, we show that one form of the left-hand-side of the Boltzmann equation (in the local rest frame) is

$$\begin{aligned}
\frac{df_a^{\rm eq}}{dt} &= f_a^{\rm eq}\left[\frac{|\mathbf{p}_a^*|^2}{3TE_a^*} + v_n^2 T\frac{\partial}{\partial T}\left(\frac{E_a-\mu_a}{T}\right)_\sigma\right]\partial_\rho u^\rho \\
&+ f_a^{\rm eq}\left(b_a - \frac{nE_a}{w}\right)\frac{p_a^\mu}{E_a^*}D_\mu\left(\frac{\mu}{T}\right) \\
&- f_a^{\rm eq}\frac{p_a^\mu p_a^\nu}{2TE_a^*}\left(D_\mu u_\nu + D_\nu u_\mu + \frac{2}{3}\Delta_{\mu\nu}\partial_\rho u^\rho\right) .
\end{aligned} \tag{4.123}$$

Now $E_a - \mu_a$ in the first line could be replaced by $E_a^* - \mu_a^*$, and E_a in the second line could be replaced by $E_a^* + g_{\omega a}\bar{\omega}^0$. With a little manipulation this can be shown to be equivalent to Sasaki and Redlich [112] who, however, did not include a vector field nor the $D_\mu(\mu/T)$ term. Another form is to write out the derivatives in the first line explicitly. This results in

$$\begin{aligned}
\frac{df_a^{\rm eq}}{dt} &= f_a^{\rm eq}\frac{1}{3TE_a^*}\left\{|\mathbf{p}_a^*|^2 - 3v_n^2\left[E_a^{*2} - T^2\left(\frac{\partial m_a^{*2}}{\partial T^2}\right)_\sigma + T^2\frac{\partial}{\partial T}\left(\frac{\mu_a^*}{T}\right)_\sigma E_a^*\right]\right\}\partial_\rho u^\rho \\
&+ f_a^{\rm eq}\left(b_a - \frac{nE_a}{w}\right)\frac{p_a^\mu}{E_a^*}D_\mu\left(\frac{\mu}{T}\right) \\
&- f_a^{\rm eq}\frac{p_a^\mu p_a^\nu}{2TE_a^*}\left(D_\mu u_\nu + D_\nu u_\mu + \frac{2}{3}\Delta_{\mu\nu}\partial_\rho u^\rho\right) .
\end{aligned} \tag{4.124}$$

In the limit that the chemical potential goes to zero this reproduces the results of Jeon and Yaffe [89] and of Chakraborty and Kapusta [76].

Now we subtract the right-hand-side from the left-hand-side and set the resulting expression to zero. This leads to

$$\mathcal{A}_a\left(\partial_\rho u^\rho\right) + \mathcal{B}_a^\mu D_\mu\left(\frac{\mu}{T}\right) - \mathcal{C}_a^{\mu\nu}\left(D_\mu u_\nu + D_\nu u_\mu + \tfrac{2}{3}\Delta_{\mu\nu}\partial_\rho u^\rho\right) = 0 \tag{4.125}$$

where

$$\mathcal{A}_a = \frac{1}{3TE_a^*}\left\{|\mathbf{p}_a^*|^2 - 3v_n^2\left[E_a^{*2} - T^2\left(\frac{\partial m_a^{*2}}{\partial T^2}\right)_\sigma + T^2\frac{\partial}{\partial T}\left(\frac{\mu_a^*}{T}\right)_\sigma E_a^*\right]\right\}$$

$$
\begin{aligned}
&+ \sum_{bcd} \frac{1}{1+\delta_{ab}} \int d\Gamma_b^* \, d\Gamma_c^* \, d\Gamma_d^* \, f_b^{\rm eq} \, W(a,b|c,d) \, [A_c + A_d - A_a - A_b] \\
&+ \sum_{cd} \int d\Gamma_c^* \, d\Gamma_d^* \, W(a|c,d) \, [A_c + A_d - A_a] \\
&+ \sum_{bc} \int d\Gamma_b^* \, d\Gamma_c^* \, f_b^{\rm eq} \, W(c|a,b) \, [A_c - A_a - A_b] \qquad (4.126)
\end{aligned}
$$

and

$$
\begin{aligned}
\mathcal{B}_a^\mu &= \left(b_a - \frac{nE_a}{w} \right) \frac{p_a^\mu}{E_a^*} \\
&+ \sum_{bcd} \frac{1}{1+\delta_{ab}} \int d\Gamma_b^* \, d\Gamma_c^* \, d\Gamma_d^* \, f_b^{\rm eq} \, W(a,b|c,d) \left[B_c p_c^\mu + B_d p_d^\mu - B_a p_a^\mu - B_b p_b^\mu \right] \\
&+ \sum_{cd} \int d\Gamma_c^* \, d\Gamma_d^* \, W(a|c,d) \left[B_c p_c^\mu + B_d p_d^\mu - B_a p_a^\mu \right] \\
&+ \sum_{bc} \int d\Gamma_b^* \, d\Gamma_c^* \, f_b^{\rm eq} \, W(c|a,b) \left[B_c p_c^\mu - B_a p_a^\mu - B_b p_b^\mu \right] \qquad (4.127)
\end{aligned}
$$

and

$$
\begin{aligned}
\mathcal{C}_a^{\mu\nu} &= \frac{p_a^\mu p_a^\nu}{2E_a^* T} \\
&+ \sum_{bcd} \frac{1}{1+\delta_{ab}} \int d\Gamma_b^* \, d\Gamma_c^* \, d\Gamma_d^* \, f_b^{\rm eq} \, W(a,b|c,d) \left[C_c p_c^\mu p_c^\nu + C_d p_d^\mu p_d^\nu - C_a p_a^\mu p_a^\nu - C_b p_b^\mu p_b^\nu \right] \\
&+ \sum_{cd} \int d\Gamma_c^* \, d\Gamma_d^* \, W(a|c,d) \left[C_c p_c^\mu p_c^\nu + C_d p_d^\mu p_d^\nu - C_a p_a^\mu p_a^\nu \right] \\
&+ \sum_{bc} \int d\Gamma_b^* \, d\Gamma_c^* \, f_b^{\rm eq} \, W(c|a,b) \left[C_a p_a^\mu p_a^\nu + C_b p_b^\mu p_b^\nu - C_c p_c^\mu p_c^\nu \right] . \qquad (4.128)
\end{aligned}
$$

Due to the tensorial structure of these equations the solution requires that $\mathcal{A}_a = 0$, $\mathcal{B}_a^\mu = 0$, and $\mathcal{C}_a^{\mu\nu} = 0$. These are integral equations for the functions A_a, B_a, and C_a which depend on the magnitude of the momentum $\mathbf{p}^*$. In general, these integral equations may be solved numerically to compute particular solutions for A_a, B_a, and C_a.

4.8 Landau-Lifshtiz Conditions of Fit

The set of equations (4.126)-(4.128) are integral equations for the functions A_a, B_a, and C_a. Consider the equation for A_a. If we have a particular solution $A_a^{\rm par}$, we can generate

another solution $A_a = A_a^{\rm par} - a_E E_a - a_B b_a$ where the constant coefficients a_E and a_B are independent of particle type a. The reason is that energy and baryon number are conserved in the collision, decay, and fusion processes. Thus, if one inserts A_a into Eq. (4.126), the E_a and b_a terms are canceled out, so the equation is identical whether using A_a or $A_a^{\rm par}$. Thus, we need additional constraints to select a unique solution. (Very loosely speaking, a similar phenomena occurs when solving differential equations: one typically finds a family of solutions and requires initial or boundary conditions to select a unique solution.)

Physically, this arbitrariness exists because of the freedom to define the local rest frame or, equivalently, the flow four-velocity u^μ. For example, using the Landau-Lifshitz definition, fluid velocity is defined as the velocity of energy flow. In the alternative Eckart definition, it is the velocity of baryon charge flow. We choose the Landau-Lifshitz definition in this thesis.

Hence, we remove this arbitrariness from our equations by imposing the Landau-Lifshitz conditions of fit. Mathematically, the conditions (in the rest frame) are

$$\delta J^0 = 0 \tag{4.129}$$

$$\delta T^{0\nu} = 0\,. \tag{4.130}$$

Requiring that $\delta T^{00} = 0$ in the local rest frame results in

$$\begin{aligned} & a_E \sum_a \int d\Gamma_a^* E_a^2 \left[1 - \frac{T(\partial E_a/\partial T)_\sigma}{E_a - \mu_a + T\left(\partial \mu_a/\partial T\right)_\sigma}\right] f_a^{\rm eq} \\ & + a_B \sum_a b_a \int d\Gamma_a^* E_a \left[1 - \frac{T(\partial E_a/\partial T)_\sigma}{E_a - \mu_a + T\left(\partial \mu_a/\partial T\right)_\sigma}\right] f_a^{\rm eq} \\ & = \sum_a \int d\Gamma_a^* E_a \left[1 - \frac{T(\partial E_a/\partial T)_\sigma}{E_a - \mu_a + T\left(\partial \mu_a/\partial T\right)_\sigma}\right] A_a^{\rm par}\, f_a^{\rm eq}\,. \end{aligned} \tag{4.131}$$

Requiring that $\delta J^0 = 0$ in the local rest frame results in

$$\begin{aligned} & a_E \sum_a b_a \int d\Gamma_a^* E_a \left[1 - \frac{T(\partial E_a/\partial T)_\sigma}{E_a - \mu_a + T\left(\partial \mu_a/\partial T\right)_\sigma}\right] f_a^{\rm eq} \\ & + a_B \sum_a b_a^2 \int d\Gamma_a^* \left[1 - \frac{T(\partial E_a/\partial T)_\sigma}{E_a - \mu_a + T\left(\partial \mu_a/\partial T\right)_\sigma}\right] f_a^{\rm eq} \end{aligned}$$

$$= \sum_a b_a \int d\Gamma_a^* \left[1 - \frac{T(\partial E_a/\partial T)_\sigma}{E_a - \mu_a + T\left(\partial \mu_a/\partial T\right)_\sigma}\right] A_a^{\rm par}\, f_a^{\rm eq}\,. \tag{4.132}$$

Let us express these equations as

$$\begin{aligned} a_E X_E + a_B X_B &= Z_E\,, \\ a_E Y_E + a_B Y_B &= Z_B\,. \end{aligned} \tag{4.133}$$

The solutions are

$$\begin{aligned} a_B &= \frac{Y_E Z_E - X_E Z_B}{Y_E X_B - X_E Y_B}\,, \\ a_E &= \frac{X_B Z_B - Y_B Z_E}{Y_E X_B - X_E Y_B}\,. \end{aligned} \tag{4.134}$$

When these are substituted into the expression (4.112) for the bulk viscosity we get

$$\zeta = \frac{1}{3}\sum_a \int d\Gamma_a^* \frac{|\mathbf{p}_a^*|^2}{E_a^*} f_a^{\rm eq} A_a - T n a_B - T w a_E\,. \tag{4.135}$$

It is not easy to find simple expressions for X_E, X_B, Y_E, Y_B when mean fields are included, hence there are no simple expressions for a_E and a_B. Fortunately, the individual expressions for a_E and a_B are not needed to find a simple expression for the bulk viscosity. Returning to Eq. (4.112) we have

$$\zeta = \frac{1}{3}\sum_a \int d\Gamma_a^* \frac{|\mathbf{p}_a^*|^2}{E_a^*} f_a^{\rm eq} (A_a^{\rm par} - a_E E_a - a_B b_a)\,. \tag{4.136}$$

Now the trick is to take a clever combination of the conditions of fit. Add $T\left(\partial\mu/\partial T\right)_\sigma - \mu$ times (4.132) to (4.131). This gives

$$\begin{aligned} a_B \sum_a b_a \int d\Gamma_a^* \left(\frac{\partial f_a^{\rm eq}}{\partial T}\right)_\sigma + a_E \sum_a \int d\Gamma_a^* E_a \left(\frac{\partial f_a^{\rm eq}}{\partial T}\right)_\sigma \\ = -\sum_a \int d\Gamma_a^* f_a^{\rm eq} A_a^{\rm par} \frac{\partial}{\partial T}\left(\frac{E_a - \mu_a}{T}\right)_\sigma\,. \end{aligned} \tag{4.137}$$

The coefficient of a_B is just $(\partial n/\partial T)_\sigma$, and from Eq. (4.93) the coefficient of a_E is just $(\partial \epsilon/\partial T)_\sigma$. Therefore we have

$$a_B \left(\frac{\partial n}{\partial T}\right)_\sigma + a_E \left(\frac{\partial \epsilon}{\partial T}\right)_\sigma = -\sum_a \int d\Gamma_a^* f_a^{\rm eq} A_a^{\rm par} \frac{\partial}{\partial T}\left(\frac{E_a - \mu_a}{T}\right)_\sigma\,. \tag{4.138}$$

Next, we need to derive the thermodynamic relations

$$Tv_n^2 = \frac{w}{(\partial\epsilon/\partial T)_\sigma} = \frac{n}{(\partial n/\partial T)_\sigma}\,. \tag{4.139}$$

First, we derive the relation between the derivatives appearing in the above equations. Using $d\epsilon = Tds + \mu dn$ and $ds = nd\sigma + \sigma dn$, we obtain

$$\left(\frac{\partial\epsilon}{\partial T}\right)_\sigma = \frac{w}{n}\left(\frac{\partial n}{\partial T}\right)_\sigma\,. \tag{4.140}$$

Now for $(\partial n/\partial T)_\sigma$ we use Eq. (4.104), the third equality of Eq. (4.97), and the first equality of Eq. (4.98) to obtain

$$T\left(\frac{\partial n}{\partial T}\right)_\sigma = \frac{n}{v_n^2}\,. \tag{4.141}$$

Together with the previous equation we obtain the desired result (4.139). Using these results in Eq. (4.138) we have

$$Tna_B + Twa_E = -v_n^2T^2\sum_a\int d\Gamma_a^* f_a^{\rm eq}A_a^{\rm par}\frac{\partial}{\partial T}\left(\frac{E_a-\mu_a}{T}\right)_\sigma\,. \tag{4.142}$$

Making this substitution in Eq. (4.135) we obtain the expression

$$\zeta = \frac{1}{3}\sum_a\int d\Gamma_a^*\left[\frac{|\mathbf{p}_a^*|^2}{E_a^*} + 3v_n^2T^2\frac{\partial}{\partial T}\left(\frac{E_a-\mu_a}{T}\right)_\sigma\right]A_a^{\rm par}f_a^{\rm eq}\,, \tag{4.143}$$

This makes perfect sense because the modification of the integrand compared to Eq. (4.112) matches the structure of the source of A_a in Eq. (4.126).

A similar arbitrariness arises in Eq. (4.127). Due to energy-momentum conservation, if we have a particular solution $B_a^{\rm par}$ we can generate another solution as $B_a = B_a^{\rm par} - b$, where b is a constant independent of particle species a. This freedom is resolved by the Landau-Lifshitz condition of fit which requires that $\delta T^{0j} = 0$ in the local rest frame. Starting with expression (4.107) we have

$$\delta T^{0j} = \sum_a\int d\Gamma_a^*\frac{p_a^{*j}}{E_a^*}E_a\left[-\left(B_a^{\rm par}-b\right)p_a^{*i}D_i\left(\frac{\mu}{T}\right)\right]f_a^{\rm eq}\,. \tag{4.144}$$

Factoring out the spatial derivative, and making use of the momentum space isotropy, we require that

$$b\sum_a\int d\Gamma_a^*\frac{|\mathbf{p}_a^*|^2}{E_a^*}E_af_a^{\rm eq} = \int d\Gamma_a^*\frac{|\mathbf{p}_a^*|^2}{E_a^*}E_aB_a^{\rm par}f_a^{\rm eq}\,. \tag{4.145}$$

The integral multiplying b is just $3Tw$ so that

$$b = \frac{1}{3Tw} \int d\Gamma_a^* \frac{|\mathbf{p}_a^*|^2}{E_a^*} E_a B_a^{\rm par} f_a^{\rm eq} \,. \tag{4.146}$$

Substitution into expression (4.114) gives

$$\lambda = \frac{1}{3} \left(\frac{w}{nT}\right)^2 \sum_a \int d\Gamma_a^* \frac{|\mathbf{p}_a^*|^2}{E_a^*} \left(b_a - \frac{nE_a}{w}\right) B_a^{\rm par} f_a^{\rm eq} \,. \tag{4.147}$$

There is no ambiguity in the solution to Eq. (4.128) for C_a, so the expression for the shear viscosity (4.111) is unchanged.

4.9 Relaxation-Time Approximation

At this point, it is convenient to derive the relaxation time approximation formulas for the shear and bulk viscosities and thermal conductivity. We start with the Boltzmann equation with the Chapman-Enskog expansion:

$$\frac{df_a^{\rm eq}}{dt} = \mathcal{C}_a \,. \tag{4.148}$$

The left-hand-side of Eq. (4.148) is given by Eq. (4.123) while $\mathcal{C}_a$ can be found in Eq. (4.118). In the energy-dependent relaxation time approximation [76], we assume particle species a is out of equilibrium ($\phi_a \neq 0$) while all other particle species are in equilibrium ($\phi_b = \phi_c = \phi_d = 0$). Using Eq. (4.118), the collision integral $\mathcal{C}_a$ greatly simplifies, and the Boltzmann equation becomes

$$\frac{df_a^{\rm eq}}{dt} = \mathcal{C}_a = -\frac{f_a^{\rm eq}\phi_a}{\tau_a} \tag{4.149}$$

where the relaxation time $\tau_a(E_a^*)$ for species a is given by

$$\begin{aligned} \frac{1}{\tau_a(E_a^*)} &= \sum_{bcd} \frac{1}{1+\delta_{ab}} \int d\Gamma_b^* \, d\Gamma_c^* \, d\Gamma_d^* \, f_b^{\rm eq} W(a,b|c,d) \\ &+ \sum_{cd} \int d\Gamma_c^* \, d\Gamma_d^* \, W(a|c,d) \\ &+ \sum_{bc} \int d\Gamma_b^* \, d\Gamma_c^* \, f_b^{\rm eq} W(c|a,b) \,. \end{aligned} \tag{4.150}$$

Next, we replace the left-hand-side of Eq. (4.149) using Eq. (4.123). Into the right-hand-side, we substitute ϕ_a using Eq. (4.79). Then we equate terms on the left- and right-hand-sides by matching tensor structures, and we obtain particular solutions for the functions A_a, B_a, and C_a from ϕ_a:

$$A_a^{\text{par}} = \frac{\tau_a}{3T}\left[\frac{|\mathbf{p}_a^*|^2}{E_a^*} + 3v_n^2 T^2 \frac{\partial}{\partial T}\left(\frac{E_a - \mu_a}{T}\right)_\sigma\right], \tag{4.151}$$

$$B_a^{\text{par}} = \frac{\tau_a}{E_a^*}\left(b_a - \frac{nE_a}{w}\right), \tag{4.152}$$

$$C_a^{\text{par}} = \frac{\tau_a}{2TE_a^*}. \tag{4.153}$$

Finally, we substitute Eqs. (4.151)-(4.153) into Eqs. (4.111), (4.143), and (4.147) and obtain the desired relaxation time formulas:

$$\eta = \frac{1}{15T}\sum_a \int d\Gamma_a^* \frac{|\mathbf{p}_a^*|^4}{E_a^{*2}} \tau_a(E_a^*) f_a^{\text{eq}}, \tag{4.154}$$

$$\zeta = \frac{1}{9T}\sum_a \int d\Gamma_a^* \frac{\tau_a(E_a^*)}{E_a^{*2}}\left[|\mathbf{p}_a^*|^2 + 3v_n^2 T^2 E_a^* \frac{\partial}{\partial T}\left(\frac{E_a - \mu_a}{T}\right)_\sigma\right]^2 f_a^{\text{eq}}, \tag{4.155}$$

$$\lambda = \frac{1}{3}\left(\frac{w}{nT}\right)^2 \sum_a \int d\Gamma_a^* \frac{|\mathbf{p}_a^*|^2}{E_a^{*2}} \tau_a(E_a^*)\left(b_a - \frac{nE_a}{w}\right)^2 f_a^{\text{eq}}. \tag{4.156}$$

A few observations are in order. First, the transport coefficients computed with Eqs. (4.154)-(4.156) are strictly non-negative, as they must be. Second, this non-negativity is ensured by the squares in the integrands which came from enforcing the Landau-Lifshitz conditions of fit. (Recall the derivation of Eqs. (4.143) and Eqs. (4.147).) This shows that it is absolutely vital that the Landau-Lifshitz conditions are carefully enforced in order to obtain the correct results. A third point is that Eqs. (4.154) and (4.155) are obvious generalizations of the formulas obtained in previous works [76, 89] to finite baryon chemical potential. The crucial insight is that entropy per baryon ($\sigma = s/n$) is conserved in zeroth-order (ideal) hydrodynamics, so that variable that must be held fixed when deriving the variations from equilibrium.

4.10 Quantum Statistics

In this section, we generalize the material from this chapter to include the effects of quantum statistics. The limit of classical statistics is attained when $|f_a| \ll 1$.

Departures from local kinetic and chemical equilibrium for particle species a are once again expressed in terms of the function ϕ_a as

$$f_a = f_a^{\rm eq}\left(1+\phi_a\right) . \tag{4.157}$$

We let δf_a represent the deviation expressed in terms of the equilibrium energy E_a^0 while $\delta\tilde{f}_a$ represents the deviation expressed in terms of the total nonequilibrium energy E_a; it is the latter which is conserved in local collisions and the one relevant for transport coefficients. The deviations are related to each other by

$$\delta f_a = \delta\tilde{f}_a + \left(\frac{\partial f_a^{\rm eq}}{\partial E_a}\right)_{T^0,\,\mu^0}\delta E_a = \delta\tilde{f}_a - \frac{\delta E_a}{T} f_a^{\rm eq}\left(1+d_a f_a^{\rm eq}\right) . \tag{4.158}$$

Here the notation is $d_a = (-1)^{2s_a}$. We need to relate the variations in T and μ to the variation $\delta\tilde{f}_a$. The latter variation is done at fixed E_a and is

$$\delta\tilde{f}_a = f_a^{\rm eq}\left[E_a - \mu_a + T\left(\frac{\partial\mu_a}{\partial T}\right)_\sigma\right]\left(1+d_a f_a^{\rm eq}\right)\frac{\delta T}{T^2} \tag{4.159}$$

Here in what follows, the derivative is carried out at fixed entropy per baryon σ. The factor from Eq. (4.158) which needs to be rewritten is

$$\frac{\delta E_a}{T} f_a^{\rm eq}\left(1+d_a f_a^{\rm eq}\right) = \left[\frac{T(\partial E_a/\partial T)_\sigma}{E_a - \mu_a + T\left(\partial\mu_a/\partial T\right)_\sigma}\right]\delta\tilde{f}_a . \tag{4.160}$$

In terms of $\delta\tilde{f}_a$ the deviations in the energy-momentum tensor and baryon current are as follows.

$$\delta T^{ij} = \sum_a \int d\Gamma_a^* \frac{p_a^{*i} p_a^{*j}}{E_a^*}\delta\tilde{f}_a \tag{4.161}$$

$$\delta T^{0j} = \sum_a \int d\Gamma_a^* \frac{p_a^{*j}}{E_a^*} E_a \delta\tilde{f}_a . \tag{4.162}$$

$$\delta T^{00} = \sum_a \int d\Gamma_a^* E_a \left\{1 - \frac{T(\partial E_a/\partial T)_\sigma}{E_a - \mu_a + T\left(\partial\mu_a/\partial T\right)_\sigma}\right\}\delta\tilde{f}_a . \tag{4.163}$$

$$\delta J^i = \sum_a b_a \int d\Gamma_a^* \frac{p_a^{*i}}{E_a^*}\delta\tilde{f}_a . \tag{4.164}$$

$$\delta J^0 = \sum_a b_a \int d\Gamma_a^* \left\{1 - \frac{T(\partial E_a/\partial T)_\sigma}{E_a - \mu_a + T\left(\partial\mu_a/\partial T\right)_\sigma}\right\}\delta\tilde{f}_a \tag{4.165}$$

In deriving the previous equations, one encounters generalized versions of Eqs. (4.89) and (4.90):

$$\delta\bar{\omega}^0 \sum_a g_{\omega a} \int d\Gamma_a^* \left(1 - \frac{|\mathbf{p}_a^*|^2}{3E_a^*} \frac{(1 + d_a f_a^{\rm eq})}{T}\right) f_a^{\rm eq} \tag{4.166}$$

$$\sum_a \delta m_a^* \int d\Gamma_a^* \frac{m_a^*}{E_a^*} \left(1 - \frac{|\mathbf{p}_a^*|^2}{3E_a^{*2}} - \frac{|\mathbf{p}_a^*|^2}{3E_a^*} \frac{(1 + d_a f_a^{\rm eq})}{T}\right) f_a^{\rm eq} \,. \tag{4.167}$$

At first glance, these equations appear far more complex, so it is not obvious that they vanish. However, we can rewrite the $1/T$ terms using

$$\frac{f_a^{\rm eq}(1 + d_a f_a^{\rm eq})}{T} = -\frac{\partial f_a^{\rm eq}}{\partial E_a^*} \tag{4.168}$$

and integrate by parts exactly as before, so indeed both integrals exactly vanish.

The collision term on the right side of the Boltzmann equation reads

$$\begin{aligned}
\mathcal{C}_a = \sum_{bcd} \frac{1}{1 + \delta_{ab}} \int d\Gamma_b^* \, d\Gamma_c^* \, d\Gamma_d^* \, W(a, b|c, d) \\
\times \Big\{ f_c f_d \, (1 + d_a f_a) \, (1 + d_b f_b) - f_a f_b \, (1 + d_c f_c) \, (1 + d_d f_d) \Big\} \\
+ \sum_{cd} \int d\Gamma_c^* \, d\Gamma_d^* \, W(a|c, d) \\
\times \Big\{ f_c f_d \, (1 + d_a f_a) - f_a \, (1 + d_c f_c) \, (1 + d_d f_d) \Big\} \\
+ \sum_{bc} \int d\Gamma_b^* \, d\Gamma_c^* \, W(c|a, b) \\
\times \Big\{ f_c \, (1 + d_a f_a) \, (1 + d_b f_b) - f_a f_b \, (1 + d_c f_c) \Big\} \,.
\end{aligned} \tag{4.169}$$

This expression explicitly includes $2 \leftrightarrow 2$ and $2 \leftrightarrow 1$ reactions. Higher order reactions are included in an obvious way.

We now consider small departures from equilibrium, meaning that we keep terms only linear in the ϕ_a. We use chemical equilibrium; for example, $a + b \leftrightarrow c + d$ gives

$$f_c^{\rm eq} f_d^{\rm eq} \, (1 + d_a f_a^{\rm eq}) \left(1 + d_b f_b^{\rm eq}\right) = f_a^{\rm eq} f_b^{\rm eq} \, (1 + d_c f_c^{\rm eq}) \left(1 + d_d f_d^{\rm eq}\right) \,.$$

Then the collision integral becomes

$$\begin{aligned}
\mathcal{C}_a &= \sum_{bcd} \frac{1}{1+\delta_{ab}} \int d\Gamma_b^*\, d\Gamma_c^*\, d\Gamma_d^*\, W(a,b|c,d) \\
&\times \left\{ f_a^{\rm eq} f_b^{\rm eq} \left[\left(1+d_d f_d^{\rm eq}\right) \phi_c + \left(1+d_c f_c^{\rm eq}\right) \phi_d \right] - f_c^{\rm eq} f_d^{\rm eq} \left[\left(1+d_b f_b^{\rm eq}\right) \phi_a + \left(1+d_a f_a^{\rm eq}\right) \phi_b \right] \right\} \\
&+ \sum_{cd} \int d\Gamma_c^*\, d\Gamma_d^*\, W(a|c,d) \Big\{ f_a^{\rm eq} \left[\left(1+d_d f_d^{\rm eq}\right) \phi_c + \left(1+d_c f_c^{\rm eq}\right) \phi_d \right] - f_c^{\rm eq} f_d^{\rm eq} \phi_a \Big\} \\
&+ \sum_{bc} \int d\Gamma_b^*\, d\Gamma_c^*\, W(c|a,b) \Big\{ - f_c^{\rm eq} \left[\left(1+d_b f_b^{\rm eq}\right) \phi_a + \left(1+d_a f_a^{\rm eq}\right) \phi_b \right] + f_a^{\rm eq} f_b^{\rm eq} \phi_c \Big\} . \qquad (4.170)
\end{aligned}$$

The left-hand-side of the Boltzmann equation is computed using the local equilibrium form of the distribution function. One form of the left-hand-side (in the local rest frame) is

$$\begin{aligned}
\frac{df_a^{\rm eq}}{dt} &= f_a^{\rm eq} \left(1+d_a f_a^{\rm eq}\right) \left[\frac{|\mathbf{p}_a^*|^2}{3TE_a^*} + v_n^2 T \frac{\partial}{\partial T} \left(\frac{E_a-\mu_a}{T} \right)_\sigma \right] \partial_\rho u^\rho \\
&+ f_a^{\rm eq} \left(1+d_a f_a^{\rm eq}\right) \left(b_a - \frac{nE_a}{w} \right) \frac{p_a^\mu}{E_a^*} D_\mu \left(\frac{\mu}{T} \right) \\
&- f_a^{\rm eq} \left(1+d_a f_a^{\rm eq}\right) \frac{p_a^\mu p_a^\nu}{2TE_a^*} \left(D_\mu u_\nu + D_\nu u_\mu + \frac{2}{3} \Delta_{\mu\nu} \partial_\rho u^\rho \right) . \qquad (4.171)
\end{aligned}$$

Now we subtract the right-hand-side from the left-hand-side and set the resulting expression to zero. This leads to

$$\mathcal{A}_a \left(\partial_\rho u^\rho \right) + \mathcal{B}_a^\mu D_\mu \left(\frac{\mu}{T} \right) - \mathcal{C}_a^{\mu\nu} \left(D_\mu u_\nu + D_\nu u_\mu + \tfrac{2}{3} \Delta_{\mu\nu} \partial_\rho u^\rho \right) = 0 \qquad (4.172)$$

where

$$\begin{aligned}
\mathcal{A}_a &= \left[\frac{|\mathbf{p}_a^*|^2}{3TE_a^*} + v_n^2 T \frac{\partial}{\partial T} \left(\frac{E_a-\mu_a}{T} \right)_\sigma \right] f_a^{\rm eq} \left(1+d_a f_a^{\rm eq}\right) \\
&+ \sum_{bcd} \frac{1}{1+\delta_{ab}} \int d\Gamma_b^*\, d\Gamma_c^*\, d\Gamma_d^*\, W(a,b|c,d) \\
&\times \Big\{ f_a^{\rm eq} f_b^{\rm eq} \left[\left(1+d_d f_d^{\rm eq}\right) A_c + \left(1+d_c f_c^{\rm eq}\right) A_d \right] \\
&- f_c^{\rm eq} f_d^{\rm eq} \left[\left(1+d_b f_b^{\rm eq}\right) A_a + \left(1+d_a f_a^{\rm eq}\right) A_b \right] \Big\} \\
&+ \sum_{cd} \int d\Gamma_c^*\, d\Gamma_d^*\, W(a|c,d) \Big\{ f_a^{\rm eq} \left[\left(1+d_d f_d^{\rm eq}\right) A_c + \left(1+d_c f_c^{\rm eq}\right) A_d \right] - f_c^{\rm eq} f_d^{\rm eq} A_a \Big\} \\
&+ \sum_{bc} \int d\Gamma_b^*\, d\Gamma_c^*\, W(c|a,b) \Big\{ - f_c^{\rm eq} \left[\left(1+d_b f_b^{\rm eq}\right) A_a + \left(1+d_a f_a^{\rm eq}\right) A_b \right] + f_a^{\rm eq} f_b^{\rm eq} A_c \Big\} , \\
& \qquad (4.173)
\end{aligned}$$

$$
\begin{aligned}
\mathcal{B}_a^\mu &= \left(b_a - \frac{nE_a}{w}\right)\frac{p_a^\mu}{E_a^*} f_a^{\rm eq}\left(1+d_a f_a^{\rm eq}\right) \\
&+ \sum_{bcd}\frac{1}{1+\delta_{ab}}\int d\Gamma_b^*\, d\Gamma_c^*\, d\Gamma_d^*\, W(a,b|c,d) \\
&\times \Big\{ f_a^{\rm eq} f_b^{\rm eq}\left[\left(1+d_d f_d^{\rm eq}\right) B_c p_c^\mu + \left(1+d_c f_c^{\rm eq}\right) B_d p_d^\mu\right] \\
&- f_c^{\rm eq} f_d^{\rm eq}\left[\left(1+d_b f_b^{\rm eq}\right) B_a p_a^\mu + \left(1+d_a f_a^{\rm eq}\right) B_b p_b^\mu\right]\Big\} \\
&+ \sum_{cd}\int d\Gamma_c^*\, d\Gamma_d^*\, W(a|c,d)\Big\{ f_a^{\rm eq}\left[\left(1+d_d f_d^{\rm eq}\right) B_c p_c^\mu + \left(1+d_c f_c^{\rm eq}\right) B_d p_d^\mu\right] - f_c^{\rm eq} f_d^{\rm eq} B_a p_a^\mu\Big\} \\
&+ \sum_{bc}\int d\Gamma_b^*\, d\Gamma_c^*\, W(c|a,b)\Big\{ - f_c^{\rm eq}\left[\left(1+d_b f_b^{\rm eq}\right) B_a p_a^\mu + \left(1+d_a f_a^{\rm eq}\right) B_b p_b^\mu\right] + f_a^{\rm eq} f_b^{\rm eq} B_c p_c^\mu\Big\},
\end{aligned}
\tag{4.174}
$$

$$
\begin{aligned}
\mathcal{C}_a^{\mu\nu} &= \frac{p_a^\mu p_a^\nu}{2E_a^* T} f_a^{\rm eq}\left(1+d_a f_a^{\rm eq}\right) \\
&+ \sum_{bcd}\frac{1}{1+\delta_{ab}}\int d\Gamma_b^*\, d\Gamma_c^*\, d\Gamma_d^*\, W(a,b|c,d) \\
&\times \Big\{ f_a^{\rm eq} f_b^{\rm eq}\left[\left(1+d_d f_d^{\rm eq}\right) C_c p_c^\mu p_c^\nu + \left(1+d_c f_c^{\rm eq}\right) C_d p_d^\mu p_d^\nu\right] \\
&- f_c^{\rm eq} f_d^{\rm eq}\left[\left(1+d_b f_b^{\rm eq}\right) C_a p_a^\mu p_a^\nu + \left(1+d_a f_a^{\rm eq}\right) C_b p_b^\mu p_b^\nu\right]\Big\} \\
&+ \sum_{cd}\int d\Gamma_c^*\, d\Gamma_d^*\, W(a|c,d)\Big\{ f_a^{\rm eq}\left[\left(1+d_d f_d^{\rm eq}\right) C_c p_c^\mu p_c^\nu + \left(1+d_c f_c^{\rm eq}\right) C_d p_d^\mu p_d^\nu\right] - f_c^{\rm eq} f_d^{\rm eq} C_a p_a^\mu p_a^\mu\Big\} \\
&+ \sum_{bc}\int d\Gamma_b^*\, d\Gamma_c^*\, W(c|a,b)\Big\{ - f_c^{\rm eq}\left[\left(1+d_b f_b^{\rm eq}\right) C_a p_a^\mu p_a^\nu + \left(1+d_a f_a^{\rm eq}\right) C_b p_b^\mu p_b^\nu\right] + f_a^{\rm eq} f_b^{\rm eq} C_c p_c^\mu p_c^\nu\Big\}.
\end{aligned}
\tag{4.175}
$$

Due to the tensorial structure of these equations the solution requires that $\mathcal{A}_a = 0$, $\mathcal{B}_a^\mu = 0$, and $\mathcal{C}_a^{\mu\nu} = 0$. These are integral equations for the functions A_a, B_a, and C_a which depend on the magnitude of the momentum $\mathbf{p}^*$.

The solutions for A_a and B_a are not unique. Starting from particular solutions $A_a^{\rm par}$ and $B_a^{\rm par}$, we can generate additional solutions

$$
A_a = A_a^{\rm par} - a_E\left(1+d_a f_a^{\rm eq}\right) E_a - a_B\left(1+d_a f_a^{\rm eq}\right) b_a \tag{4.176}
$$

$$
B_a = B_a^{\rm par} - b\left(1+d_a f_a^{\rm eq}\right). \tag{4.177}
$$

These forms differ from those in Sec. 4.8 due to the altered form of the collision integral (4.170) which now incorporates quantum statistics.

Once again, it is necessary to specify whether u^μ represents the flow of energy (Landau-Lifshitz) or baryon number (Eckart) in order to select unique solutions. We enforce the Landau-Lifshitz conditions, which in the rest frame are $\delta J^0 = 0$ and $\delta T^{0\nu} = 0$. The derivation proceeds in the same manner as in Sec. 4.8. The results for the transport coefficients are

$$\zeta = \frac{1}{3} \sum_a \int d\Gamma_a^* \left[\frac{|\mathbf{p}_a^*|^2}{E_a^*} + 3 v_n^2 T^2 \frac{\partial}{\partial T} \left(\frac{E_a - \mu_a}{T} \right)_\sigma \right] A_a^{\rm par} f_a^{\rm eq} \,, \tag{4.178}$$

$$\lambda = \frac{1}{3} \left(\frac{w}{nT} \right)^2 \sum_a \int d\Gamma_a^* \frac{|\mathbf{p}_a^*|^2}{E_a^*} \left(b_a - \frac{n E_a}{w} \right) B_a^{\rm par} f_a^{\rm eq} \,, \tag{4.179}$$

$$\eta = \frac{2}{15} \sum_a \int d\Gamma_a^* \frac{|\mathbf{p}_a^*|^4}{E_a^*} C_a^{\rm par} f_a^{\rm eq} \,. \tag{4.180}$$

We next generalize the energy-dependent relaxation time approximation. Again, we assume that only one ϕ_a is nonzero and the others vanish. Then the Boltzmann equation is approximated by

$$\frac{df_a^{\rm eq}}{dt} = \mathcal{C}_a = -\frac{f_a^{\rm eq} \phi_a}{\tau_a} \,, \tag{4.181}$$

where the relaxation time $\tau_a(E_a^*)$ for species a is given by

$$\begin{aligned} \frac{1 + d_a f_a^{\rm eq}}{\tau_a(E_a^*)} &= \sum_{bcd} \frac{1}{1 + \delta_{ab}} \int d\Gamma_b^* \, d\Gamma_c^* \, d\Gamma_d^* \, W(a,b|c,d) f_b^{\rm eq} \left(1 + d_c f_c^{\rm eq}\right) \left(1 + d_d f_d^{\rm eq}\right) \\ &+ \sum_{cd} \int d\Gamma_c^* \, d\Gamma_d^* \, W(a|c,d) \left(1 + d_c f_c^{\rm eq}\right) \left(1 + d_d f_d^{\rm eq}\right) \\ &+ \sum_{bc} \int d\Gamma_b^* \, d\Gamma_c^* \, W(c|a,b) f_b^{\rm eq} \left(1 + d_c f_c^{\rm eq}\right) \,. \end{aligned} \tag{4.182}$$

The particular solutions are

$$A_a^{\rm par} = \frac{\tau_a}{3T} \left[\frac{|\mathbf{p}_a^*|^2}{E_a^*} + 3 v_n^2 T^2 \frac{\partial}{\partial T} \left(\frac{E_a - \mu_a}{T} \right)_\sigma \right] \left(1 + d_a f_a^{\rm eq}\right) \tag{4.183}$$

$$B_a^{\rm par} = \frac{\tau_a}{E_a^*} \left(b_a - \frac{n E_a}{w} \right) \left(1 + d_a f_a^{\rm eq}\right) \,, \tag{4.184}$$

$$C_a^{\rm par} = \frac{\tau_a}{2TE_a^*}\left(1 + d_a f_a^{\rm eq}\right) . \tag{4.185}$$

Substitution gives the transport coefficients

$$\eta = \frac{1}{15T}\sum_a \int d\Gamma_a^* \frac{|\mathbf{p}_a^*|^4}{E_a^{*2}} \tau_a(E_a^*) f_a^{\rm eq}\left(1 + d_a f_a^{\rm eq}\right) , \tag{4.186}$$

$$\zeta = \frac{1}{9T}\sum_a \int d\Gamma_a^* \frac{\tau_a(E_a^*)}{E_a^{*2}} \left[|\mathbf{p}_a^*|^2 + 3v_n^2 T^2 E_a^* \frac{\partial}{\partial T}\left(\frac{E_a - \mu_a}{T}\right)_\sigma\right]^2 f_a^{\rm eq}\left(1 + d_a f_a^{\rm eq}\right) , \tag{4.187}$$

$$\lambda = \frac{1}{3}\left(\frac{w}{nT}\right)^2 \sum_a \int d\Gamma_a^* \frac{|\mathbf{p}_a^*|^2}{E_a^{*2}} \tau_a(E_a^*) \left(b_a - \frac{nE_a}{w}\right)^2 f_a^{\rm eq}\left(1 + d_a f_a^{\rm eq}\right) . \tag{4.188}$$

These are clearly non-negative.

4.11 Conclusion

In this chapter, we developed a flexible relativistic quasiparticle theory of transport coefficients in hot and dense hadronic matter. A major goal was the simultaneous inclusion of temperature- and baryon chemical potential-dependent quasiparticle masses with scalar and vector mean fields, all in a thermodynamically self-consistent way. Classical statistics were used throughout to simplify the presentation, although complete results with quantum statistics are given in Sec. 4.10. From the dispersion relations for the quasiparticles, we derived the Boltzmann equation and then the transport coefficients using the Chapman-Enskog expansion. Next, we derived compact analytic expressions for the shear and bulk viscosities and thermal conductivity. These formulas can be used with the relaxation time approximation; alternatively, we have provided integral equations which may be solved for greater accuracy. We have shown that the transport coefficients are non-negative in the relaxation time approximation (as they must be) which is a direct consequence of carefully enforcing the Landau-Lifshitz conditions of fit.

We also showed that previous bulk viscosity formulas (derived assuming zero baryon chemical potential) generalize straightforwardly to finite baryon chemical potential if one recalls that entropy per baryon is conserved in ideal hydrodynamics. This was the crucial detail that allowed us to compute the variations from equilibrium and use them to derive the bulk viscosity and thermal conductivity formulas.

Chapter 5

Conclusion and Discussion

In this thesis, we developed theoretical models to predict the equilibrium and non-equilibrium thermodynamic properties of QCD matter, with an emphasis on modeling QCD matter at finite baryon chemical potentials. The results of this work should be useful, for instance, to improve state-of-the art hydrodynamic modeling of heavy-ion collisions at finite baryon densities, and thus aid in the search for the QCD critical point in upcoming experiments at heavy-ion colliders.

In Chapter 2, we modeled the QCD equation of state, which is a vital input for all hydrodynamic simulations. To start, we reviewed the popular hadron resonance gas model, which has been shown to accurately describe the QCD equation of state at low temperatures below the deconfinement transition. That model neglects repulsive forces between hadrons, which become important at higher densities. Hence, we derived a hadron gas model which included repulsive forces via an excluded volume approximation. We next compared several hadron models to lattice QCD calculations. We showed, for instance, that excluded volume models perform much better than the point hadron resonance gas model, but they still fail at high temperatures above the deconfinement transition. Next, we used thermodynamic switching functions to build phenomenological equations of state which smoothly interpolate from a hadronic description at low temperatures and densities to a perturbative QCD equation of state at high temperatures and densities. We carefully constructed a switching function which would not introduce phase transitions, since lattice QCD suggests none are present at small baryon chemical potentials. We next showed that these crossover equations of

state are in excellent agreement with lattice QCD calculations, and they describe the lattice results over a wider range of temperatures than either hadron gas or perturbative QCD models do alone. Finally, we used the models to predict the equation of state at larger baryon chemical potentials where lattice results are unavailable.

In Chapter 3, we continued our study of the hadronic and crossover models developed in Chapter 2. First, we computed the speed of sound, which is a sensitive measure of the equation of state as it involves first and second derivatives of the pressure. We compared the speed of sound to lattice calculations, and we again found that crossover models were superior to hadronic (only) models. We found that crossover models which incorporated hadronic repulsion (via excluded volumes) performed the best. Next, we predicted baryon number fluctuations using our models, such as susceptibility, skewness, and kurtosis. These are even more sensitive measures of the equation of state which involve second through fourth derivatives of the pressure. Here, the crossover models showed some disagreement with lattice QCD, especially near and above the deconfinement temperature, but they nevertheless showed much better agreement than hadron gas models. We also compared the predictions to net-proton fluctuations from the STAR Collaboration at RHIC. Importantly, we find the best agreement if fluctuations freeze-out significantly after chemical freeze-out. This suggests previous papers may have over-estimated the fluctuation freeze-out temperature. We then used our crossover models to infer the freeze-out surface, which again showed cooler freeze-out temperatures. We saw no indications of the critical point in the STAR fluctuation data.

In Chapter 4, we turned towards a complementary task: computing the shear and bulk viscosity and thermal conductivity of hot and dense hadronic matter. These quantities determine, in essence, how sticky the fluid is and how readily heat flows through it. Obviously, these are critical inputs for hydrodynamic simulations, in addition to the equation of state and speed of sound. Again, the goal was developing results valid at finite baryon chemical potentials. We built upon the work of Ref. [76] and developed a relativistic quasiparticle theory of hadrons which included attractive and repulsive forces via scalar and vector mean fields. The main contributions of this work were including a baryon chemical potential and a vector mean field, both of which were neglected in [76]. We then employed the Chapman-Enskog expansion to derive formulas for the shear and bulk viscosity and thermal conductivity. Importantly, we showed how to maintain

thermodynamic self-consistency in the presence of mean fields. We also showed how to enforce the Landau-Lifshitz conditions of fit. Together, these ensured the transport coefficients remain non-negative—a strict requirement of thermodynamics.

In closing, we mention several natural extensions to this work which merit further study. First, the formulas developed in Chapter 4 provide a clear avenue for predicting transport coefficients at finite baryon chemical potentials. In the future, these formulas will be applied to specific hadronic models to yield numerical predictions for the transport coefficients, generalizing Ref. [76] which only considered zero baryon chemical potential. These will then be incorporated into hydrodynamic codes. A second interesting project would be adding additional mean fields and conserved charges into the framework of Chapter 4. Finally, it would be interesting to build upon the ideas of Chapters 2 and 3 and design switching functions which incorporate a first-order phase transition line and a critical point. The resulting equations of state would facilitate modeling the influence of the critical point on observables, such as baryon number fluctuations, and would greatly aid in the search for the critical point.

References

[1] M. Albright, J. Kapusta, and C. Young, Phys. Rev. C **90**, 024915 (2014).

[2] M. Albright, J. Kapusta, and C. Young, Phys. Rev. C **92**, 044904 (2015).

[3] M. Albright and J. Kapusta, submitted to Phys. Rev. C, preprint, arXiv:1508.02696.

[4] B. V. Jacak and B. Müller, Science **337**, 310 (2012).

[5] M. Alford, Annu. Rev. Nucl. Part. Sci. **51**, 131 (2001).

[6] M. G. Alford, A. Schmitt, K. Rajagopal, and T. Schäfer, Rev. Mod. Phys. **80**, 1455 (2008).

[7] A. Kurkela, E. S. Fraga, J. Schaffner-Bielich, and A. Vuorinen, Astrophys. J. **789**, 127 (2014).

[8] J. M. Lattimer, Annu. Rev. Nucl. Part. Sci. **62**, 485 (2012).

[9] K. Fukushima and T. Hatsuda, Rept. Prog. Phys. **74**, 014001 (2011).

[10] A. Masayuki and Y. Koichi, Nucl. Phys. A **504**, 668 (1989).

[11] A. Barducci, R. Casalbuoni, S. De Curtis, R. Gatto, and G. Pettini, Phys. Lett. B **231**, 463 (1989); Phys. Rev. D **41**, 1610 (1990).

[12] J. Berges and K. Rajagopal, Nucl. Phys. B **538**, 215 (1999).

[13] M. A. Halasz, A. D. Jackson, R. E. Shrock, M. A. Stephanov, and J. J. M. Verbaarschot, Phys. Rev. D **58**, 096007 (1998).

[14] F. R. Brown, F. P. Butler, H. Chen, N. H. Christ, Z. Dong, W. Schaffer, L. I. Unger, and A. Vaccarino, Phys. Rev. Lett. **65**, 2491 (1990).

[15] Y. Aoki, G. Endrődi, Z. Fodor, S. D. Katz, and K. K. Szabó, Nature (London) **443**, 675 (2006).

[16] M. Stephanov, Prog. Theor. Phys. Suppl. **153**, 139 (2004); Int. J. Mod. Phys. A **20**, 4387 (2005); PoS(LAT2006)024.

[17] B. Mohanty, Nucl. Phys. A **830**, 899c (2009).

[18] R. Stock, J. Phys. G **30**, 633 (2004).

[19] U. Heinz and M. Jacob, preprint, arxiv:nucl-th/0002042v1.

[20] A. Adare *et al.* (PHENIX Collaboration), Phys. Rev. C **81**, 034911 (2010).

[21] L. Arsene *et al.* (BRAHMS Collaboration), Nucl. Phys. A **757**, 1 (2005).

[22] B. B. Back *et al.* (PHOBOS Collaboration), Nucl. Phys. A **757**, 28 (2005).

[23] J. Adams *et al.* (STAR Collaboration), Nucl. Phys. A **757**, 102 (2005).

[24] K. Adcox *et al.* (PHENIX Collaboration), Nucl. Phys. A **757**, 184 (2005).

[25] M. Gyulassy and L. McLerran, Nucl. Phys. A **750**, 30 (2005).

[26] E. Shuryak, Prog. Part. Nucl. Phys. **53**, 273 (2004).

[27] C. V. Johnson and P. Steinberg, Phys. Today **63**, 29 (2010).

[28] H. Song, S. A. Bass, U. Heinz, T. Hirano, and C. Shen, Phys. Rev. Lett. **106**, 192301 (2011); *ibid.* **109**, 139904 (2012).

[29] P. K. Kovtun, D. T. Son, and A. O. Starinets, Phys. Rev. Lett. **94**, 111601 (2005).

[30] M. Gyulassy, in *Structure and Dynamics of Elementary Matter*, NATO Science Series, **166**, 159 (2004), preprint, arXiv:nucl-th/0403032.

[31] K. Adcox *et al.* (PHENIX Collaboration), Phys. Rev. Lett. **88**, 022301 (2001).

[32] J. Adams *et al.* (STAR Collaboration), Phys. Rev. Lett. **91**, 172302 (2003).

[33] L. Adamczyk *et al.* (STAR Collaboration), Phys. Rev. Lett. **112**, 032302 (2014).

[34] R. A. Lacey, Phys. Rev. Lett. **114**, 142301 (2015).

[35] G. Odyniec, EPJ Web of Conferences **95**, 3027 (2015).

[36] D. J. Gross and F. Wilczek, Phys. Rev. Lett. **30**, 1343 (1973).

[37] H. D. Politzer, Phys. Rev. Lett. **30**, 1346 (1973).

[38] Y. Aoki, S. Borsányi, S. Dürr, Z. Fodor, S. D. Katz, S. Krieg, and K. Szabó, J. High Energy Phys. 06 (2009) 088.

[39] S. Borsányi, Z. Fodor, C. Hoelbling, S. D. Katz, Stefan Krieg, C. Ratti, and K. K. Szabó, J. High Energy Phys. 09 (2010) 073.

[40] A. Bazavov, T. Bhattacharya, M. Cheng, C. DeTar, H.-T. Ding, Steven Gottlieb, R. Gupta, P. Hegde, U. M. Heller, F. Karsch, E. Laermann, L. Levkova, S. Mukherjee, P. Petreczky, C. Schmidt, R. A. Soltz, W. Soeldner, R. Sugar, D. Toussaint, W. Unger, and P. Vranas, Phys. Rev. D **85**, 054503 (2012).

[41] S. Borsányi, Z. Fodor, C. Hoelbling, S. D. Katz, S. Krieg, and K. K. Szabó, Phys. Lett. B **730**, 99 (2014).

[42] P. de Forcrand, PoS(LAT2009)010.

[43] F. Karsch, K. Redlich, and A. Tawfik, Eur. Phys. J. C **29** 549 (2003).

[44] J. Cleymans, H. Oeschler, K. Redlich, and S. Wheaton, Phys. Rev. C **73**, 034905 (2006).

[45] J. I. Kapusta, in *Relativistic Heavy Ion Physics*, Landolt-Börnstein New Series, Vol. I/23, edited by R. Stock (Springer Verlag, New York, 2010).

[46] R. Dashen, S.-K. Ma, and H. J. Bernstein, Phys. Rev. **187**, 345 (1969).

[47] A. Baran, W. Broniowski, and W. Florkowski, Acta Phys. Polon. B **35**, 779 (2004).

[48] W. Broniowski, F. Giacosa, and V. Begun, Phys. Rev. C **92**, 034905 (2015).

[49] R. Hagedorn and J. Rafelski, Phys. Lett. **B97**, 136 (1980).

[50] R. Hagedorn, Z. Phys. C **17**, 265 (1983).

[51] M. I. Gorenstein, V. K. Petrov, and G. M. Zinovjev, Phys. Lett. **B106**, 327 (1981).

[52] J. I. Kapusta and K. A. Olive, Nucl. Phys. **A408**, 478 (1983).

[53] D. H. Rischke, M. I. Gorenstein, H. Stöcker, and W. Greiner, Z. Phys. C **51**, 485 (1991).

[54] J. Cleymans, M. I. Gorenstein, J. Stalnacke, and E. Suhonen, Physica Scripta **48**, 277 (1993).

[55] G. D. Yen, M. I. Gorenstein, W. Greiner, and S. N. Yang, Phys. Rev. C **56**, 2210 (1997).

[56] Sz. Borsányi, G. Endrődi, Z. Fodor, A. Jakovác, S. D. Katz, S. Krieg, C. Ratti, and K. K. Szabó, J. High Energy Phys. 11 (2010) 077 .

[57] A. Vuorinen, Phys. Rev. D **67**, 074032 (2003); *ibid.* **68**, 054017 (2003).

[58] N. Haque, M. G. Mustafa, and M. Strickland, Phys. Rev. D **87**, 105007 (2013).

[59] J. Beringer *et al.* (Particle Data Group), Phys. Rev. D **86**, 010001 (2012).

[60] J. I. Kapusta, Nucl. Phys. **B148**, 461 (1979).

[61] H. W. Woolley, Int. J. Thermophys. **4**, 51 (1983).

[62] J. I. Kapusta, Phys. Rev. C **81**, 055201 (2010).

[63] Sz. Borsányi, G. Endrődi, Z. Fodor, S. D. Katz, S. Krieg, C. Ratti, and K. K. Szabó, J. High Energy Phys. 08 (2012) 053.

[64] M. A. Stephanov, Phys. Rev. Lett. **102**, 032301 (2009).

[65] M. Asakawa, S. Ejiri, and M. Kitazawa, Phys. Rev. Lett. **103**, 262301 (2009).

[66] F. Karsch and K. Redlich, Phys. Lett. B **695**, 136 (2011).

[67] K. Fukushima, Phys. Rev. C **91**, 044910 (2015).

[68] S. Borsányi, Z. Fodor, S. D. Katz, S. Krieg, C. Ratti, and K. K. Szabó, Phys. Rev. Lett. **113**, 052301 (2014).

[69] S. Borsányi, Z. Fodor, S. D. Katz, S. Krieg, C. Ratti, and K. K. Szabó, Phys. Rev. Lett. **111**, 062005 (2013).

[70] A. Bazavov *et al.* (HotQCD Collaboration), Phys. Rev. D **86**, 034509 (2012).

[71] B. Schenke, S. Jeon, and C. Gale, Phys. Rev. C **82**, 014903 (2010).

[72] C. Shen, U. W. Heinz, P. Huovinen, and H. Song, Phys. Rev.C **82**, 054904 (2010); *ibid.* **84**, 044903 (2011).

[73] P. Alba, W. Alberico, R. Bellwied, M. Bluhm, V. Mantovani Sarti, M. Nahrgang, and C. Ratti, Phys. Lett. B **738**, 305 (2014).

[74] P. Garg, D. K. Mishra, P. K. Netrakanti, B. Mohanty, A. K. Mohanty, B. K. Singh, and N. Xu, Phys. Lett. B **726**, 691 (2013).

[75] A. Bhattacharyya, S. Das, S. K. Ghosh, R. Ray, S. Samanta, Phys. Rev. C **90**, 034909 (2014).

[76] P. Chakraborty and J. I. Kapusta, Phys. Rev. C **83**, 014906 (2011).

[77] H. Song and U. Heinz, Phys. Lett. B **658**, 279 (2008).

[78] P. Bożek, Phys. Rev. C **81**, 034909 (2010).

[79] K. Dusling and T. Schäfer, Phys. Rev. C **85**, 044909 (2012).

[80] J. Noronha-Hostler, J. Noronha, and F. Grassi, Phys. Rev. C **90**, 034907 (2014).

[81] R. Kubo, J. Phys. Soc. Jpn. **12**, 570 (1957).

[82] F. Karsch and H. W. Wyld, Phys. Rev. D **35**, 2518 (1987).

[83] S. Sakai, A. Nakamura, and T. Saito, Nucl. Phys. A **638**, 535c (1998).

[84] A. Hosoya and K. Kajantie, Nucl. Phys. B **250**, 666 (1985).

[85] S. Gavin, Nucl. Phys. A **435**, 826 (1985).

[86] P. Danielewicz and M. Gyulassy, Phys. Rev. D **31**, 53 (1985).

[87] M. Prakash, M. Prakash, R. Venugopalan, and G. Welke, Phys. Rep. **227**, 321 (1993).

[88] S. Jeon, Phys. Rev. D **52**, 3591 (1995).

[89] S. Jeon and L. G. Yaffe, Phys. Rev. D **53**, 5799 (1996).

[90] G. Baym, H. Monien, C. J. Pethick, and D. G. Ravenhall, Phys. Rev. Lett. **64**, 1867 (1990).

[91] G. Baym, H. Monien, C. J. Pethick, and D. G. Ravenhall, Nucl. Phys. A **525**, 415c (1991).

[92] P. Arnold, G. D. Moore, and L. G. Yaffe, J. High Energy Phys. 11 (2000) 001.

[93] P. Arnold, G. D. Moore, and L. G. Yaffe, J. High Energy Phys. 01 (2003) 030.

[94] P. Arnold, G. D. Moore, and L. G. Yaffe, J. High Energy Phys. 05 (2003) 051.

[95] J.-S. Gagnon and S. Jeon, Phys. Rev. D **76**, 105019 (2007).

[96] J.-S. Gagnon and S. Jeon, Phys. Rev. D **75**, 025014 (2007).

[97] J.-S. Gagnon and S. Jeon, Phys. Rev. D **76**, 089902 (2007).

[98] J. E. Davis and R. J. Perry, Phys. Rev. C **43**, 1893 (1991).

[99] G. Baym and C. Pethick, *Landau Fermi-Liquid Theory: Concepts and Applications* (Wiley Interscience, New York, 1991).

[100] P. Romatschke, Phys. Rev. D **85**, 065012 (2012).

[101] M. I. Gorenstein and S. N. Yang, Phys. Rev. D **52**, 5206 (1995).

[102] A. Nakamura and S. Sakai, Phys. Rev. Lett. **94**, 072305 (2005).

[103] S. Sakai and A. Nakamura, PoS(LAT2005)186.

[104] H. B. Meyer, Phys. Rev. D **76**, 101701 (2007).

[105] H. B. Meyer, Nucl. Phys. A **830**, 641c (2009).

[106] J.-W. Chen, Y.-H. Li, Y.-F. Liu, and E. Nakano, Phys. Rev. D **76**, 114011 (2007).

[107] K. Itakura, O. Morimatsu, and H. Otomo, Phys. Rev. D **77**, 014014 (2008).

[108] A. Dobado, F. J. Llanes-Estrada, and J. M. Torres-Rincon, Phys. Lett. B **702**, 43 (2011).

[109] M. I. Gorenstein, M. Hauer, and O. N. Moroz, Phys. Rev. C **77**, 024911 (2008).

[110] J. Noronha-Hostler, J. Noronha, and C. Greiner, Phys. Rev. Lett. **103**, 172302 (2009).

[111] J. Noronha-Hostler, J. Noronha, and C. Greiner, Phys. Rev. C **86**, 024913 (2012).

[112] C. Sasaki and K. Redlich, Phys. Rev. C **79**, 055207 (2009).

[113] M. Bluhm, B. Kämpfer, and K. Redlich, Phys. Rev. C **84**, 025201 (2011).

[114] J.-W. Chen, Y.-F. Liu, Y.-K. Song, and Q. Wang, Phys. Rev. D **87**, 036002 (2013).

[115] A. S. Khvorostukhin, V. D. Toneev, and D. N. Voskresensky, Nucl. Phys. A **915**, 158 (2013).

[116] A. S. Khvorostukhin, V. D. Toneev, and D. N. Voskresensky, Nucl. Phys. A **845**, 106 (2010).

[117] A. S. Khvorostukhin, V. D. Toneev, and D. N. Voskresensky, Phys. Rev. C **84**, 035202 (2011).

[118] S. R. de Groot, W. A. van Leeuwen and Ch. G. van Weert, *Relativistic Kinetic Theory: Principles and Applications*, North-Holland (1980).

[119] S. Weinberg, *Gravitation and Cosmology*, Wiley, New York (1972).

[120] L. D. Landau and E. M. Lifshitz, *Fluid Mechanics*, Pergamon Press, Oxford (1987).

[121] A. B. Larionov, O. Buss, K. Gallmeister, and U. Mosel, Phys. Rev. C **76**, 044909 (2007).

Appendix A

List of Particles in Hadronic Gas Calculations

This appendix contains a listing of the hadrons included in the calculations in Chapters 2 and 3. The particles and their properties are taken from the Particle Data Group [59]. There are a few baryons whose spins are not known; in these cases we conservatively take them to be spin 1/2. This table does not include hadrons with charm, bottom, or top quarks, and is therefore the appropriate set of particles for comparisons of equations of state with lattice QCD results including only up, down and strange quarks. The table also omits the σ meson since its contribution to averaged thermal observables is canceled by other repulsive channels [48]. The degeneracies of the hadrons includes isospin degeneracy when the mass splitting is small (for example, for the Δ baryons); otherwise the hadrons are listed separately (for example, p and n). Antibaryons are not listed in the table but are included in the calculations. The columns indicate, from left to right, the hadron's identity, mass, degeneracy, and baryon charge.

hadron	m_a(GeV)	degen	b_a	hadron	m_a(GeV)	degen	b_a	hadron	m_a(GeV)	degen	b_a
π^0	0.135	1	0	$K_2^{*0}(1430)$	1.432	10	0	$K_3^*(1780)$	1.776	28	0
$\pi^\pm$	0.140	2	0	$N(1440)$	1.440	4	1	$\Lambda(1800)$	1.800	2	1
$K^\pm$	0.494	2	0	$\rho(1450)$	1.465	9	0	$\Lambda(1810)$	1.810	2	1
K^0	0.498	2	0	$a_0(1450)$	1.474	3	0	$\pi(1800)$	1.812	3	0
η	0.548	1	0	$\eta(1475)$	1.476	1	0	$K_2(1820)$	1.816	20	0
ρ	0.775	9	0	$f_0(1500)$	1.505	1	0	$\Lambda(1820)$	1.820	6	1
ω	0.783	3	0	$\Lambda(1520)$	1.520	4	1	$\Xi(1820)$	1.823	8	1
$K^{*\pm}(892)$	0.892	6	0	$N(1520)$	1.520	8	1	$\Lambda(1830)$	1.830	6	1
$K^{*0}(892)$	0.896	6	0	$f_2^{'}(1525)$	1.525	5	0	$\phi_3(1850)$	1.854	7	0
p	0.938	2	1	$\Xi^0(1530)$	1.532	4	1	$N(1875)$	1.875	8	1
n	0.940	2	1	$N(1535)$	1.535	4	1	$\Delta(1905)$	1.880	24	1
$\eta^{'}$	0.958	1	0	$\Xi^-(1530)$	1.535	4	1	$\Delta(1910)$	1.890	8	1
a_0	0.980	3	0	$\Delta(1600)$	1.600	16	1	$\Lambda(1890)$	1.890	4	1
f_0	0.990	1	0	$\Lambda(1600)$	1.600	2	1	$\pi_2(1880)$	1.895	15	0
ϕ	1.019	3	0	$\eta_2(1645)$	1.617	5	0	$N(1900)$	1.900	8	1
Λ	1.116	2	1	$\Delta(1620)$	1.630	8	1	$\Sigma(1915)$	1.915	18	1
h_1	1.170	3	0	$N(1650)$	1.655	4	1	$\Delta(1920)$	1.920	16	1
Σ^+	1.189	2	1	$\Sigma(1660)$	1.660	6	1	$\Delta(1950)$	1.930	32	1
Σ^0	1.193	2	1	$\pi_1(1600)$	1.662	9	0	$\Sigma(1940)$	1.940	12	1
Σ^-	1.197	2	1	$\omega_3(1670)$	1.667	7	0	$f_2(1950)$	1.944	5	0
b_1	1.230	9	0	$\omega(1650)$	1.670	3	0	$\Delta(1930)$	1.950	24	1
a_1	1.230	9	0	$\Lambda(1670)$	1.670	2	1	$\Xi(1950)$	1.950	4	1
Δ	1.232	16	1	$\Sigma(1670)$	1.670	12	1	$a_4(2040)$	1.996	27	0
$K_1(1270)$	1.272	12	0	$\pi_2(1670)$	1.672	15	0	$f_2(2010)$	2.011	5	0
f_2	1.275	5	0	Ω^-	1.673	4	1	$f_4(2050)$	2.018	9	0
f_1	1.282	3	0	$N(1675)$	1.675	12	1	$\Xi(2030)$	2.025	12	1
$\eta(1295)$	1.294	1	0	$\phi(1680)$	1.680	3	0	$\Sigma(2030)$	2.030	24	1
$\pi(1300)$	1.300	3	0	$N(1680)$	1.685	12	1	$K_4^*(2045)$	2.045	36	0
Ξ^0	1.315	2	1	$\rho_3(1690)$	1.689	21	0	$\Lambda(2100)$	2.100	8	1
a_2	1.318	15	0	$\Lambda(1690)$	1.690	4	1	$\Lambda(2110)$	2.110	6	1
Ξ^-	1.322	2	1	$\Xi(1690)$	1.690	4	1	$\phi(2170)$	2.175	3	0
$f_0(1370)$	1.350	1	0	$N(1700)$	1.700	8	1	$N(2190)$	2.190	16	1
$\pi_1(1400)$	1.354	9	0	$\Delta(1700)$	1.700	16	1	$N(2200)$	2.250	20	1
$\Sigma(1385)$	1.385	12	1	$N(1710)$	1.710	4	1	$\Sigma(2250)$	2.250	6	1
$K_1(1400)$	1.403	12	0	$K^*(1680)$	1.717	12	0	$\Omega^-(2250)$	2.252	2	1
$\Lambda(1405)$	1.405	2	1	$\rho(1700)$	1.720	9	0	$N(2250)$	2.275	20	1
$\eta(1405)$	1.409	1	0	$f_0(1710)$	1.720	1	0	$f_2(2300)$	2.297	5	0
$K^*(1410)$	1.414	12	0	$N(1720)$	1.720	8	1	$f_2(2340)$	2.339	5	0
$\omega(1420)$	1.425	3	0	$\Sigma(1750)$	1.750	6	1	$\Lambda(2350)$	2.350	10	1
$K_0^*(1430)$	1.425	4	0	$K_2(1770)$	1.773	20	0	$\Delta(2420)$	2.420	48	1
$K_2^{*\pm}(1430)$	1.426	10	0	$\Sigma(1775)$	1.775	18	1	$N(2600)$	2.600	24	1
$f_1(1420)$	1.426	3	0								

Table A.1: A list of hadrons included in calculations in Chapters 2 and 3. (Antibaryons are omitted from the table but are included in the calculations.)

Appendix B

Details About the Speed of Sound

Abundant experimental evidence has demonstrated that the hot and dense matter formed in high-energy heavy-ion collisions behaves as a fluid. Just like in familiar, nonrelativistic fluids, sound waves can propagate through quark-gluon plasmas and hadronic gases. The speed of sound through these forms of matter is an interesting quantity in and of itself, but it is also a sensitive measure of the equation of state. It is therefore useful to compare model predictions of the speed of sound to lattice QCD calculations; see Chapter 3 for the results. In this appendix we provide additional details about calculating the speed of sound from thermodynamic models. We begin by discussing the basic physics of sound. Then we derive the wave equation to obtain an expression for the sound speed. Finally, we give technical details on how to calculate the sound speed from the equation of state.

At a fundamental level, the phenomena of sound is a pressure wave which propagates through a fluid. Typically, the compression and rarefaction of the fluid occurs *fast* enough that negligible entropy is produced over one period of the wave—sound waves are approximately adiabatic. Mathematically, this requires that the divergence of the entropy four-current vanish. Using the notation of Chapter 4, we have

$$\partial_\mu s^\mu = 0\,. \tag{B.1}$$

Since we are ignoring viscous effects, the entropy current in equilibrium is

$$s^\mu = s u^\mu\,, \tag{B.2}$$

where s is the local entropy density and u^μ is the fluid four-velocity. Recalling the useful formulas

$$D = u^\mu \partial_\mu \tag{B.3}$$

$$D_\mu = \partial_\mu - u_\mu D\,, \tag{B.4}$$

we can rewrite Eq. (B.1) as a continuity equation

$$Ds = -s\partial_\mu u^\mu\,. \tag{B.5}$$

Physically, D is a time derivative in the local rest frame while D_μ is a spacial gradient in the local rest frame: in the rest frame, $D = \partial_0$, $D_0 = 0$, and $D_i = \partial_i$. In equilibrium, the baryon current is nu^μ, where n is the baryon density. Baryon charge is exactly conserved in QCD; its conservation law in ideal hydrodynamics is

$$Dn = -n\partial_\mu u^\mu\,. \tag{B.6}$$

Note that while the total entropy and baryon number are conserved in an adiabatic sound wave, the densities of those quantities do change as the fluid expands and contracts. One quantity which is unchanged is the entropy per baryon

$$\sigma = \frac{s}{n}\,. \tag{B.7}$$

We can see this from Eq. (B.7) using Eqs. (B.5) and (B.6):

$$D\sigma = n^{-1}Ds - sn^{-2}Dn = (-sn^{-1} + sn^{-1})\partial_\mu u^\mu = 0\,. \tag{B.8}$$

Hence, σ is unchanged with time. This fact was used in Chapter 4 when deriving deviations of the distribution function from equilibrium since entropy production was negligible in that calculation.

We proceed to derive the wave equation. The energy momentum tensor in ideal hydrodynamics is

$$T^{\mu\nu} = -Pg^{\mu\nu} + (P+\epsilon)u^\mu u^\nu\,. \tag{B.9}$$

Conservation of energy and momentum requires $\partial_\mu T^{\mu\nu} = 0$, which we can write as

$$0 = u^\nu\left[D\epsilon + (P+\epsilon)\partial_\mu u^\mu\right] + \left[-D^\nu P + (P+\epsilon)Du^\nu\right]\,. \tag{B.10}$$

The first term is parallel to the fluid four-velocity u^ν while the second is orthogonal to it; hence both terms independently vanish. For simplicity, we evaluate both in the rest frame and take the nonrelativistic limit, where $u^0 \approx 1$ and $\partial_\mu u^\mu \to \partial_i u^i$. We get

$$\partial_0 \epsilon = -w \partial_i u^i \tag{B.11}$$

$$\partial_i P = w \partial_0 u_i = -w \partial_0 u^i \,, \tag{B.12}$$

where $w = (P + \epsilon)$ is the enthalpy density.

We need one additional expression which we can find if we treat P as a function of ϵ and σ instead of the more typical T and μ. Since σ is constant during adiabatic processes, we can write

$$\partial_0 P = \left(\frac{\partial P}{\partial \epsilon} \right)_\sigma \partial_0 \epsilon \,. \tag{B.13}$$

Next, we linearize the system assuming small perturbations around global equilibrium:

$$P(x) = P^{\rm eq} + \delta P(x) \tag{B.14}$$

$$\epsilon(x) = \epsilon^{\rm eq} + \delta\epsilon(x) \,. \tag{B.15}$$

Thus

$$\partial_0 \delta P = \left(\frac{\partial P}{\partial \epsilon} \right)_\sigma \partial_0 \delta\epsilon = -w \left(\frac{\partial P}{\partial \epsilon} \right)_\sigma \partial_i u^i \,. \tag{B.16}$$

Differentiating again gives

$$\partial_0 \partial_0 \delta P = -w \left(\frac{\partial P}{\partial \epsilon} \right)_\sigma \partial_i \partial_0 u^i = \left(\frac{\partial P}{\partial \epsilon} \right)_\sigma \partial_i \partial_i \delta P \,. \tag{B.17}$$

This is the famous wave equation

$$\frac{\partial^2 P}{\partial t^2} = \left(\frac{\partial P}{\partial \epsilon} \right)_\sigma \nabla^2 P \tag{B.18}$$

with speed of sound c_s given by

$$c_s^2 = \left(\frac{\partial P}{\partial \epsilon} \right)_\sigma \,. \tag{B.19}$$

Note that we must hold constant the entropy per baryon σ when evaluating the derivative in Eq. (B.19).

The models presented in this thesis predict the pressure $P(T, \mu)$ as a function of temperature T and baryon chemical potential μ, so we need a practical way to evaluate

Eq. (B.19). We begin by deriving two useful thermodynamic relations. We start with the thermodynamic identity

$$d\epsilon = Tds + \mu dn\,, \tag{B.20}$$

where s and n are the entropy and baryon densities, respectively. Using $\sigma = s/n$, $ds = d(n\sigma)$, so

$$\begin{aligned} d\epsilon &= Tnd\sigma + (T\sigma + \mu)dn \\ &= Tnd\sigma + \frac{w}{n}dn\,. \end{aligned} \tag{B.21}$$

Thus, at fixed σ,

$$d\epsilon = \frac{w}{n}dn\,. \tag{B.22}$$

Next, we note that if σ is fixed, then $d\sigma = d(s/n) = 0$ implies that

$$sdn = nds\,. \tag{B.23}$$

Combining Eqs. (B.22) and (B.23) gives (at fixed σ)

$$d\epsilon = \frac{w}{s}ds\,. \tag{B.24}$$

Using Eq. (B.24) with (B.19), we find

$$c_s^2 = \frac{\left(\frac{\partial P}{\partial T}\right)_\sigma}{\left(\frac{\partial \epsilon}{\partial T}\right)_\sigma} = \frac{s}{w}\frac{\left(\frac{\partial P}{\partial T}\right)_\sigma}{\left(\frac{\partial s}{\partial T}\right)_\sigma}\,. \tag{B.25}$$

From the chain rule,

$$c_s^2 = \frac{s}{w}\frac{\left[\left(\frac{\partial P}{\partial T}\right)_\mu + \left(\frac{\partial \mu}{\partial T}\right)_\sigma \left(\frac{\partial P}{\partial \mu}\right)_T\right]}{\left[\left(\frac{\partial s}{\partial T}\right)_\mu + \left(\frac{\partial \mu}{\partial T}\right)_\sigma \left(\frac{\partial s}{\partial \mu}\right)_T\right]}\,. \tag{B.26}$$

To find the link between μ and T at fixed σ, we turn to Eq. (B.23), which we can expand as

$$s\left[\left(\frac{\partial n}{\partial T}\right)_\mu dT + \left(\frac{\partial n}{\partial \mu}\right)_T d\mu\right] = n\left[\left(\frac{\partial s}{\partial T}\right)_\mu dT + \left(\frac{\partial s}{\partial \mu}\right)_T d\mu\right]\,. \tag{B.27}$$

Solving for $d\mu/dT$ gives

$$\left(\frac{\partial \mu}{\partial T}\right)_\sigma = \frac{s\left(\frac{\partial n}{\partial T}\right)_\mu - n\left(\frac{\partial s}{\partial T}\right)_\mu}{n\left(\frac{\partial s}{\partial \mu}\right)_T - s\left(\frac{\partial n}{\partial \mu}\right)_T}\,. \tag{B.28}$$

The speed of sound is now readily calculable from Eqs. (B.26) and (B.28) since all of the required quantities come directly from $P(T, \mu)$ or its first or second derivatives with respect to T and μ. For completeness, we provide a few additional details. Recall the thermodynamic identities for entropy density and baryon density:

$$s = \left(\frac{\partial P}{\partial T}\right)_{\mu} \tag{B.29}$$

$$n = \left(\frac{\partial P}{\partial \mu}\right)_{T} . \tag{B.30}$$

Let us also recall the susceptibility formula

$$\chi_{xy} = \frac{\partial^2 P}{\partial x \partial y} , \tag{B.31}$$

where x and y are either T or μ. Combining Eqs. (B.26) and (B.28), we find

$$c_s^2 = \frac{n^2 \chi_{TT} - sn(\chi_{T\mu} + \chi_{\mu T}) + s^2 \chi_{\mu\mu}}{w(\chi_{TT}\chi_{\mu\mu} - \chi_{T\mu}\chi_{\mu T})} . \tag{B.32}$$

If derivatives commute (as in this thesis, where there is no strong phase transition or the accompanying discontinuities in thermodynamic derivatives), then

$$c_s^2 = \frac{n^2 \chi_{TT} - 2sn\chi_{\mu T} + s^2 \chi_{\mu\mu}}{w(\chi_{TT}\chi_{\mu\mu} - (\chi_{\mu T})^2)} . \tag{B.33}$$

The pressure derivatives appearing in Eq. (B.33) are readily evaluated using finite difference methods.

Appendix C

Deriving the Conservation Equations

In this appendix, we outline the derivation of the conservation equations from their microscopic origins. This is straightforward but requires a special identity involving the Boltzmann equation. Then, we use the results to obtain constraints for the mean fields. Finally, we highlight the close connection between energy and momentum conservation and thermodynamic self-consistency.

The derivations in this section require frequent raising and lowering of vector indices using the metric $g_{\mu\nu} = (+,-,-,-)$. To avoid potential confusion between particle labels and vector indices, we will not write the particle label on momentum variables in this section:

$$p_a^{*\mu} \to p^{*\mu}\,. \tag{C.1}$$

Then, for example, we can raise and lower vector indices like

$$\begin{aligned} p^{*0} &= p^*_0 \\ p^{*i} &= -p^*_i \end{aligned} \tag{C.2}$$

(and similarly for other vectors) with no confusion.

In QCD, baryon charge, energy, and momentum are conserved at a microscopic level during collisions between particles. Let χ_a represent any such conserved quantity carried by particle a. Then, for instance, in collision events $a + b \to c + d$, we will have

$\chi_a + \chi_b = \chi_c + \chi_d$. One can show that for any conserved quantity χ_a,

$$\sum_a \int d\Gamma^*_a \chi_a \mathcal{C}_a = 0\,, \tag{C.3}$$

where $\mathcal{C}_a$ is the collision integral for the Boltzmann equation. For a proof, see Part A, Chapter II.1 of de Groot's book [118]. Note that while de Groot proves Eq. (C.3) assuming classical statistics, it is easy to show that Eq. (C.3) is unchanged by the inclusion of quantum statistics.

We can derive macroscopic conservation equations from Eq. (C.3) by replacing the collision integral $\mathcal{C}_a$ with the left-hand-side the Boltzmann equation (4.25), which we rewrite as

$$\mathcal{C}_a = \frac{p^{*\mu}}{E^*_a}\partial_\mu f_a + \left(\partial^i E^*_a + g_{\omega a}\frac{p^*_\mu}{E^*_a}\,\bar{\omega}^{i\mu}\right)\frac{\partial f_a}{\partial p^{*i}}\,. \tag{C.4}$$

Recall that the vector mean field $\bar{\omega}^\mu(x)$ depends on the space-time coordinate x^μ but not momentum. The antisymmetric stress tensor is

$$\bar{\omega}^{\mu\nu}(x) = \partial^\mu \bar{\omega}^\nu(x) - \partial^\nu \bar{\omega}^\mu(x)\,. \tag{C.5}$$

Also recall that

$$E^*_a = \sqrt{|\mathbf{p}^*|^2 + m^{*2}_a(x)} \tag{C.6}$$

depends on x^μ via m^{*2}_a and also depends on momentum p^{*i}.

First, we substitute Eq. (C.4) into Eq. (C.3). In the first term, we integrate by parts with respect to the space-time variable x while in the second term we integrate by parts with respect to momentum p^*. Note that the boundary term vanishes when integrating by parts with momentum. Two useful intermediate results are

$$\begin{aligned}
\partial_\mu\left(\frac{p^{*\mu}}{E^*_a}\right) &= \partial_0(1) + \partial_i\left(\frac{p^{*i}}{E^*_a}\right) = -\frac{p^{*i}}{E^{*2}_a}\partial_i E^*_a \\
\frac{\partial}{\partial p^{*i}}\left(\partial^i E^*_a\right) &= -\frac{p^{*i}}{E^{*2}_a}\partial^i E^*_a = \frac{p^{*i}}{E^{*2}_a}\partial_i E^*_a\,.
\end{aligned} \tag{C.7}$$

Also,

$$\frac{\partial}{\partial p^{*i}}\left(\frac{p^*_\mu \bar{\omega}^{i\mu}}{E^*_a}\right) = \bar{\omega}^{ij}\left[\frac{\delta^{ij}}{E^*_a} - \frac{p^{*i}p^{*j}}{E^{*3}_a}\right] = 0 \tag{C.8}$$

due to the product of antisymmetric and symmetric tensors. Thus Eq. (C.3) becomes

$$\begin{aligned} 0 &= \partial_\mu \left(\sum_a \int d\Gamma^*_a \, f_a \frac{p^{*\mu} \chi_a}{E^*_a} \right) \\ &- \sum_a \int d\Gamma^*_a \, f_a \left[\frac{p^{*\mu}}{E^*_a} \partial_\mu \chi_a + \left(\partial^i E^*_a + \frac{g_{\omega a} p^*_\mu \bar{\omega}^{i\mu}}{E^*_a} \right) \frac{\partial \chi_a}{\partial p^{*i}} \right] . \end{aligned} \tag{C.9}$$

This is a very general result for any conserved quantity χ_a, regardless of whether one uses classical or quantum statistics.

As a practical example, let $\chi_a = b_a$ be the baryon charge. Then all derivatives of χ_a vanish, so Eq. (C.9) becomes

$$0 = \partial_\mu \left(\sum_a b_a \int d\Gamma^*_a f_a \frac{p^{*\mu}}{E^*_a} \right) = \partial_\mu J^\mu \, . \tag{C.10}$$

This is clearly the conservation law for the baryon current, just as expected.

Next, we consider energy conservation. Note that it is the full particle energy E_a which is conserved in particle collisions. Hence let $\chi_a = E_a = E^*_a + g_{\omega a} \bar{\omega}^0$. To simplify the result, we note that

$$p^*_i p^*_\mu \bar{\omega}^{i\mu} = E^*_a p^*_i \bar{\omega}^{i0} \tag{C.11}$$

since the antisymmetric and symmetric parts vanish upon contraction. Then, after much simplification, Eq. (C.9) becomes

$$\begin{aligned} 0 &= \partial_\mu \left(\sum_a \int d\Gamma^*_a f_a \frac{p^{*\mu} E^*_a}{E^*_a} \right) - \sum_a \int d\Gamma^*_a f_a \partial^0 E^*_a \\ &+ \bar{\omega}^0 \partial_\mu \left(\sum_a g_{\omega a} \int d\Gamma^*_a f_a \frac{p^{*\mu}}{E^*_a} \right) + \bar{\omega}^{\mu 0} \sum_a g_{\omega a} \int d\Gamma^*_a f_a \frac{p^*_\mu}{E^*_a} \, . \end{aligned} \tag{C.12}$$

Next, we consider conservation of momentum p^j, so let $\chi_a = p^j = p^{*j} + g_{\omega a} \bar{\omega}^j$. After simplifying, Eq. (C.9) becomes

$$\begin{aligned} 0 &= \partial_\mu \left(\sum_a \int d\Gamma^*_a f_a \frac{p^{*\mu} p^{*j}}{E^*_a} \right) - \sum_a \int d\Gamma^*_a f_a \partial^j E^*_a \\ &+ \bar{\omega}^j \partial_\mu \left(\sum_a g_{\omega a} \int d\Gamma^*_a f_a \frac{p^{*\mu}}{E^*_a} \right) + \bar{\omega}^{\mu j} \sum_a g_{\omega a} \int d\Gamma^*_a f_a \frac{p^*_\mu}{E^*_a} \, . \end{aligned} \tag{C.13}$$

Upon examination, we see that we can combine Eqs. (C.12) and (C.13) into one energy and momentum conservation law

$$\begin{aligned} 0 &= \partial_\mu \left(\sum_a \int d\Gamma_a^* f_a \frac{p^{*\mu} p^{*\nu}}{E_a^*} \right) - \sum_a \int d\Gamma_a^* f_a \partial^\nu E_a^* \\ &+ \bar{\omega}^\nu \partial_\mu \left(\sum_a g_{\omega a} \int d\Gamma_a^* f_a \frac{p^{*\mu}}{E_a^*} \right) + \bar{\omega}^{\mu\nu} \sum_a g_{\omega a} \int d\Gamma_a^* f_a \frac{p_\mu^*}{E_a^*} \,. \end{aligned} \tag{C.14}$$

Analogously to the case of baryon current, this expression gives the divergence of the energy-momentum tensor

$$0 = \partial_\mu T^{\mu\nu} \,. \tag{C.15}$$

Indeed, we recognize the first term on the right-hand-side of Eq. (C.14) as the kinetic theory contribution to the energy-momentum tensor. Hence, the remaining terms must originate in the mean fields. We can begin to see how by recalling the equation of motion for the ω^μ field from Chapter 4. In Eq. (4.40), we found that to first-order in viscous hydrodynamics,

$$m_\omega^2 \bar{\omega}^\mu = \sum_a g_{\omega a} \int d\Gamma_a^* \frac{p^{*\mu}}{E_a^*} f_a \,. \tag{C.16}$$

Hence, we may rewrite Eq. (C.14) as

$$\begin{aligned} 0 &= \partial_\mu \left(\sum_a \int d\Gamma_a^* f_a \frac{p^{*\mu} p^{*\nu}}{E_a^*} \right) - \sum_a \int d\Gamma_a^* f_a \partial^\nu E_a^* \\ &+ m_\omega^2 \bar{\omega}^\nu \partial_\mu \bar{\omega}^\mu + m_\omega^2 \bar{\omega}^{\mu\nu} \bar{\omega}_\mu \,. \end{aligned} \tag{C.17}$$

Thus, we can immediately see the influence of the vector mean field.

To understand the effects of the scalar mean field, we must recall the form of the energy momentum tensor used in Chapter 4. From Eq. (4.36), it was

$$T^{\mu\nu} = \sum_a \int d\Gamma_a^* \frac{p^{*\mu} p^{*\nu}}{E_a^*} f_a + g^{\mu\nu} U(\bar{\sigma}, \bar{\omega}^\rho \bar{\omega}_\rho) + m_\omega^2 \bar{\omega}^\mu \bar{\omega}^\nu \,. \tag{C.18}$$

We require energy and momentum are conserved, so Eq. (C.18) implies

$$\begin{aligned} 0 &= \partial_\mu T^{\mu\nu} \\ &= \partial_\mu \left(\sum_a \int d\Gamma_a^* f_a \frac{p^{*\mu} p^{*\nu}}{E_a^*} \right) + \partial^\nu U \\ &+ m_\omega^2 \left(\bar{\omega}^\nu \partial_\mu \bar{\omega}^\mu + \bar{\omega}_\mu \partial^\mu \bar{\omega}^\nu \right) \,. \end{aligned} \tag{C.19}$$

By equating expressions (C.17) and (C.19) and canceling terms, we find that U must be constrained by the equation

$$\partial^\nu U = -\sum_a \int d\Gamma_a^* f_a \partial^\nu E_a^* - m_\omega^2 \bar{\omega}_\mu \partial^\nu \bar{\omega}^\mu \tag{C.20}$$

We recall that in Chapter 4 we assumed hadron effective masses were shifted by the scalar field $\bar{\sigma}$ according to

$$m_a^* = m_a - g_{\sigma a}\bar{\sigma}\,, \tag{C.21}$$

where m_a is the bare mass and $g_{\sigma a}$ is the hadron-sigma coupling constant. Then we can rewrite Eq. (C.20) as

$$\partial^\nu U(\bar{\sigma}, \bar{\omega}^\rho\bar{\omega}_\rho) = \left(\sum_a g_{\sigma a} \int d\Gamma_a^* f_a \frac{m_a^*}{E_a^*}\right) \partial^\nu \bar{\sigma} + \left(-\tfrac{1}{2}m_\omega^2\right) \partial^\nu \left(\bar{\omega}^\rho\bar{\omega}_\rho\right) \tag{C.22}$$

From the chain rule, we see conservation of energy and momentum require that we enforce the constraints

$$\frac{\partial U(\bar{\sigma}, \bar{\omega}^\rho\bar{\omega}_\rho)}{\partial \bar{\sigma}} = \sum_a g_{\sigma a} \int d\Gamma_a^* \frac{m_a^*}{E_a^*} f_a \tag{C.23}$$

$$\frac{\partial U(\bar{\sigma}, \bar{\omega}^\rho\bar{\omega}_\rho)}{\partial \left(\bar{\omega}^\rho\bar{\omega}_\rho\right)} = -\tfrac{1}{2}m_\omega^2\,, \tag{C.24}$$

in addition to Eq. (C.16).

In light of the constraint (C.24), we can split U into simpler independent parts

$$U(\bar{\sigma}, \bar{\omega}^\rho\bar{\omega}_\rho) = V(\bar{\sigma}) - \tfrac{1}{2}m_\omega^2 \left(\bar{\omega}^\rho\bar{\omega}_\rho\right)\,. \tag{C.25}$$

Now $V(\bar{\sigma})$ must obey the constraint

$$\frac{dV(\bar{\sigma})}{d\bar{\sigma}} = \sum_a g_{\sigma a} \int d\Gamma_a^* \frac{m_a^*}{E_a^*} f_a\,. \tag{C.26}$$

We comment on a few practical considerations for numerical computations. In a numerical calculation of transport coefficients, one would need to specify details of the specific model under investigation, such as $V(\bar{\sigma})$ and the particle-mean field coupling constants. Then, one would need to determine the equilibrium state of the system: at each temperature T and baryon chemical potential μ, one would simultaneously solve Eqs. (C.16) and (C.26) numerically (in the rest frame) to obtain $\bar{\sigma}(T,\mu)$ and $\bar{\omega}^0(T,\mu)$.

Note that one would use the equilibrium distribution function $f_a^{\rm eq}$. Thus, since the mean fields would obey the constraints (C.16) and (C.26), the model constructed would conserve energy and momentum. (It would also be thermodynamically self-consistent, as we will discuss shortly.) Then, one could straightforwardly compute the equilibrium thermodynamic quantities like pressure, energy density, etc. After that, one could apply the formulas from Chapter 4 to compute the shear and bulk viscosities and thermal conductivity.

Eq. (C.25) is somewhat simple, so one may ask whether or not it is possible to construct a more complicated potential $U(\bar{\sigma}, \bar{\omega}^\rho \bar{\omega}_\rho)$? For instance, might one allow extra terms in U containing products of $\bar{\sigma}$ and $\bar{\omega}^\rho \bar{\omega}_\rho$? The answer is yes, one could construct more elaborate forms of U, but one would need to add extra terms to the energy momentum tensor (C.18). Furthermore, it would have to be done in such a way that Eq. (C.14) still holds. This represents one potential avenue to generalize the model of quasiparticles and mean fields developed in this thesis. Another avenue would be inclusion of additional conserved charges and additional scalar and vector mean fields. In either case, energy and momentum must be carefully conserved in order to build a realistic model.

We conclude this section by illustrating the connection between energy momentum conservation and thermodynamic self-consistency. As a bonus, this will prove that several formulas used in Chapter 4 are unchanged by the inclusion of quantum statistics. For simplicity, we work in the fluid's local rest frame. Also, we shall work to first-order in space-time gradients, which is consistent with the rest of this appendix. In equilibrium and in the rest frame, only the $\bar{\omega}^0$ component of is non-zero. (Otherwise $\bar{\omega}^i$ would break rotational symmetry.) So we can say to first-order

$$\bar{\omega}_\mu \partial^\nu \bar{\omega}^\mu \cong \bar{\omega}_0 \partial^\nu \bar{\omega}^0 = \bar{\omega}^0 \partial^\nu \bar{\omega}^0 \,. \tag{C.27}$$

We substitute this result into Eq. (C.20). Then we use the equation of motion for $\bar{\omega}^\mu$ (C.16) to replace the term $m_\omega^2 \bar{\omega}^0$. We obtain, to first-order accuracy,

$$\begin{aligned} \partial^\nu U &= -\sum_a \int d\Gamma_a^* \, \partial^\nu \left(E_a^* + g_{\omega a} \bar{\omega}^0 \right) f_a^{\rm eq} \\ &= -\sum_a \int d\Gamma_a^* \, \partial^\nu \left(E_a \right) f_a^{\rm eq} \,. \end{aligned} \tag{C.28}$$

Hence, if we consider $U(T,\mu)$ a function of temperature and baryon chemical potential and apply the chain rule to Eq. (C.28), we find

$$\left(\frac{\partial U}{\partial T}\right)_{\mu} = -\sum_{a}\int d\Gamma_a^* \left(\frac{\partial E_a}{\partial T}\right)_{\mu} f_a^{\rm eq}\,. \tag{C.29}$$

$$\left(\frac{\partial U}{\partial \mu}\right)_{T} = -\sum_{a}\int d\Gamma_a^* \left(\frac{\partial E_a}{\partial \mu}\right)_{T} f_a^{\rm eq}\,. \tag{C.30}$$

These formulas were crucial for proving the thermodynamic self-consistency of the theory in Sec. 4.5. Thus, we see that energy and momentum conservation are critical to maintaining thermodynamic self-consistency—a well-known result [101, 113]. Since we have not assumed classical statistics in this section, the last two formulas are equally valid for quantum or classical statistics.

Appendix D

The Chapman-Enskog Expansion

In this appendix, we derive Eq. (4.123). Recall that we are we are working with first-order hydrodynamics. This means that we assume space-time gradients are small, so we keep terms up to first-order in gradients and neglect all higher terms. Practically, this means that inside terms which are already first-order in gradients, we can use ideal (zeroth-order) hydrodynamic equations to transform terms into equivalent forms.

The goal is to evaluate Eq. (4.25), which we can recast as

$$\frac{df_a^{\rm eq}}{dt} = \frac{p^{*\mu}}{E_a^*}\partial_\mu f_a^{\rm eq} + \left(\partial^i E_a^* + g_{\omega a}\frac{p_\mu^*}{E_a^*}\,\bar{\omega}^{i\mu}\right)\frac{\partial f_a^{\rm eq}}{\partial p^{*i}}\,. \tag{D.1}$$

Recall that we use Einstein notation where we sum over repeated indices. Also, Greek indices like μ run over space-time variables 0-3 while Roman indices like i run over spacial variables 1-3. Also note that

$$\bar{\omega}^{i\mu} = \partial^i\bar{\omega}^\mu - \partial^\mu\bar{\omega}^i \tag{D.2}$$

is antisymmetric. We recall that the equilibrium distribution function takes the form (using classical statistics)

$$f_a^{\rm eq} = e^{-\beta(p_a^\nu u_\nu - \mu_a)}\,. \tag{D.3}$$

Also recall the identities

$$p^\nu = p^{*\nu} + g_{\omega a}\bar{\omega}^\nu(x) \tag{D.4}$$

$$E_a^* = p^{*0} = \sqrt{\mathbf{p}^{*2} + m_a^{*2}(x)}\,. \tag{D.5}$$

Note that p^{*i} is an integration variable and has no x dependence while $p^{*0} = E_a^*$ has x dependence only through $m_a^*(x)$. We also have

$$\mu_a = b_a \mu \,, \tag{D.6}$$

where μ is the baryon chemical potential and b_a is the baryon charge of particle species a. Also, μ_a^* is given by

$$\mu_a^* = \mu_a - g_{\omega a} \bar{\omega}^\nu u_\nu \,. \tag{D.7}$$

In the following derivation, we will simplify results by working extensively in the local rest frame. Hence, we recall a few useful formulas. First, the fluid four-velocity u^μ obeys the identity

$$u_\mu u^\mu = 1 \,, \tag{D.8}$$

hence

$$u_\mu \partial_\nu u^\mu = 0 \,. \tag{D.9}$$

In the local rest frame where $u_\mu = (1, 0, 0, 0)$ this becomes

$$\partial_\nu u^0 = 0 \,. \tag{D.10}$$

We also note that one must be careful when working with terms containing u_ν. In the local rest frame $u_\nu = (1, 0, 0, 0)$, but the gradients of u_ν in general are nonzero. Hence, when derivatives are involved, one should first differentiate terms involving u_ν, and then afterwards simplify using the rest frame expression $u_\nu = (1, 0, 0, 0)$. For example,

$$\partial_\mu (p^\nu u_\nu) = \partial_\mu E_a + p^\nu \partial_\mu u_\nu \,. \tag{D.11}$$

We begin the evaluation of (D.1) starting with the rightmost term. Performing the derivative, we find in the local rest frame

$$\frac{\partial f_a^{\rm eq}}{\partial p^{*i}} = -\frac{f_a^{\rm eq}}{T} \frac{p^{*i}}{E_a^*} \,. \tag{D.12}$$

From our metric $g_{\mu\nu} = (+, -, -, -)$, we can raise and lower spacial indices with a sign change: $p^{*i} = -p_i^*$. Then Eq. (D.1) becomes

$$\frac{df_a^{\rm eq}}{dt} = \frac{p^{*\mu}}{E_a^*} \partial_\mu f_a^{\rm eq} + \frac{1}{T E_a^*} \left(g_{\omega a} \frac{p_i^* p_\mu^* \bar{\omega}^{i\mu}}{E_a^*} - p^{*i} \partial^i E_a^* \right) f_a^{\rm eq} \,. \tag{D.13}$$

In $p_i^* p_\mu^* \bar{\omega}^{i\mu}$, we are contracting symmetric and antisymmetric tensors, so all but the $\mu = 0$ terms cancel. Thus

$$\frac{df_a^{\rm eq}}{dt} = \frac{p^{*\mu}}{E_a^*}\partial_\mu f_a^{\rm eq} + \frac{1}{TE_a^*}\left(g_{\omega a} p_i^* \bar{\omega}^{i0} - p^{*i}\partial^i E_a^*\right) f_a^{\rm eq}\,. \tag{D.14}$$

Next, we compute the space-time gradient term

$$\partial_\mu f_a^{\rm eq} = f_a^{\rm eq}\left[\frac{E_a}{T^2}\partial_\mu T - \frac{1}{T}\partial_\mu E_a - \frac{p^\nu \partial_\mu u_\nu}{T} + \partial_\mu\left(\frac{\mu_a}{T}\right)\right]. \tag{D.15}$$

Using Eq. (D.10), we can rewrite

$$p^\nu \partial_\mu u_\nu = p^i \partial_\mu u_i\,. \tag{D.16}$$

We also note that in the rest frame $\bar{\omega}^i = 0$ in equilibrium, so to first-order accuracy

$$p^\nu \partial_\mu u_\nu = p^{*i}\partial_\mu u_i\,. \tag{D.17}$$

Thus we find

$$\frac{p_a^{*\mu}}{E_a^*}\partial_\mu f_a^{\rm eq} = \frac{f_a^{\rm eq}}{E_a^*}\left[\frac{E_a p^{*\mu}\partial_\mu T}{T^2} - \frac{p^{*\mu}\partial_\mu E_a}{T} - \frac{p^{*\mu}p^{*i}\partial_\mu u_i}{T} + p^{*\mu}\partial_\mu\left(\frac{\mu_a}{T}\right)\right]. \tag{D.18}$$

Combining Eqs. (D.18) and (D.14) and simplifying, we find

$$\frac{df_a^{\rm eq}}{dt} = \frac{f_a^{\rm eq}}{E_a^*}\left[\frac{E_a p^{*\mu}\partial_\mu T}{T^2} + p^{*\mu}\partial_\mu\left(\frac{\mu_a}{T}\right) - \frac{E_a^*\partial_0 E_a}{T} - \frac{g_{\omega a}p^{*i}\partial_0\bar{\omega}_i}{T} - \frac{p^{*\mu}p^{*i}\partial_\mu u_i}{T}\right]. \tag{D.19}$$

We note that in equilibrium, $\bar{\omega}_\mu$ has no spacial components, so we write

$$\bar{\omega}_\mu = \bar{\omega}^0 u_\mu\,, \tag{D.20}$$

so to lowest order we have

$$\partial_0\bar{\omega}_i = \bar{\omega}^0\partial_0 u_i\,. \tag{D.21}$$

Thus, we find

$$\frac{df_a^{\rm eq}}{dt} = \frac{f_a^{\rm eq}}{E_a^*}\left[\frac{E_a p^{*\mu}\partial_\mu T}{T^2} + p^{*\mu}\partial_\mu\left(\frac{\mu_a}{T}\right) - \frac{E_a^*\partial_0 E_a}{T} - \frac{E_a p^{*i}\partial_0 u_i}{T} - \frac{p^{*i}p^{*j}\partial_j u_i}{T}\right]. \tag{D.22}$$

We can reorganize the terms to read

$$\frac{df_a^{\rm eq}}{dt} = \frac{f_a^{\rm eq}}{E_a^*}\left[-E_a^*\partial_0\left(\frac{E_a-\mu_a}{T}\right) + p^{*i}\partial_i\left(\frac{\mu_a}{T}\right) + \frac{E_a p^{*i}}{T}\left(\frac{\partial_i T}{T} - \partial_0 u_i\right) - \frac{p^{*i}p^{*j}\partial_j u_i}{T}\right]. \tag{D.23}$$

Next, we derive a needed identity. From Eq. (B.10), we see conservation of energy and momentum implies (to lowest order)

$$D_\nu P = w D u_\nu \,, \tag{D.24}$$

where $w = (P + \epsilon)$ is the enthalpy density. In the rest frame this equation is

$$\partial_i P = w \partial_0 u_i \,. \tag{D.25}$$

Employing the Gibbs-Duhem thermodynamic equation, we find

$$\begin{aligned} \partial_i P &= s\partial_i T + n\partial_i \mu \\ &= \frac{w}{T}\partial_i T + Tn\partial_i\left(\frac{\mu}{T}\right) = w\partial_0 u_i \,, \end{aligned} \tag{D.26}$$

or

$$\frac{1}{T}\left(\frac{\partial_i T}{T} - \partial_0 u_i\right) = -\frac{n}{w}\partial_i\left(\frac{\mu}{T}\right) . \tag{D.27}$$

Then recalling $\mu_a = b_a \mu$, Eq. (D.23) becomes

$$\frac{df_a^{\rm eq}}{dt} = \frac{f_a^{\rm eq}}{E_a^*}\left[-E_a^*\partial_0\left(\frac{E_a - \mu_a}{T}\right) + \left(b_a - \frac{E_a n}{w}\right)p^{*i}\partial_i\left(\frac{\mu}{T}\right) - \frac{p^{*i}p^{*j}\partial_j u_i}{T} \,.\right] \tag{D.28}$$

Next, we symmetrize the term

$$\begin{aligned} p^{*i}p^{*j}\partial_j u_i &= \tfrac{1}{2}p^{*i}p^{*j}\left(\partial_i u_j + \partial_j u_i + \tfrac{2}{3}\Delta_{ij}\partial_\rho u^\rho\right) - p^{*i}p^{*j}\tfrac{1}{3}\Delta_{ij}\partial_\rho u^\rho \\ &= \tfrac{1}{2}p^{*i}p^{*j}\left(\partial_i u_j + \partial_j u_i + \tfrac{2}{3}\Delta_{ij}\partial_\rho u^\rho\right) - \frac{|\mathbf{p}^*|^2}{3}\partial_\rho u^\rho \,. \end{aligned} \tag{D.29}$$

(Recall that in the rest frame $\Delta_{ij} = \delta_{ij}$.) We next cast this into a more covariant form by recalling that in the rest frame

$$\begin{aligned} D &= \partial_0 \\ D_i &= \partial_i \\ D_0 &= 0 \,. \end{aligned} \tag{D.30}$$

Thus Eq. (D.28) becomes

$$\begin{aligned} \frac{df_a^{\rm eq}}{dt} &= f_a^{\rm eq}\left[\frac{|\mathbf{p}^*|^2}{3TE_a^*}\partial_\rho u^\rho - D\left(\frac{E_a - \mu_a}{T}\right)\right] \\ &\quad + f_a^{\rm eq}\left(b_a - \frac{E_a n}{w}\right)\frac{p^{*\mu}}{E_a^*}D_\mu\left(\frac{\mu}{T}\right) \\ &\quad - f_a^{\rm eq}\frac{p^{*\mu}p^{*\nu}}{2TE_a^*}\left[D_\mu u_\nu + D_\nu u_\mu + \tfrac{2}{3}\Delta_{\mu\nu}\partial_\rho u^\rho\right] \,. \end{aligned} \tag{D.31}$$

Note that, working to first-order in space-time gradients, we can swap

$$p_a^{*\mu} D_\mu \to p_a^\mu D_\mu \tag{D.32}$$

since the difference is second-order in gradients. (The reason is that in equilibrium, $\bar{\omega}^\mu$ is parallel to u^μ which is orthogonal to D_μ.) Thus we find

$$\begin{aligned} \frac{df_a^{\rm eq}}{dt} &= f_a^{\rm eq}\left[\frac{|\mathbf{p}^*|^2}{3TE_a^*}\partial_\rho u^\rho - D\left(\frac{E_a-\mu_a}{T}\right)\right] \\ &\quad + f_a^{\rm eq}\left(b_a - \frac{E_a n}{w}\right)\frac{p^\mu}{E_a^*} D_\mu\left(\frac{\mu}{T}\right) \\ &\quad - f_a^{\rm eq}\frac{p^\mu p^\nu}{2TE_a^*}\left[D_\mu u_\nu + D_\nu u_\mu + \tfrac{2}{3}\Delta_{\mu\nu}\partial_\rho u^\rho\right] . \end{aligned} \tag{D.33}$$

Next, we recall Eq. (4.120) which came from ideal hydrodynamics

$$\begin{aligned} DT &= -v_n^2 T\,\partial_\rho u^\rho , \\ D\mu &= -v_s^2 \mu\,\partial_\rho u^\rho . \end{aligned} \tag{D.34}$$

Also note that

$$v_n^2 = \left(\frac{\partial P}{\partial \epsilon}\right)_n \tag{D.35}$$

as discussed in Sec. 4.6. Since entropy per baryon σ is conserved in ideal hydrodynamics, we can write (to first-order accuracy)

$$\begin{aligned} -D\left(\frac{E_a-\mu_a}{T}\right) &= -\frac{\partial}{\partial T}\left(\frac{E_a-\mu_a}{T}\right)_\sigma DT \\ &= v_n^2 T\frac{\partial}{\partial T}\left(\frac{E_a-\mu_a}{T}\right)_\sigma \partial_\rho u^\rho . \end{aligned} \tag{D.36}$$

Hence Eq. (D.33) becomes

$$\begin{aligned} \frac{df_a^{\rm eq}}{dt} &= f_a^{\rm eq}\left[\frac{|\mathbf{p}^*|^2}{3TE_a^*} + v_n^2 T\frac{\partial}{\partial T}\left(\frac{E_a-\mu_a}{T}\right)_\sigma\right]\partial_\rho u^\rho \\ &\quad + f_a^{\rm eq}\left(b_a - \frac{E_a n}{w}\right)\frac{p^\mu}{E_a^*} D_\mu\left(\frac{\mu}{T}\right) \\ &\quad - f_a^{\rm eq}\frac{p^\mu p^\nu}{2TE_a^*}\left[D_\mu u_\nu + D_\nu u_\mu + \tfrac{2}{3}\Delta_{\mu\nu}\partial_\rho u^\rho\right] . \end{aligned} \tag{D.37}$$

Thus we have derived Eq. (4.123).

We conclude this appendix by computing an alternative form of Eq. (D.37) which generalizes results found in other published works. We start with Eq. (D.36) and employ the chain rule to differentiate with respect to T and μ. We find

$$\begin{aligned} -D\left(\frac{E_a-\mu_a}{T}\right) &= \frac{1}{T^2}\left[E_a - T\left(\frac{\partial E_a}{\partial T}\right)_\mu - b_a\mu\right]DT \\ &\quad -\frac{1}{T}\left[\left(\frac{\partial E_a}{\partial \mu}\right)_T - b_a\right]D\mu\,. \end{aligned} \tag{D.38}$$

Next, we note that Eq. (D.34) is often written in an equivalent form [112] which is derived using ideal hydrodynamics and hence also conserves entropy per baryon:

$$\begin{aligned} DT &= -T\left(\frac{\partial P}{\partial \epsilon}\right)_n \partial_\rho u^\rho\,, \\ D\mu &= -\left[\mu\left(\frac{\partial P}{\partial \epsilon}\right)_n + \left(\frac{\partial P}{\partial n}\right)_\epsilon\right]\partial_\rho u^\rho\,. \end{aligned} \tag{D.39}$$

Inserting Eqs. (D.38) and (D.39) into Eq. (D.33), we find after simplification

$$\begin{aligned} \frac{df_a^{\rm eq}}{dt} &= \frac{f_a^{\rm eq}}{T}\left[\frac{|\mathbf{p}^*|^2}{3E_a^*} - \left(\frac{\partial P}{\partial \epsilon}\right)_n\left(E_a - T\left(\frac{\partial E_a}{\partial T}\right)_\mu - \mu\left(\frac{\partial E_a}{\partial \mu}\right)_T\right)\right. \\ &\quad \left. + \left(\frac{\partial P}{\partial n}\right)_\epsilon\left(\left(\frac{\partial E_a}{\partial \mu}\right)_T - b_a\right)\right]\partial_\rho u^\rho \\ &\quad + f_a^{\rm eq}\left(b_a - \frac{E_a n}{w}\right)\frac{p^\mu}{E_a^*}D_\mu\left(\frac{\mu}{T}\right) \\ &\quad - f_a^{\rm eq}\frac{p^\mu p^\nu}{2TE_a^*}\left[D_\mu u_\nu + D_\nu u_\mu + \tfrac{2}{3}\Delta_{\mu\nu}\partial_\rho u^\rho\right]\,. \end{aligned} \tag{D.40}$$

Formally, this looks very similar to the result in Ref. [112]. However, Ref. [112] did not include a baryon chemical potential nor a vector mean field (which is concealed inside E_a in Eq. (D.40)). Hence, this result is in fact a generalization of Ref. [112].